Ultrasound assisted preparation of nanoclay Bentonite-FeCo nanocomposite hybrid hydrogel: A potential responsive sorbent for removal of organic pollutant from water

S.R. Shirsath [b,1], A.P. Hage [a], M. Zhou [c], S.H. Sonawane [b,*,2], M. Ashokkumar [c]

[a] Department of Chemical Engineering, Sinhgad College of Engineering, Vadgaon (BK), Pune-411041, India
[b] Department of Chemical Engineering, Vishwakarma Institute of Technology, 666 Upper Indira Nagar, Pune-411037, India
[c] Department of Chemistry, University of Melbourne,VIC, Australia

ABSTRACT

Synthesis of poly(acrylic acid)-bentonite-FeCo (PAA-B-FeCo) hydrogel nanocomposite via ultrasound assisted in situ emulsion polymerization was carried out. Addition of exfoliated bentonite clay platelets and Fe–Co increased the strength and stability of hydrogel and assisted the adsorption of an organic pollutant. The response of the nanocomposite hydrogel was evaluated using a cationic dye, crystal violet (CV) under different temperature, pH, and cavitation environment. The optimum temperature was found to be 35 °C and basic pH (optimum at 11) was responsible for the higher adsorption of dye due to dissociation of COO^- ions at higher pH. Bimetallic components form the metal ions in hydrogel which shows repulsion at low pH resulting to lower response. Thermodynamic parameters for adsorption indicated that the dye adsorption onto PAA-B-FeCo hydrogel was spontaneous and endothermic in nature.

© 2011 Elsevier B.V. All rights reserved.

1. Introduction

Hydrogels are three dimensionally dense cross linked polymer network structures composed of functional hydrophilic groups which have the ability to absorb significant amount of water and solute molecules [1–5]. Hydrogels are also known as smart materials which show response and swelling when there is small change in external environment [4,6,7]. The response of hydrogel is dependent on the presence of hydrophilic functional groups such as − OH, − COOH [8,9]. These groups make the hydrogel hydrophilic and due to capillary action and difference in the osmotic pressure, water diffuses into the hydrogel. Polymerization methods, the presence of functional groups and the nature of cross linking agents are important parameters that control the swelling ability of the hydrogen [10]. The external environmental conditions such as, pH, temperature, electric field, ionic strength, and light act as stimuli for the responsiveness of the hydrogels [9–12]. Hydrogels are useful in a variety of applications such as tissue engineering [13], drug delivery [10], separation of bimolecules [14], separation of the metal ions, and inorganic compounds [15] etc. The pH-sensitive hydrogels contain ionizable groups in polymer, e.g. COO^- ions in polyacrylic acid, which shows response to pH change [11,16].

Nanosized magnetic iron oxide particles are extensively studied as new adsorbents with large surface area and small diffusion resistance for the separation and removal of chemical species such as metals, dyes and gasses [17]. Different types of magnetic nano-adsorbents with tailored surface reactivity by using natural or synthetic polymers such as chitosan, alginate, poly(acrylic acid) are used for heavy metal removal from waste water [18]. Zhu et al. [19] successfully used magnetically separable γ-Fe_2O_3/crosslinked chitosan adsorbent for the removal of hazardous azo dye.

A number of adsorbents are used in dye adsorption, e.g. activated charcoal, clay materials such as bentonite, flyash, kaolin and montmorillonite [20–22]. These adsorbents generate secondary waste and some of the materials are not efficient adsorbents because of their limitations in the cation exchange capacity, lower adsorption rate, etc.[23]. Hence, the enhancement of adsorption process has been achieved using cavitation, changing cation exchange capacity or hybrid nanocomposites [24]. The limitations of existing water treatment methods (ion exchange, adsorption, and wet air oxidation, etc.) could be overcome by developing efficient hydrogels to intensify the process of removal of organic components from waste water [25]. A number of attempts are made to use the hydrogels for adsorption of the dye components from water [26–28].

Ultrasonic irradiation is used to initiate the emulsion polymerization to form hydrogel through the generation of free radicals. The high shear gradients generated by the acoustic cavitation process helps to control the molecular weights of hydrogels formed in aqueous solutions. Ultrasound was found to be an effective method for polymerization of monomers and for the production of hydrogel

in the absence of a chemical initiator [29]. Several acrylic hydrogels have been prepared via ultrasonic polymerization of water soluble monomers and macro monomers [30].

Nanocomposite hydrogels are loaded with the different types of clays like bentonite, Laponite, Sepiolite. These clays enhance the mechanical properties and adsorption capacity of hydrogels. Compared to other adsorbents, clays are the natural, abundant and inexpensive materials having good mechanical strength and porous structure [31–37]. Li et al. [31] prepared nanocomposite hydrogels by incorporating Laponite clay into a poly(acryl amide) hydrogel by the in situ polymerization for the adsorption of CV. The cationic dye adsorption ability of the hydrogel increased with increasing clay content in the hydrogel.

In this manuscript attempt was made to synthesize polymer nanocomposite hydrogels using metal hybrid polymer along with clay. No reports are available in the literature on the synthesis of nanocomposite using metal and clay composite hydrogel. It is also important to note that magnetic nanoparticles were used in hydrogels so that the material can be used in a number of applications [38]. In this study, clay platelets were used as support for the metal particles and to increase the mechanical strength of the hydrogel composite. Metallic iron nanoparticles are, undoubtedly, promising materials for magnetic, drug delivery systems and other medical applications. Combination of cobalt with Fe nanoparticles may increase the magnetic characteristics [39,40]. Hence an attempt was made in this study to synthesize clay supported metal nanocomposite hydrogel using ultrasound assisted emulsion method. Clay and Fe–Co combination is used to enhance the mechanical properties and to improve the efficiency of water treatment.

The objectives of the present investigation are: (i) To synthesize poly(acrylic acid)-bentonite-FeCo (PAA-B-FeCo) hydrogel via in situ ultrasonic emulsion polymerization and (ii) To assess the feasibility of PAA-B-FeCo hydrogel for the removal of crystal violet dye. The adsorption equilibrium studies are carried out under different pH, temperature, and dye initial concentration conditions. The data obtained is processed using the adsorption isotherm models and the thermodynamic behavior of the cationic dye adsorption is also evaluated.

2. Experimental

2.1. Materials

Acrylic acid (AA), ammonium persulphate (APS), sodium dodecyl sulfate (SDS) and crystal violet dye (CV) were of analytical grade and procured from M/s CDH, India. Natural Bentonite clay was obtained from MD Chemicals, Pune, India. Millipore deionized water was used for all experiments. N-acetyl-N,N,N-trimethyl ammonium bromide (CTAB), ferric chloride, cobalt chloride and sodium borohydride (NaBH$_4$) were procured from Sigma Aldrich.

2.2. Synthesis of pure poly(acrylic acid) and PAA-B-FeCo hydrogel

Initially, pristine bentonite clay was washed 3–4 times with demineralized water. Impurities such as silica and iron oxides were removed by a differential sedimentation technique. The mixture was stirred for 1 h and kept undisturbed overnight. After filtration, the solid was exposed to slow evaporation, till the desired dryness was obtained. Modification of bentonite was carried out by ion exchange reaction. The following procedure was used to carry out ion exchange reaction so as to obtain modified bentonite nanoclay. 10 g bentonite clay (calculated on the basis of CEC of bentonite used) was mixed in 100 mL water containing 2 mL of hydrochloric acid and then solution was heated to 70 °C. HCl was added into clay solution as acidic environment facilitates the distribution of quaternary ammonium salts inside the gallery spacing of clay. CTAB solution (0.05 M) was dispersed into

bentonite containing aqueous solution. The dispersion was stirred vigorously for 12 h at 70 °C. Unreacted amines were removed by continuous washing of precipitate using hot water. The final precipitate was thoroughly dried in an oven at 80 °C for 24 h to obtain the modified bentonite nanoclay. A detailed procedure for synthesis of nanoclay bentonite using sonochemical technique has been reported by Sonawane et al. [41,42].

The synthesis of inorganic metal nanocomposite was carried out as follows: An aqueous solution containing ferric chloride (0.05 M, 100 mL) and cobalt chloride (0.05 M 100 mL) was sonicated for 10 min in an ultrasonic probe reactor (Dakshin, Mumbai India, probe diameter 22 mm). The solution was then added to 10 g of prepared nanoclay bentonite aqueous slurry. The amount of addition of precursors was decided based on the cation exchange capacity (CEC) of the bentonite clay which was 72 meq/g of clay. The mixture was sonicated for 30 min in order to disperse the chloride solution into the gallery spacing. Further, ultrasonic irradiation was carried out for 2 h using ultrasonic probe reactor with 22.5 KHz frequency and a nominal power (120 W). The total acoustic power (1.479 W/cm^2) delivered to the solution was calculated by calorimetric method [23,41]. After 30 min, sodium borohydride (0.1 M) was added drop wise to the solution containing bentonite, FeCl$_2$ and CoCl$_2$. Different procedure was followed for the preparation of Fe–Co as compared to that reported in literature. In our case we used a simple precipitation reduction route using sonochemical approach for formation of B-Fe Co nanocomposite [43].

The synthesis of insitu emulsion nanocomposite hydrogel using cavitation technique was carried out as follows: Water (69 g) containing SDS (0.54 g) was added to the reaction mixture and the entire solution was thoroughly deoxygenated by bubbling with argon for 45 min at room temperature. Initially 36 g of AA was added and the solution was irradiated for 10 min in the ultrasound reactor to form uniform monomer droplets. The temperature of the reaction mixture was maintained at 60 °C using a water bath. The liquid mixture was then subjected to sonication. 2.3 g of ammonium persulphate (APS) initiator in 5 mL distilled water was added dropwise into the reaction mixture. The polymerization reaction was completed within 40 min. Within the initial 15 min of sonication, a viscous mass was formed indicating the formation of pure poly(acrylic acid) hydrogel. The resulting polymerized hydrogel was then dried in an oven for 48 h at 85 °C.

PAA-B-FeCo hydrogel was prepared in a similar manner, except for the addition of 1 g of modified B-FeCo nanoparticles to acrylic acid during polymerization. During the studies done by different researchers on the hydrogels loaded with clays, different amounts of clays are added to the hydrogels ranging from 0.5 g clay to 2 g clay by taking basis of quantities of monomer, initiator and solvent. [31]. In the present investigation bentonite-FeCo nanoparticles were added on the weight percent basis of monomer acrylic acid. Here we have added 1 g of bentonite-FeCo nanoparticles which corresponds to 2.77% (Wt%) of acrylic acid. The addition was very small to act as crosslinking agent during polymerization as it contains the clay platelets. During the sonication of this reaction mixture, the formation of thick brown solution was initially observed which was then converted into a gel. This hydrogel was dried in an oven for 48 h at 85 °C.

2.3. Sample characterization

UV–vis spectrophotometer (SHIMADZU 160A model) was used to determine the concentration of CV dye. The wavelength of maximum absorbance (λ_{max}) of CV dye was found to be 590 nm. Demineralized water was used as a reference. FTIR spectra of the hydrogel samples were recorded on a Perkin Elmer FTIR spectrometer (Paragon 1000 PC) in the wave number range of 500–4000 cm^{-1} with resolution of 1 cm^{-1}.

2.4. Swelling behavior of PAA and nanocomposite hydrogel

The swelling behavior of pure PAA and PAA-B-FeCo hydrogels was studied at 25 °C in deionized water using a gravimetric procedure [44]. Pre-weighed PAA and PAA-B-FeCo hydrogels were kept in distilled water. After regular intervals of time, weight of swollen pieces of hydrogels was measured. The weight measurement of swollen hydrogel was continued till equilibrium was reached. The swelling ratio, S was then calculated using Eq. (1)

$$S = (W_s - W_d)/W_d \qquad (1)$$

where W_s and W_d were the swollen and dry weights of the hydrogel, respectively.

2.5. Adsorption of CV dye

To study the effects of different experimental parameters such as, pH, temperature, concentration, quantity of hydrogel and cavitation environment in batch mode on the adsorption kinetics of CV dye onto PAA-B-FeCo hydrogel, the following procedure was carried out.

During the experiment, 100 mL of the dye solution of desired concentration with 1 g hydrogel was taken in a 200 mL beaker. The desired pH value of dye solution was adjusted using a buffer solution. The effect of initial dye concentration was studied by taking different concentrations of the dye ranging from 10 to 50 mg/L. To study the effect of hydrogel loading, different quantities of PAA-B-FeCo hydrogel (0.5–2.0 g) were used by keeping all other parameters constant. A constant temperature was maintained throughout experimentation using water bath. The percentage dye removal and dye adsorbed per mg of adsorbent (q_t) were calculated using the following equations:

$$Percentage\ removal = (C_o - C_e)/C_o \times 100 \qquad (2)$$

where, C_o and C_e are the initial and equilibrium concentrations of CV dye (mg/L), respectively.

The amount of dye adsorbed per unit mass of hydrogel can be determined using following equation,

$$q_t = (C_0 - C_t)\ V/M \qquad (3)$$

V is volume of the dye solution in L and M is the mass of dry hydrogel in g.

3. Results and discussion

Nanoclay supported Fe and Co particles were initially incorporated into the gallery spacing of bentonite clay by reducing Fe and Co ions inside the clay. To facilitate the incorporation of these metal particles, initially natural bentonite clay was intercalated using quaternary ammonium salts. The long chain of CTAB molecules (C_{16}–C_{18}) of the quaternary ammonium salt increases the cation exchange capacity of bentonite clay from 96 to 120 meq/g of clay. The acoustic cavitation generated physical forces increase the diffusion of precursors inside the gallery spacing. These nanoparticles remain attached to the clay platelets because of presence of CTAB in the platelets. Exfoliation of the platelets takes place during polymerization, because of the shearing effect of acoustic cavitation and hence the platelets exfoliate into the polymer. The details of the procedure and increase in d spacing are described in the literature [41,42]. A diagrammatic representation of formation of nanocomposite hydrogel is shown in Fig. 1.

Fig. 2 shows the TEM images of B-FeCo nanoparticles dispersed in the PAA hydrogel matrix. Fig. 2A shows that the nanoparticles are uniformly distributed in the hydrogel matrix. The particle size of B-FeCo was found to be about 50 nm. Fig. 2B shows that the particles of Fe–Co are spherical in nature. TEM images indicate that the nanoparticles are uniformly dispersed in the hydrogel matrix.

When the pure poly(acrylic acid) hydrogel was put into the dye solution it was dissolved, therefore bentonite and Fe–Co was added
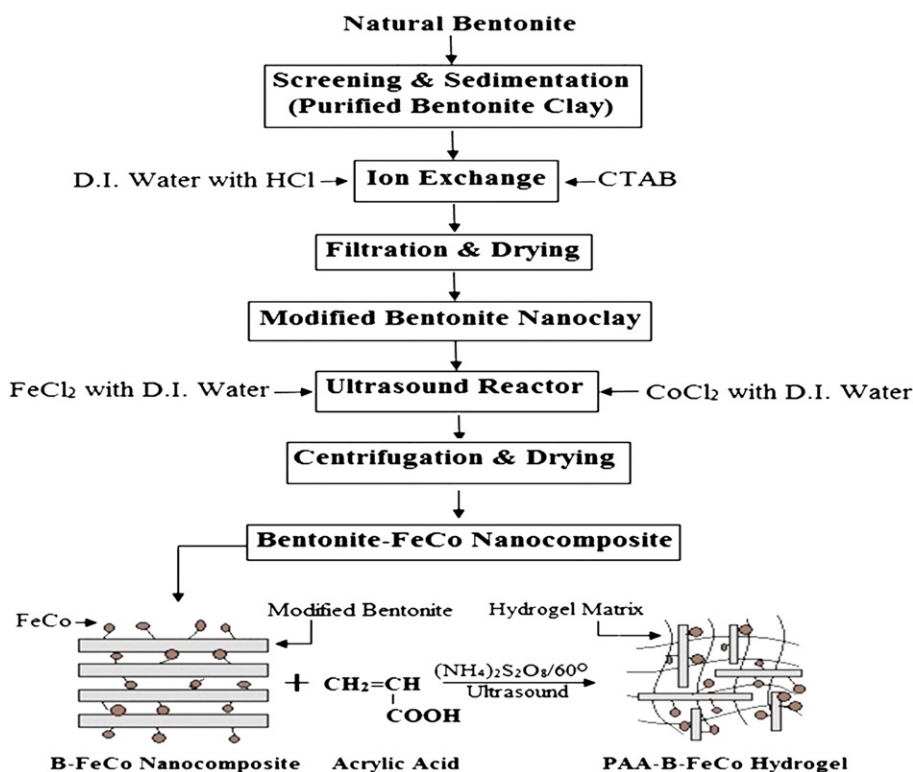
Fig. 1. Ultrasound assisted synthesis of B-FeCo nanocomposite hydrogel.
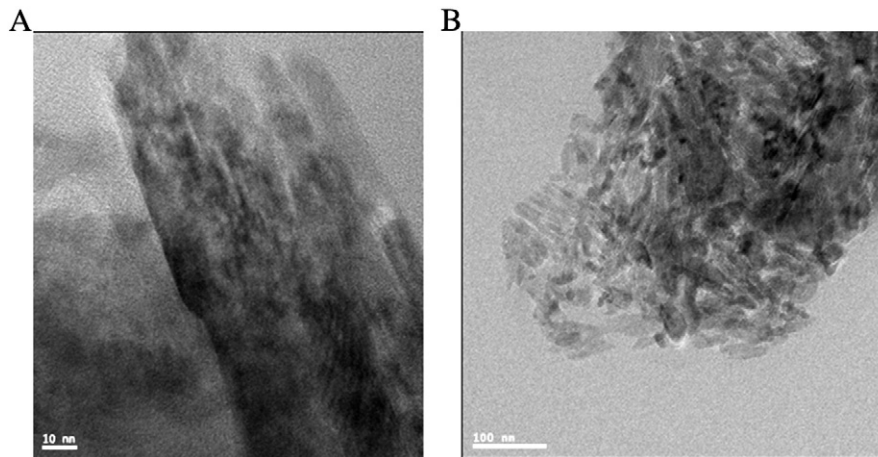
Fig. 2. TEM image of (A) Fe Co bentonite hydrogel nanocomposite, (B) Fe Co particle into present in hydrogel nanocomposite.

to the hydrogel to give it mechanical strength to prevent the collapse of hydrogel matrix. The addition of B-Fe served the dual purpose of providing the mechanical strength to the hydrogel as well as increased the adsorption capacity due to improvement in the electrostatic interaction [19].

As discussed in experimental section Fe–Co nanoparticles were surrounded with COOH groups of polyacrylic acid. It is important to note that bare magnetic particles in water based system are susceptible to oxidation and particles are aggregated which reduce the efficiency of separation and adsorption; hence the presence of COOH groups in the hydrogel offer improvement in the efficiency of the Fe–Co nanoparticles.

3.1. Swelling behavior of hydrogel

When pre-weighed samples of PAA-B-FeCo hydrogel (1 g) were kept for more than 12 h in water, the compact (dry) network structure of the polymer matrix relaxed and swollen due to the diffusion of water molecules inside the matrix, until an equilibrium was reached. At this stage, pressure inside the hydrogel matrix increased due to the presence of large amount of water molecules. The dissolution of the hydrogel did not occur due to the presence of cross linker as against pure PAA hydrogel which dissolved in water. Hence, the mechanical strength and dissolution properties could be changed by the addition of cross linker [5,32] and nanoparticles of Fe–Co during the polymerization. In this work, we have used B-FeCo as the cross linker as well as adsorbent. The B-FeCo nanocomposite hydrogel shows enhanced swelling behavior due to formation of network structure between PAA and B-FeCo.

The time dependent swelling behavior of the hydrogel is calculated by Eq. (4) [15,45].

$$F = M_t/M_s = Kt^n \qquad (4)$$

where, 'F' is the fractional uptake at time 't', K is the diffusion constant; 'M_t' and 'M_s' are the masses of water uptake at time 't' and equilibrium, respectively. Characteristic exponent 'n' is related to the transport mode of the penetrating molecule. Eq. (4) is valid for the first 60% of the fractional uptake of water. The value of 'n' for case of Fickian diffusion (rate of diffusion is slow compared to relaxation rate of hydrogel) is 0.5 and is 1 when rate of diffusion is fast compared to relaxation rate. Value of 'n' for Non-Fickian diffusion is between $0.5 < n < 1$ [45]. A graph of $\ln(M_t/M_s)$ against ln 't' can be used to evaluate 'n' as shown in Fig. 3. The value of n is found to be 0.56 indicating that the transport mode of water in the gel is non-Fickian diffusion. The diffusion constant 'K' can be calculated from the intercept of the line, which is 0.13.

3.2. Effect of pH on dye adsorption

The pH of the solution is an important parameter, which affects the adsorption process. The effect of solution pH depends on the ions present in the reaction mixture and electrostatic interactions at the adsorption surface [16,36]. To determine the effect of different pH on CV dye removal, experiments were carried out by adjusting the pH value to 4, 9 and 11 using acid/base buffer solutions. The natural pH of the solution was 6.5. Fig. 4A shows the effect of pH on the dye adsorption at an initial concentration of 30 mg/L in presence of 1 g of hydrogel nanocomposite. The maximum dye removal was observed (above 75%) in the pH range of 9 to 11. At higher pH, the COOH functional groups of acrylic acid present in the hydrogel matrix dissociates to form COO^- ions, which is responsible for higher adsorption of dye in basic pH. The electrostatic attraction between the positively charged dye and negatively charged COO^- ions, results into the formation of ionic complex which increases the dye removal. Hence for further experiments, pH 11 was used as the solution pH. Fig. 4B shows plausible responsive mechanism of adsorption of CV molecules towards hydrogel at different pH conditions.

3.3. Effect of temperature

The effect of temperature on the adsorption of CV was evaluated for 1 g hydrogel with 30 mg/L dye solution at three different temperature conditions (15, 25 and 35 °C) at 11 pH value. The initial concentration was fixed but the temperature was varied. The adsorption of the
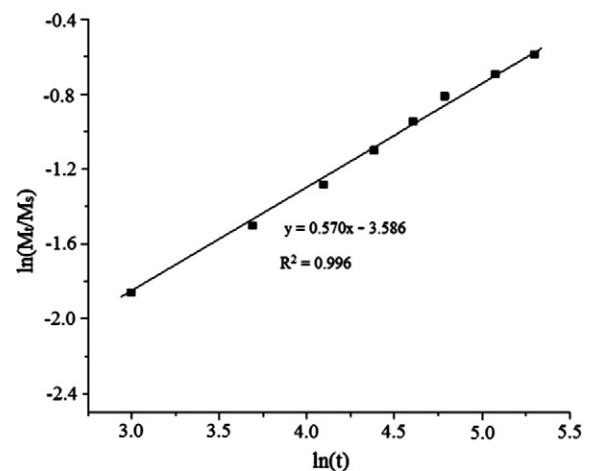
Fig. 3. Plot of ln(Mt/Ms) against ln(t) of water in PAA-B-FeCo hydrogel.

A

B
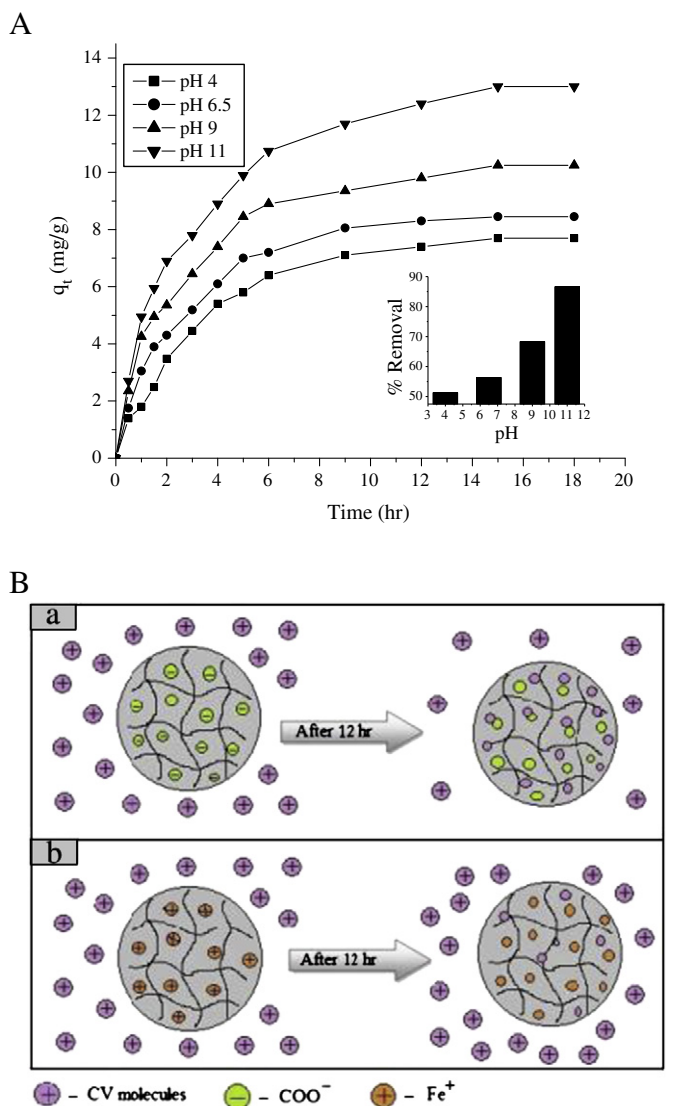
Fig. 4. (A) Time Vs amount of CV dye adsorbed onto PAA-B-FeCo hydrogel at 35 °C and different pH. (B) Adsorption mechanism of CV dye in PAA-B-FeCo hydrogel (a) pH 11 (b) pH 4.

dye increases with increase in temperature as shown in Fig. 5A. This is because at higher temperature the hydrogel network gets relaxed and dye molecules can easily diffuse through the matrix resulting into more adsorption. A maximum of about 87% removal was obtained at 35 °C, hence remaining experiments were carried out at 35 °C.

3.4. Effect of initial dye concentration

The adsorption capacity of hydrogel was determined by equilibrium adsorption studies, at different concentrations of CV dye ranging from 20 to 50 mg/L; with 1 g of PAA-B-FeCo hydrogel at pH 11 and 35 °C. Results indicated that the dye uptake by hydrogel increases sharply with increasing initial dye concentration as shown in Fig. 5B. This is because at higher initial concentration of the dye, the availability of the number of dye molecules is more, which can easily penetrate through hydrogel. However, the removal efficiency was reduced at high concentrations, because the hydrogel gets saturated. The change in color of both hydrogel and dye solutions is shown in Fig. 6. The color of the hydrogel changed from brown to dark blue.

Compared to the previous research performed by Zhang et al. [46] for adsorption of CV on composite hydrogel (adsorption capacity = 0.3 mg/

A

B
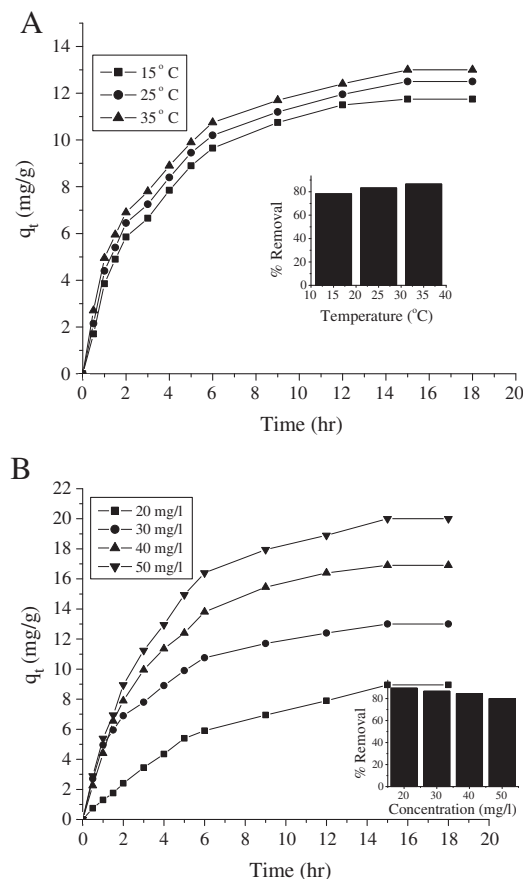
Fig. 5. (A) Time Vs amount of CV dye adsorbed onto PAA-B-FeCo hydrogel at different temperatures and 11 pH, (B) Time Vs amount of CV dye adsorbed onto PAA-B-FeCo hydrogel at different initial concentrations at 11 pH and 35 °C.

g), the PAA-B-FeCo hydrogel prepared in the present investigation shows far better results (adsorption capacity = 13 mg/g). The results are also superior in comparison with the use of wollastonite as an adsorbent (adsorption capacity = 0.88 mg/g) [47]. These results may be attributed to the fact that there may be large number of charge groups on the clay surface and absence of organic cross-linker in the composites leads to flexible polymer chains so that the cationic dye molecules can easily enter into the hydrogel network and interact with the clay [31].

3.5. Effect of quantity of hydrogel

The effect of hydrogel quantity on adsorption was studied by using different amounts of hydrogel (0.5, 1, 1.5, 2 g) in 30 mg/L concentration of 100 mL CV dye solution. Fig. 7A shows that the percent removal of the dye increases with an increase in the quantity of hydrogel. About 95% of dye was removed, when 2 g of hydrogel sample was kept in the solution. This indicates that the presence of higher quantity of hydrogel provides large number of negatively charged ions to adsorb more amount of CV dye due to electrostatic force.

3.6. Effect of ultrasound in dye removal

In this experiment, combined effect of ultrasound and hydrogel adsorption was evaluated and compared. In both the experiments 100 mL solution of 30 mg/L concentration and 1 g of hydrogel was used. The removal efficiencies for hydrogel alone and the combined effect of ultrasound and hydrogel are shown in Fig. 7B, which indicates that combination of hydrogel and ultrasound gives higher dye removal
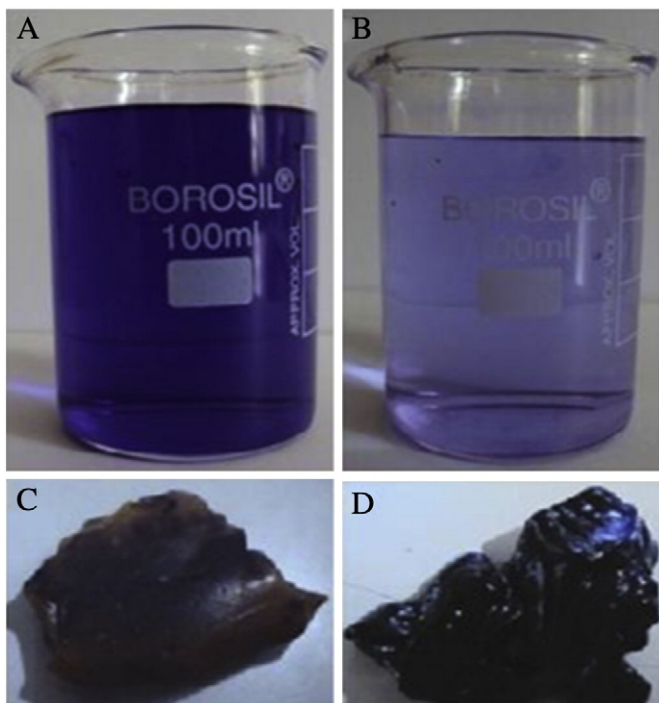
Fig. 6. Color change of CV dye and hydrogel before (A), (C) and after adsorption (B), (D).

as compared to hydrogel adsorption alone. With hydrogel alone, 87% removal was achieved in 15 h and with combination of ultrasound 97% removal was achieved in only 5 h. This enhancement could be due to the mechanical agitation generated by the physical forces generated by acoustic cavitation.

3.7. FTIR study

Fig. 8 shows FTIR spectra of pure PAA, PAA-B-FeCo hydrogel, before and after adsorption of the dye respectively. The FTIR spectra of the pure PAA and PAA-B-FeCo hydrogel show the peak at 1700 cm^{-1}, which is characteristic peak of the C=O stretching due to presence of carboxyl groups in poly(acrylic acid). After the adsorption of the dye, this band is shifted to 1690 cm^{-1} . The FTIR spectra of PAA-B-FeCo hydrogel after the adsorption of CV dye shows a peak at 3500 cm^{-1} which originates due to the formation of hydrogen bond between hydrogel and the dye. The presence of band at 3610 cm^{-1} indicates the OH stretching vibration of bentonite clay [38]. There are small bands originating at 1539 and 1400 cm^{-1} which are due to the stretching of −COOH and −COO$^-$ groups at higher pH value.

3.8. Adsorption isotherm model

Equilibrium data in terms of adsorption isotherm is a basic requirement for the design of adsorption systems. The equilibrium removal of dyes was mathematically expressed in terms of Langmuir and Freundlich adsorption isotherms. The Langmuir equation is based on the assumption that maximum adsorption corresponds to saturated monolayer of the adsorbate molecule on the adsorbent surface [26]. In Langmuir equation,

$$C_e/q_e = 1/(\alpha Q_m) + C_e/Q_m \tag{5}$$

the constant α is related to the energy of adsorption, C_e (mg/L) is the equilibrium concentration of the dye in solution, q_e (mg/g) is the amount of adsorbed dye on the adsorbent surface and the constant
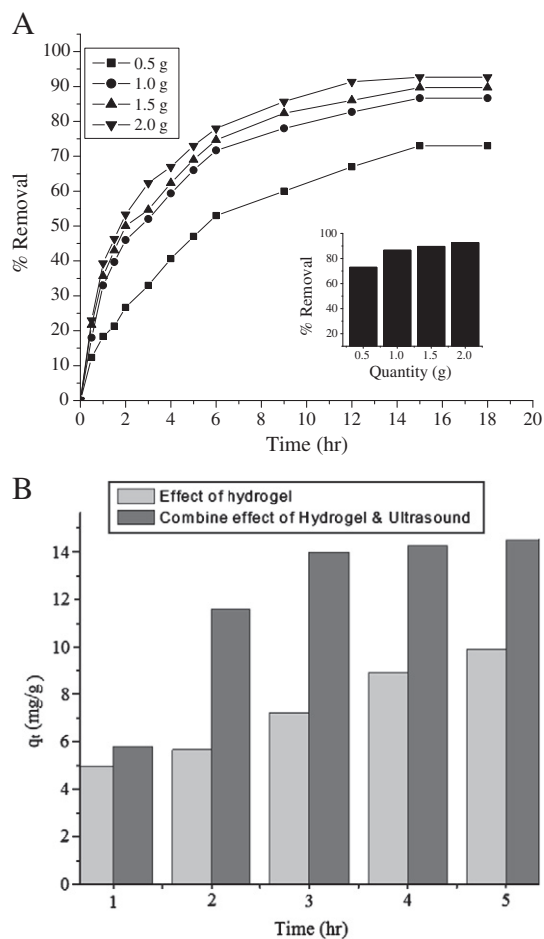
Fig. 7. (A) Time vs percentage removal of CV dye at different initial quantity of PAA-B-FeCo hydrogel at 11 pH and 35 °C (B) Time Vs quantity of CV dye adsorbed using hydrogel & hydrogel with ultrasound at pH 11 and temperature 35 °C.

Q_m represents the maximum binding at the complete saturation of adsorbent binding sites [28]. Q_m and α values can be obtained from slope and intercept of the linear plot of C_e/q_e vs C_e (Fig. 9A), respectively. The values of Q_m and α are given in Table 1a. It can be seen that the adsorption of the dye on PAA-B-FeCo hydrogel followed the Langmuir model.

The Freundlich isotherm model suggests that sorption energy exponentially decreases on completion of the sorptional sites of adsorbent. This isotherm is an empirical equation employed to
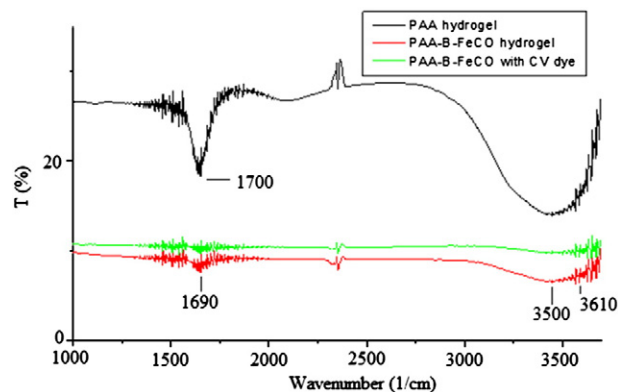
Fig. 8. FTIR spectra of pure PAA hydrogel, PAA-B-FeCo hydrogel before and after adsorption of CV.
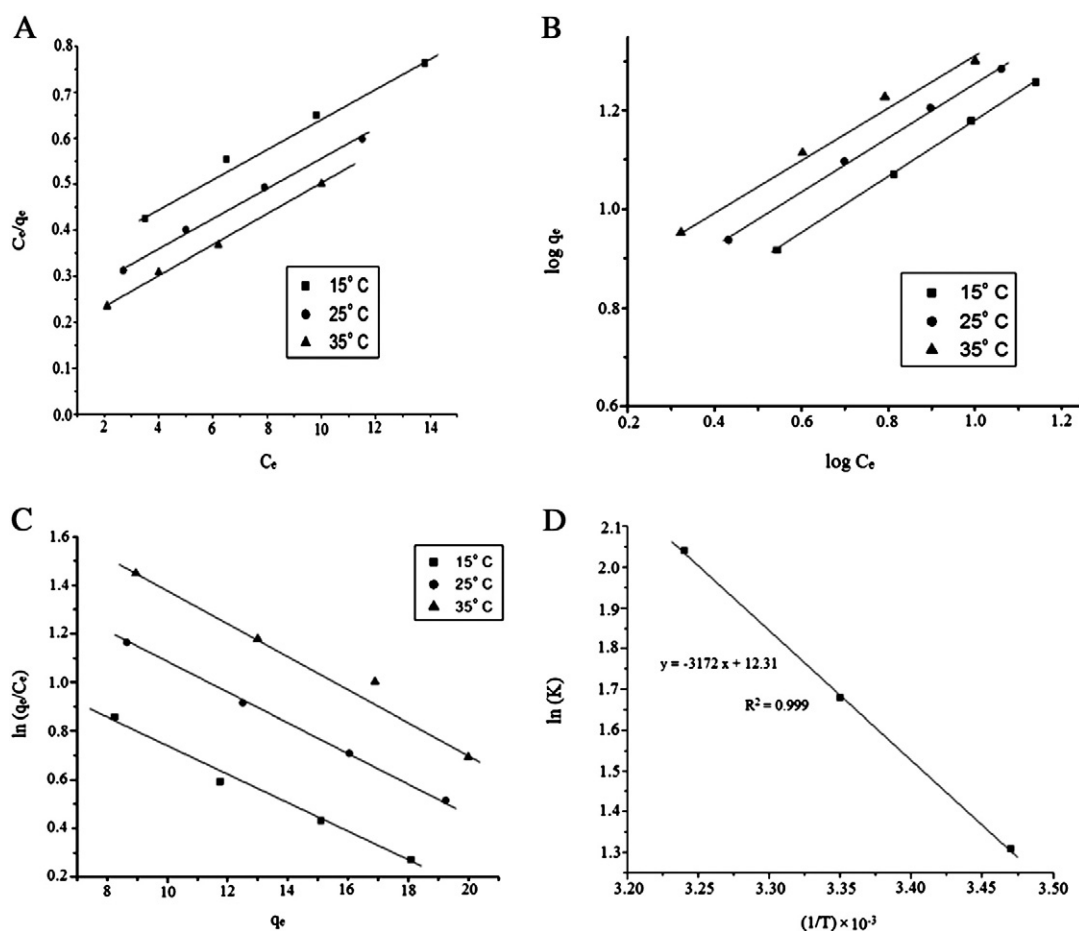
Fig. 9. Plot of (A) C_e/q_e vs C_e for Langmuir isotherm, (B) log qe vs log Ce for Freundlich isotherm, (C) ln (q_e/C_e) vs q_e for K values at different temperatures and (D) plot of ln K vs 1/T.

describe heterogeneous systems [21,26,28]. The Freundlich isotherm is described by equation

$$q_e = K_F \times log C_e^{(1/n)} \tag{6}$$

Taking log on both sides,

$$log\ q_e = log\ K_F + (1/n) log\ C_e \tag{7}$$

where, K_F and n are the physical constants of the Freundlich isotherm. The slope and intercept of the linear plot of log q_e vs log C_e (Fig. 9B) give the values of n and K_F. Values 1/n indicate the type of isotherm to be irreversible (1/n = 0), favorable (0 < 1/n < 1) or unfavorable (1/n > 1) [21,26,28]. The results showed that besides the Langmuir isotherm, Freundlich isotherm is also suitable for describing the adsorption of CV dye on PAA-B-FeCo hydrogel. The Freundlich constants are given in Table 1a.

3.9. Thermodynamic parameters

The thermodynamic parameters $\Delta G°$, $\Delta S°$ and $\Delta H°$ for this adsorption process are determined by using following equations [48,49].

$$\Delta G° = -RT\ lnK \tag{8}$$

where K is the thermodynamic equilibrium constant. The effect of temperature on thermodynamic constant is determined by

$$d\ lnK/dt = \Delta H°/RT^2 \tag{9}$$

Integrating & rearranging Eq. (9)

$$lnK = -(\Delta H°/RT) + \Delta S°/R \tag{10}$$

and Gibbs free energy is given by

$$\Delta G° = \Delta H° - T\Delta S° \tag{11}$$

where $\Delta G°$ is the free energy change (J/mol); R is the universal constant (8.314 J/mol K) and T the absolute temperature (K).

The values of K can be determined by plotting $ln(q_e/C_e)$ against q_e and extrapolating to zero [31,35] (Fig. 9C). The $\Delta H°$ and $\Delta S°$ values were calculated from slope and intercept of the linear plot, of lnK vs 1/T as shown in Fig. 9D. The corresponding values of thermodynamic parameters are presented in Table 1b. The negative values of $\Delta G°$ indicate that the dye adsorption process is spontaneous and feasible. The positive value of $\Delta H°$ shows the adsorption process is endothermic in nature.

Table 1a
Langmuir and Freundlich isotherm constants.

Temperature (K)	Langmuir constants			Freundlich constants		
	Q_m (mg/g)	α	R^2	K_F	n	R^2
288	30.30	0.098	0.989	3.98	1.754	0.999
298	31.15	0.138	0.996	5.01	1.818	0.998
308	31.25	0.197	0.997	6.16	1.923	0.988

Table 1b
Thermodynamic parameters of adsorption of dye onto nanocomposite hydrogel.

Temperature (K)	lnK	$\Delta G°$ (J/mol)	$\Delta H°$ (J/mol)	$\Delta S°$ (J/(mol K))
298	1.31	− 3358.86	26,372	99.77
308	1.68	− 4354.08		
318	2.04	− 5351.68		

4. Conclusion

PAA-B-FeCo hydrogel was synthesized by ultrasonic polymerization of AA and cross-linked by B-FeCo. The network formation of crosslinked polymer hydrogels shows a good swelling behavior due to the presence of B-FeCo. Adsorption process for dye removal was shown to be highly efficient for higher pH and temperature. The lower concentration and higher quantity of hydrogel is more favorable for maximum removal efficiency. The combined effect of hydrogel and ultrasound show a higher percent removal of the dye as compared to hydrogel alone. The FTIR spectrum confirms the presence of carboxyl group in all hydrogel samples. The equilibrium data for adsorption was followed using both Langmuir and Freundlich isotherms. The negative value of $\Delta G°$ indicates the feasibility and spontaneity of the adsorption process. The positive value of $\Delta H°$ suggests the endothermic nature of the adsorption.

Acknowledgment

References

[1] B. Peppas, N. Peppas, Equilibrium swelling behavior of pH-sensitive hydrogels, Chem. Eng. Sci. 46 (1991) 715–722.

[2] H. Kazutoshi, Nanocomposite hydrogels, Rev. Art. Curr. Opin. Solid State Mater. Sci. 11 (2007) 47–54.

[3] G. Fu, W.O. Soboyejo, Swelling and diffusion characteristics of modified poly (N-isopropylacrylamide) hydrogels, Mater. Sci. Eng., C 30 (2010) 8–13.

[4] S.K. Samba, K.Y. Rhee, Preparation and characterization of pH-responsive hydrogel magnetite nanocomposite, Colloids Surf., A 349 (2009) 29–34.

[5] M. Guilherme, A. Fajardo, T. Moia, M. Kunita, M. Goncalves, A. Rubira, E. Tambourgi, Porous nanocomposite hydrogel of vinyled montmorillonite-crosslinked maltodextrin-co-dimethylacrylamide as a highly stable polymer carrier for controlled release system, Eur. Polym. J. 46 (2010) 1465–1474.

[6] Y. Hou, A. Matthews, A. Smitherman, A. Bulick, M. Hahn, H. Hou, A. Han, M. Grunlan, Thermoresponsive nanocomposite hydrogels with cell-releasing behavior, Biomaterials 22 (2008) 3175–3184.

[7] D. Roy, J. Cambre, B. Sumerlin, Future perspectives and recent advances in stimuli-responsive materials, Prog. Polym. Sci. 35 (2010) 278–301.

[8] B. Zkahraman, A. Emik, Removal of cationic dyes from aqueous solutions with poly (N-isopropylacrylamide-co-itaconic acid) hydrogel, Polym. Bull. 66 (2011) 551–570.

[9] K. Pal, A. Banthia, D. Majumdar, Biomedical evaluation of polyvinyl alcohol–gelatin esterified hydrogel for wound dressing, J. Mater. Sci. Mater. Med. 18 (2007) 1889–1894.

[10] K. Liu, T. Liu, S. Chen, D.M. Liu, Drug release behavior of chitosan–montmorillonite nanocomposite hydrogels following electrostimulation, Acta Biomater. 4 (2008) 1038–1045.

[11] M. Bernardo, M. Blanco, R. Olmo, J. Teijon, Delivery of bupivacaine included in poly(acrylamide-co-monomethyl itaconate) hydrogels as a function of the pH swelling medium, J. Appl. Polym. Sci. 86 (2002) 327–334.

[12] F. Carillo, B. Defays, X. Colom, Surface modification of lyocell fibres by graft copolymerization of thermo-sensitive poly-N-isopropylacrylamide, Eur. Polym. J. 44 (2008) 4020–4028.

[13] K. Lee, D. Mooney, Hydrogels for tissue engineering, Chem. Rev. 101 (2001) 1869–1879.

[14] S. Christopher, S. Putka, M. Gehrke, D. Stafford, J. Bryant, Recovery and separation of cell lysate proteins using hydrogels guided by aqueous two-phase extraction principles, Biotechnol. Bioeng. 80 (2002) 139–143.

[15] O. Ozay, S. Ekici, Y. Baran, S. Kubilay, N. Aktas, N. Sahiner, Utilization of magnetic hydrogels in the separation of toxic metal ions from aqueous environments, Desalination 260 (2010) 57–64.

[16] W. Li, J. Wang, L. Zou, S. Zhu, Synthesis and characteristic of the thermo- and pH sensitive hydrogel and microporous hydrogel induced by the NP-10 aqueous two-phase system, Eur. Polym. J. 44 (2008) 3688–3699.

[17] S. Shariati, M. Faraji, Y. Yamini, A. Rajabi, Fe$_3$O$_4$ magnetic nanoparticles modified with sodium dodecyl sulfate for removal of safranin O dye from aqueous solutions, Desalination 270 (2011) 160–165.

[18] A. Badruddoza, A. Tay, P. Tan, K. Hidajat, M. Uddin, Carboxymethyl-β-cyclodextrin conjugated magnetic nanoparticles as nano-adsorbents for removal of copper ions: synthesis and adsorption studies, J. Hazard. Mater. 185 (2011) 1177–1186.

[19] H. Zhua, R. Jiang, L. Xiao, W. Li, A novel magnetically separable γ-Fe$_2$O$_3$/cross-linked chitosan adsorbent: preparation characterization and adsorption application for removal of hazardous azo dye, J. Hazard. Mater. 179 (2010) 251–257.

[20] C. Ozcan, Y. Omeroglu, A. Erdogan, A. Ozacan, Modification of bentonite with a cationic surfactant: an adsorption study of textile dye Reactive Blue-19, J. Hazard. Mater. 140 (2007) 173–179.

[21] N. Emad, J. Qada, G. Stephen, Adsorption of Methylene Blue onto activated carbon produced from steam activated bituminous coal: a study of equilibrium adsorption isotherm, Chem. Eng. J. 124 (2006) 103–110.

[22] M. Dogan, O. Demirbaş, Y. Ozdemir, C. Ozmetin, Adsorption kinetics of maxilon blue GRL onto sepiolite from aqueous solutions, Chem. Eng. J. 124 (2006) 89–101.

[23] S. Sonawane, P. Chaudhari, S. Ghodke, S. Phadtare, S. Meshram, Ultrasound assisted adsorption of basic dye onto organically modified bentonite (nanoclay), J. Sci. Ind. Res. 68 (2009) 162–164.

[24] K. Mishra, P. Gogate, Intensification of degradation of Rhodamine B using hydrodynamic cavitation in the presence of additives, Sep. Purif. Technol. 20 (2010) 385–391.

[25] J. Yun, D. Jin, Y. Lee, H. Kim, Photocatalytic treatment of acidic waste water by electrospun composite nanofibers of pH-sensitive hydrogel and TiO$_2$, Mater. Lett. 30 (2010) 2431–2434.

[26] S. Mak, D. Chen, Fast adsorption of methylene blue on polyacrylic acid-bound iron oxide magnetic nanoparticles, Dyes Pigm. 61 (2004) 93–98.

[27] A. Paulino, M. Guilherme, A. Reis, G. Campese, E. Muniz, J. Nozaki, Removal of methylene blue dye from an aqueous media using superabsorbent hydrogel supported on modified polysaccharide, J. Colloid Interface Sci. 301 (2006) 55–62.

[28] S. Li, Removal of crystal violet from aqueous solution by sorption into semi-interpenetrated networks hydrogels constituted of poly(acrylic acid-acrylamide-methacrylate) and amylase, Bioresour. Technol. 101 (2010) 2197–2204.

[29] B. Teo, S. Prescott, G. Price, F. Grieser, M. Ashokkumar, Synthesis of temperature responsive poly(N-isopropylacrylamide) using ultrasound irradiation, J. Phys. Chem. B 9 (2010) 3178–3184.

[30] P. Cass, W. Knower, E. Pereeia, N. Holmes, T. Hughes, Preparation of hydrogels via ultrasonic polymerization, Ultrason. Sonochem. 17 (2010) 326–332.

[31] L. Peng, Siddaramaiah, N. Kim, S. Heo, J. Lee, Novel PAAm/Laponite clay nanocomposite hydrogels with improved cationic dye adsorption behavior, Composites Part B 39 (2008) 756–763.

[32] Y. Xiang, Z. Peng, D. Chen, A new polymer/clay nano-composite hydrogel with improved response rate and tensile mechanical properties, Eur. Polym. J. 42 (2006) 2125–2132.

[33] N. Churochkina, S. Starodoubtsev, A. Khokhlov, Swelling and collapse of the gel composites based on neutral and slightly charged poly(acrylamide) gels containing Namontmorillonite, Polym. Gels Netw 6 (1998) 205–215.

[34] K. Kabiri, M. Zohuriaan, Superabsorbent hydrogel composites, Polym. Adv. Technol 14 (2003) 438–444.

[35] J. Lin, J. Wu, Z. Yang, M. Pu, Synthesis and properties of poly(acrylic acid)/mica superabsorbent nanocomposite, Macromol. Rapid Commun. 22 (2001) 422–424.

[36] S. Starodoubtsev, N. Churochkina, A. Khokhlov, Hydrogel composites of neutral and slightly charged poly(acrylamide) gels with incorporated bentonite interaction with salt and ionic surfactants, Langmuir 16 (2000) 1529–1534.

[37] J. Wu, J. Lin, M. Zhou, M. Pu, Synthesis and properties of starch-graft polyacrylamide/clay superabsorbent composite, Macromol. Rapid Commun. 21 (2000) 1032–1034.

[38] R. Olsson, A. Samir, G. Alvarez, L. Belova, V. Stro, L. Berglund, O. Ikkala, J. Nogue, U. Geddemaking, Flexible magnetic aerogels and stiff magnetic nanopaper using cellulose nanofibrils as templates, Nat. Nanotechnol. 5 (2010) 584–588.

[39] D. Kim, N. Yuzh, B. Kim, E. Vasileva, E. Kaidash, O. Tolochko, Magnetic properties of iron nanoparticles alloyed with cobalt, Glass Phys. Chem. 33 (2007) 214–216.

[40] G. Chaubey, C. Barcena, N. Poudyal, R. Chuanbing, J. Gao, S. Shouheng, J. Ping, Synthesis and stabilization of FeCo nanoparticles, J. Am. Chem. Soc. 129 (2007) 7214–7215.

[41] S. Sonawane, P. Chaudhari, S. Ghodke, S. Ambade, A. Gulig, A. Mirikar, A. Bane, Combined effect of ultrasound and nanoclay on adsorption of phenol, Ultrason. Sonochem. 15 (2008) 1033–1037.

[42] S. Sonawane, P. Chaudhari, S. Ghodke, M. Parande, V. Bhandari, S. Mishra, R. Kulkarni, Ultrasound assisted synthesis of polyacrylic acid–nanoclay nanocomposite and its application in sonosorption studies of malachite green dye, Ultrason. Sonochem. 16 (2009) 351–355.

[43] C. Wang, S. Peng, L. Lacroix, S. Sun, Synthesis of high magnetic moment CoFe nanoparticles via interfacial diffusion in core/shell structured Co/Fe nanoparticles, Nano Res. 2 (2009) 380–385.

[44] T. Caykara, S. Kiper, D. khan, Thermosensitive poly(N-isopropylacrylamide-co-acrylamide) hydrogels: synthesis, swelling and interaction with ionic surfactants, Eur. Polym. J. 42 (2006) 348–355.

[45] N. Peppas, N. Franson, The swelling interface number as a criterion for prediction of diffusional solute release mechanisms in swellable polymers, J. Polym. Sci. 21 (1983) 983–997.

[46] L.M. Zhang, Y.J. Zhou, Y. Wang, Novel hydrogel composite for the removal of water-soluble cationic dye, J. Chem. Technol. Biotechnol. 81 (2006) 799–804.

[47] S.K. Khare, R.M. Srivastava, K.K. Panday, V.N. Singh, Removal of basic dye (crystal violet) from waste water using wollastonite as adsorbent, Environ. Technol. Lett. 9 (1988) 1163–1172.

[48] M. Purkait, S. Dasgupta, S. De, Determination of thermodynamic parameters for the cloud point extraction of different dyes using TX-100 and TX-114, Desalination 244 (2009) 130–138.

[49] M. Ghouti, M. Khraisheh, M. Ahmad, S. Allen, Thermodynamic behaviour and the effect of temperature on the removal of dyes from aqueous solution using modified diatomite: a kinetic study, J. Colloid Interface Sci. 287 (2005) 6–13.

Ultrasound assisted synthesis of doped TiO$_2$ nano-particles: Characterization and comparison of effectiveness for photocatalytic oxidation of dyestuff effluent

S.R. Shirsath [a], D.V. Pinjari [c], P.R. Gogate [c], S.H. Sonawane [b,*], A.B. Pandit [c]

[a] Department of Chemical Engineering, Vishwakarma Institute of Technology, 666 Upper Indira Nagar, Pune 411037, India
[b] Chemical Engineering Department, National Institute of Technology, Warangal, AP 506007, India
[c] Chemical Engineering Division, Institute of Chemical Technology, Matunga, Mumbai 400019, India

A B S T R A C T

The present work deals with the synthesis of titanium dioxide nanoparticles doped with Fe and Ce using sonochemical approach and its comparison with the conventional doping method. The prepared samples have been characterized using X-ray diffraction (XRD), FTIR, transmission electron microscopy (TEM) and UV–visible spectra (UV–vis). The effectiveness of the synthesized catalyst for the photocatalytic degradation of crystal violet dye has also been investigated considering crystal violet degradation as the model reaction. It has been observed that the catalysts prepared by sonochemical method exhibit higher photocatalytic activity as compared to the catalysts prepared by the conventional methods. Also the Ce-doped TiO$_2$ exhibits maximum photocatalytic activity followed by Fe-doped TiO$_2$ and the least activity was observed for only TiO$_2$. The presence of Fe and Ce in the TiO$_2$ structure results in a significant absorption shift towards the visible region. Detailed investigations on the degradation indicated that an optimal dosage with 0.8 mol% doping of Ce and 1.2 mol% doping of Fe in TiO$_2$ results in higher extents of degradation. Kinetic studies also established that the photocatalytic degradation followed the pseudo first-order reaction kinetics. Overall it has been established that ultrasound assisted synthesis of doped photocatalyst significantly enhances the photocatalytic activity.

© 2012 Elsevier B.V. All rights reserved.

1. Introduction

Over the last decade different catalytic techniques have been investigated as a possible solution for the ever increasing serious environmental pollution problems. Heterogeneous photocatalysis is a well accepted technique with a great potential to control aqueous contaminants or air pollutants. Among various oxide semiconductor photocatalysts, titanium dioxide has attracted interest of many researchers in recent years because of its applicability for all the three classes of water contaminants viz., organic, inorganic and microbiological with a minimal risk of the production of harmful byproducts [1–5]. Titanium dioxide has been proven to be the most suitable photocatalyst because of its chemical inertness, strong oxidizing power, long-term stability against photo and chemical corrosion, suitable band gap energy and electronic and optical properties. Also titanium dioxide is photocatalytically stable, relatively easy to produce and is able to efficiently catalyze reactions [6–9]. It is also used in cosmetics, paints, electronic paper, filter materials, anti-reflection films, sensors, and dye-sensitive solar cells [10,11].

Undesirable recombination of electrons and holes, and low efficiency under irradiation in the visible region are the two main drawbacks associated with the use of TiO$_2$ for environmental applications [12,13]. Efforts have been made to extend the light absorption range of TiO$_2$ from UV to visible light and to improve the photocatalytic activity of TiO$_2$ [14]. The current research on nanoscience and nanotechnology has been oriented towards the fabrication, characterization, and manipulation of novel materials, broadly referred as nanocomposites, which can be used as catalysts, adsorbents and sensors in optical, electronic and magnetic devices [15]. Dopants, such as transitional metals can be added to TiO$_2$ to improve its catalytic activity and also reduce the recombination of photo-generated electrons and photo-generated holes. Noble metals doped or deposited on TiO$_2$ also show effect on the photocatalytic activity by extending excitation wavelength from the UV to the visible light range [11–14,16,17].

There have been many reports of transition metals (Fe, Al, Ni, Cr, Co, W, V and Zr), metal oxides (Fe$_2$O$_3$, Cr$_2$O$_3$, CoO$_2$, MgO + CaO and SiO$_2$), transition metal ceramics (WO$_3$, MoO$_3$, Nb$_2$O$_5$, SnO$_2$ and ZnO) and anionic compounds (C, N, and S) being used to dope TiO$_2$ to improve its applicability [2,18–20]. Zeleska [21] has reviewed the preparation methods of doped TiO$_2$ with metallic and

nonmetallic species, including various types of dopants and doping methods. Rauf [14] has given an overview on the photocatalytic degradation of azo dyes in the presence of TiO_2 doped with selective transition metals.

Higher catalytic activity has been reported for the Ce and CeO_2 doped TiO_2 materials for photo-degradation of dyes and other pollutants [13,22,23]. Titanium dioxide nanopowders doped with visible responsive catalyst may shift the UV absorption threshold of TiO_2 into visible spectrum range and photocatalytic activities can be higher than those of pure TiO_2 and Degussa P25 [6,24–27]. Effect of silver, platinum and gold doping on the TiO_2 for photocatalytic reduction of CO_2 and sonophotocatalytic degradation of methyl orange and organic pollutant nonylphenol ethoxylate has been investigated [7,15,16,28]. Also there are reports of tin, calcium, sulfur and zirconia doped TiO_2 being used for photo-degradation of model pollutants [29–32].

The synthesis of metal-loaded semiconductor oxide materials by conventional physical blending or chemical precipitation followed by surface adsorption usually yields insoluble materials for which the control over size, morphology and dispersion of the metal component remains inherently difficult. These methods often require a long time and are inherently multi-step procedures. Sonochemistry has been proven to be an excellent method for the preparation of mesoporous materials. The physical and chemical effects generated by acoustic cavitation can be expected to significantly influence the properties of doped materials [6,15]. Ultrasound has been very useful in the synthesis of a wide range of nanostructured materials, including high-surface area transition metals, alloys, carbides, oxides, and colloids. The collapse of cavitation bubbles generates localized hot spots with transient temperature of about 10000 K, pressures of about 1000 atm or more and cooling rates in excess of 10^9 K/s. Under such extreme conditions, various chemical reactions and physical changes occur and numerous nano-structured materials such as metals, alloys, oxides and biomaterials can be effectively synthesized with required particle size distribution [6,33–35]. In the past the sonochemical method has been applied to prepare various TiO_2 and doped nanomaterials and photocatalytic activity has been evaluated by different researchers [36–41].

Yu et al. [37] synthesized pure TiO_2 particles using ultrasonically-induced hydrolysis reaction and compared the photocatalytic activity of prepared samples with Degussa P 25 and samples prepared by conventional hydrolysis method. Neppolian et al. [39] also prepared nano TiO_2 photocatalysts using sol–gel and ultrasonic-assisted sol–gel methods using two different sources of ultrasonicator, i.e., a bath type and horn type. The effect of ultrasonic irradiation time, power density, the ultrasonic sources (bath-type and horn-type), magnetic stirring, initial temperatures and sizes of the reactors has been investigated. Li et al. [38] used the combination of ultrasonic and hydrothermal method for preparing Fe-doped TiO_2 for photo-degradation of methyl orange. Zhou et al. [6] used ultrasonicaly-induced hydrolysis reaction for the preparation of Fe-doped TiO_2 whereas Huang et al. [36] synthesized and characterized $Fe_xO_y-TiO_2$ via the sonochemical method.

As mentioned earlier there are many reports of Fe doping on TiO_2 to improve its photocatalytic activity. Amongst a variety of transitional metals, iron has been considered to be an appropriate material due to the fact that the radius of Fe^{3+} (0.79 Å) is similar to that of Ti^{4+} (0.75 Å), so that Fe^{3+} can be easily incorporated into the crystal lattice of TiO_2. Fe^{3+} has proved to be a successful doping element due to its half-filled electronic configuration [2,6,24,26,27]. Cerium oxides have attracted much attention due to the optical and catalytic properties associated with the redox pair of Ce^{3+}/Ce^{4+}. Ce-doped TiO_2 materials have been synthesized by the sol–gel and hydrothermal methods and used in the photocatalytic degradation applications. But there are very few reports on Ce doped catalysts

and the beneficial effect of Ce doped TiO_2 catalysts are known to depend on different factors, such as the synthesis method and the cerium content. [13,22,23]. The photocatalytic performance of TiO_2 catalysts depends strongly on the methods of metal ion doping and the amount of doping material, since they have a decisive influence on the properties of the catalysts. Therefore, it is necessary to investigate the effects of doping method and doping material content on the photocatalytic performance of TiO_2 nanocatalysts.

The present work deals with a detailed study about establishing the influence of ultrasound on the phase composition, structure and performance of pure and doped TiO_2 nanocatalysts. Cerium and Fe-doped TiO_2 nanocatalysts with different amounts of doping elements were prepared by a single-step sonochemical method and conventional method at room temperature. Photocatalytic activity of the prepared composites has been evaluated for the degradation of crystal violet dye. Dye stuffs are a ubiquitous class of synthetic organic pigments that represent increasing environmental issues. As a widely used cationic triphenylmethane dye, crystal violet has high stability because of the electron-donating groups in its unique structure. Crystal violet is a non-biodegradable mutagen and mitotic poison and hence is associated with considerable environmental and health concerns. Considering the Indian context, crystal violet is extensively used in industries such as textile, paper, leather, additives, foodstuffs, cosmetics, and analytical chemistry. Considering the widespread use and toxic nature, it was thought imperative to evaluate the degradation patterns and hence crystal violet has been selected as a model pollutant.

2. Experimental

2.1. Materials

Titanium isopropoxide, propanol, cerium nitrate, and ferric nitrate were procured from S. D. Fine Chemicals Ltd., Mumbai, India. Sodium hydroxide was obtained from Merck Ltd., Mumbai, India. Crystal violet dye was procured from M/s., CDH, India. All the chemicals were of analytical grade and were used as received from the supplier. Freshly prepared distilled water was used in all the experiments.

2.2. Synthesis of TiO_2 by conventional method (CV)

Cerium (III) nitrate, Ferric nitrate and titanium (IV) isopropoxide were used as precursors and 2-propanol was used as solvent. In conventional synthesis procedure, 50 ml of 2-propanol was taken in a 250 ml beaker and 5 ml of titanium isopropoxide was added at room temperature (35 ± 2 °C). The beaker was placed in a constant temperature bath. Solution of cerium nitrate was prepared in 20 ml distilled water. Sodium hydroxide was dissolved in 50 ml distilled water separately and 5 ml of sodium hydroxide solution and 2 ml of cerium nitrate solution were added simultaneously to the titanium isopropoxide solution in propanol after every 30 s until a total of 50 ml sodium hydroxide solution and 20 ml of cerium nitrate solution were added into the beaker. After the addition of all the chemicals, the reaction was allowed to proceed for 4 h under stirring at a temperature of 35 ± 2 °C. After 4 h, the resulting precipitate was centrifuged, filtered, dried and calcined at 450 °C for 3 h. For preparing Fe doped TiO_2, ferric nitrate was used as iron precursor and similar procedure was followed. The catalysts prepared by this method are hereafter named as TiO_2 (CV), Fe–TiO_2 (CV) and Ce–TiO_2 (CV) where CV stands for conventional method of preparation. Pure TiO_2 sample was prepared according to the above procedure without the addition of cerium/iron precursor.

2.3. Synthesis of TiO$_2$ by sonochemical method (US)

In a typical synthesis procedure involving ultrasound, 50 ml of 2-propanol was taken in a 250 ml beaker and 5 ml of titanium iso-propoxide was added. The beaker was placed in a constant temperature bath and the sonication was carried out by employing a direct immersion titanium horn in the sonication cell. Solutions of five different concentrations of cerium nitrate were prepared to get 0.4, 0.8, 1.2, 1.6 and 2 (mol%) of Ce to TiO$_2$ in 20 ml distilled water. 5 ml of sodium hydroxide solution and 2 ml of cerium nitrate solution were added simultaneously after every 30 s till a total of 50 ml sodium hydroxide solution and 20 ml of cerium nitrate solution were added into the ultrasound reactor. After the addition of all the solutions, the mixture was sonicated for further 30 min. After 30 min of irradiation the solution was kept undisturbed for settling of the precipitate. The resulting precipitate was centrifuged, filtered, dried and calcined at 450 °C for 3 h. Similar procedure was adopted for the synthesis of Fe doped TiO$_2$ nanocatalyst with molar ratios of 0.4, 0.8, 1.2, 1.6 and 2 (mol%) of Fe to TiO$_2$. Pure TiO$_2$ sample was also prepared according to the above procedure except the addition of cerium/iron precursor. Synthesis procedure for cerium doped TiO$_2$ is schematically shown in Fig. 1. An ultrasonic horn has been used as a source of ultrasonic irradiations for the synthesis of TiO$_2$ doped composite. The specifications of the horn are as follows: Make: Sonics and Materials, USA; Operating frequency: 22 kHz; rated output power: 750 W; diameter of stainless steel tip: 1.3×10^{-2} m, surface area of ultrasound irradiating face: 1.32×10^{-4} m^2, expected ultrasound intensity: 3.4×10^5 W/m^2 and the horn was operated at 40% amplitude. The catalysts prepared by this method are hereafter described as TiO$_2$ (US), Fe–TiO$_2$ (US) and Ce–TiO$_2$ (US) where US stands for sonochemical method of preparation. The experimental set up for the sonochemical synthesis is schematically shown in Fig. 2.

The reaction time required for the conventional synthesis was 4 h while during sonochemical synthesis the precipitate was formed within 30 min. Zhou et al. [6] has investigated the ultrasound assisted synthesis of Fe doped TiO$_2$ and reported that the reaction time was observed to be 45 min at 20 °C temperature. The reduction in the reaction time compared to conventional synthesis is due to the cavitational effect. Further, the rapid
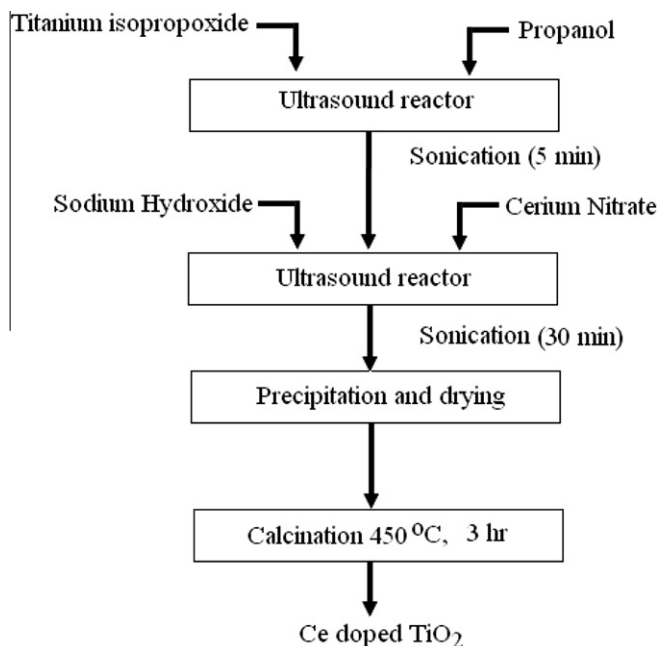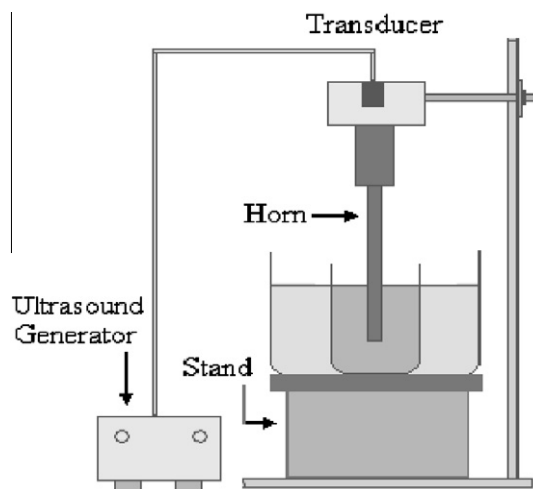
Fig. 2. Experimental setup for sonochemical synthesis.

micromixing and implosive collapse of bubbles in a liquid solution results in extremely high temperatures during ultrasound induced hydrolysis, which results into accelerated hydrolysis reaction.

2.4. Characterization of TiO$_2$ catalysts

XRD diffraction patterns of TiO$_2$ samples were recorded by means of powder X-ray diffractometer (Philips PW 1800). The XRD patterns were recorded at angles between 20° and 70° with a scan rate of 2°/min. FTIR Spectra of the samples were recorded on Perkin Elmer FTIR spectrometer (Paragon 1000 PC) in the wave number range of 500–4000 cm^{-1}. Transmission electron microscopy (TEM, magnification 7,50,000×) image was taken on a Philips Tecnai 20 model.

2.5. Photocatalytic degradation experiments

In order to compare the photocatalytic activity of synthesized catalysts, crystal violet dye degradation studies have been carried out in a laboratory scale reactor. The solution was irradiated in a closed box with a UV lamp Spectroline XX-15 N which emits radiation at 365 nm with intensity of 2000 W/cm^2. All the photocatalytic degradation experiments were carried out at a pH of 6.5 which is the natural pH of the crystal violet solution and the temperature was maintained at 35 °C. The effect of various operating parameters such as catalyst loading and initial dye concentration was studied for the different photocatalysts. For all experiments, 150 ml of crystal violet dye solution was taken in a beaker and appropriate quantity of catalyst was added.

Initially, the time required for reaching the adsorption equilibrium as well as the maximum amount of dye adsorbed on the TiO$_2$ surface under dark and stirred conditions was established using preliminary studies prior to the actual experiments (using UV irradiations). The mixture was stirred with magnetic stirrer for 120 min in the dark to establish the equilibrium adsorption characteristics. The results indicated that maximum of 1.5% of crystal violet dye could be adsorbed on the TiO$_2$ (0.3 g/l loading) and adsorption equilibrium was obtained within 15 min of contact time. The absorbance value did not change with extended time of contact beyond 15 min. Considering this observation, all the photocatalytic degradation experiments have been carried out with 15 min of soaking period under stirring. The time duration of 15 min matches with the studies related to the degradation of methyl orange reported elsewhere [7]. After the attainment of adsorption equilibrium, the suspensions were irradiated with UV

Fig. 1. Synthesis of Ce doped TiO$_2$ by sonochemical method.

lamp at constant stirring speed. Samples were withdrawn regularly from the reactor and centrifuged prior to analysis, in order to separate any suspended solids. UV–vis spectrophotometer (SHIMA-DZU 160A model) was used to determine the concentration of crystal violet dye. The wavelength of maximum absorbance (λ_{max}) of dye was found to be 590 nm. Demineralized water was used as a reference.

Reproducibility of the obtained experimental data is very important in investigation related to the effects of the operating parameters. In the current work, all the experiments were carried out at least two times to estimate the reproducibility of the obtained data. The graphs were plotted using mean values obtained from the data. The standard deviation of the replicate values is shown as error bars in the values depicted on Y axis. All the experimental errors were found to be within ±4% of the mean reported value.

3. Results and discussion

3.1. XRD analysis of pure and doped TiO_2 nanoparticles prepared by conventional and sonochemical method

The wide angle X-ray diffraction pattern was used to investigate the phase structures of the prepared TiO_2 powders. Fig. 3 shows the XRD patterns of the TiO_2 powder samples prepared by ultrasonic method and the conventional method. Neat TiO_2 prepared by both the methods, shows the presence of the main peaks at $2\theta = 25.2°$, 38°, 47.6°, 55.1° and 61.9° and hence confirms that the catalysts have been predominantly crystalline in nature with anatase as the major phase. For Fe doped TiO_2 nanoparticles the mole ratio of Fe/Ti was 2% for both the methods. The XRD patterns for Fe doped TiO_2 prepared by both the methods showed the peaks at $2\theta = 25.8°$, 36.9°, 48.1°, 54.1° and 62.4° corresponding to the anatase phase and hence it can be established that doping with metal ions did not influence the crystal structure of the TiO_2 particle. The XRD pattern also showed the peaks at 34.4° which can be assigned to the presence of Fe in hematite form in TiO_2 [10,18]. Similarly the XRD patterns of Ce doped TiO_2 for Ce/Ti molar ratio of 2% showed the presence of main peaks at $2\theta = 25.4°$, 37.4°, 47.8°, 54.5° and 62.7° again corresponding to the anatase phase. Compared with JCPDS card No. 21–1272 data files, it was found that all peaks observed in the XRD patterns are consistent with anatase (1 0 1), (0 0 4), (2 0 0), (2 1 1) and (2 0 4) spacing, respectively [2,4,11,13,31]. In addition, a broad peak was observed at $2\theta = 29.1°$. Some of literature reports indicate that the Ce-doped TiO_2 materials shows the presence of prominent peaks at 30° and 30.6° which are assigned to cerium titanate–$Ce_x Ti_{(1-x)} O_2$ [13,42]. Thus, in the present case as there was no peak observed at 30°, peak corresponding to 29.1° can be assigned to the presence of cerium as a separate cubic CeO_2, or as cerium titanate in the TiO_2 phase. From the figure, it is also found that the intensities of peaks prepared by sonochemical method are higher as compared to the conventional method and also the peaks are sharper. This clearly indicates the increase in the crystallinity of TiO_2, Fe and Ce doped TiO_2 nanoparticles prepared with sonochemical method leading to the enhanced formation of crystalline particles with anatase phase.

3.2. FTIR analysis of pure and doped TiO_2 nanoparticles prepared by conventional and sonochemical method

The FTIR spectra of pure TiO_2 and doped TiO_2 nanoparticles prepared by sonochemical method are shown in Fig. 4. The absorption bands in the region of 3420–3450 cm^{-1} are generally assigned to the stretching vibrations whereas the bands in the region 1630–1640 cm^{-1} are assigned to the bending vibrations of the hydroxyl on the surface of TiO_2 catalysts [9,17,43]. The absorption bands in the region of 520–580 cm^{-1} are assigned to the stretching vibration of Ti–O. In the present work, results of FTIR analysis shows four main absorption peaks located in the regions 482–507, 1687–1760, 2360–2393, 3568–3651 cm^{-1}. The absorption bands in the region of 1687–1760 cm^{-1} are attributed to the bending vibration of the hydroxyl on the surface of TiO_2-based catalysts, while the bands in the region 3568–3651 cm^{-1} may be assigned to the stretching vibration of the hydroxyl on the surface of the catalysts, since there were no absorption peaks in the region of 3420–3450 cm^{-1}. The absorption bands in the region of 482–507 cm^{-1} can be assigned to the stretching vibration of Ti–O. In addition, peaks in the range of 883–945 cm^{-1} are observed. These peaks can be assigned to the main band (944 cm^{-1}) corresponding to TiO_2 [13]. No additional peaks are present upon Fe and Ce doping, supporting the efficient dispersion of doping elements.

3.3. UV–visible absorption spectra of pure and doped TiO_2 nanoparticles

The increase in the absorption in the visible region depends not only on the type of dopant but also on the method of preparation. The method of preparation plays a significant role in controlling the properties of the TiO_2 nano-particles which could be identified using UV spectroscopic analysis. Fig. 5 shows the UV–visible spectra of the pure TiO_2 and doped TiO_2 samples prepared by using
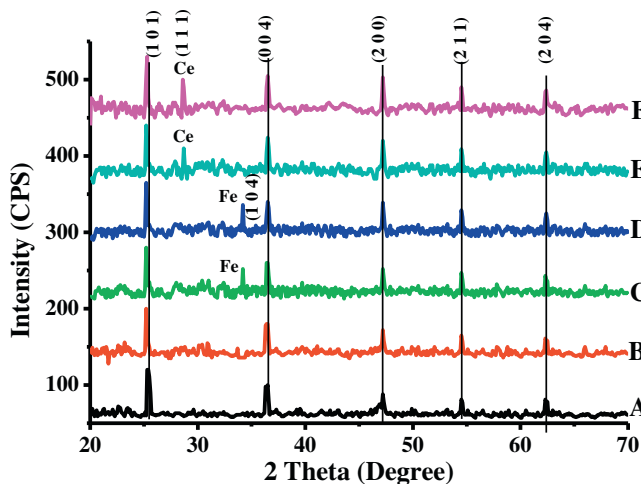
Fig. 3. XRD patterns of Ce-doped TiO_2, Fe-doped TiO_2 and undoped TiO_2 powder prepared by conventional and sonochemical method [A – TiO_2 (CV), B – TiO_2 (US), C – Fe–TiO_2 (CV), D – Fe–TiO_2 (US), E – Ce–TiO_2 (CV), F – Ce–TiO_2 (US)].
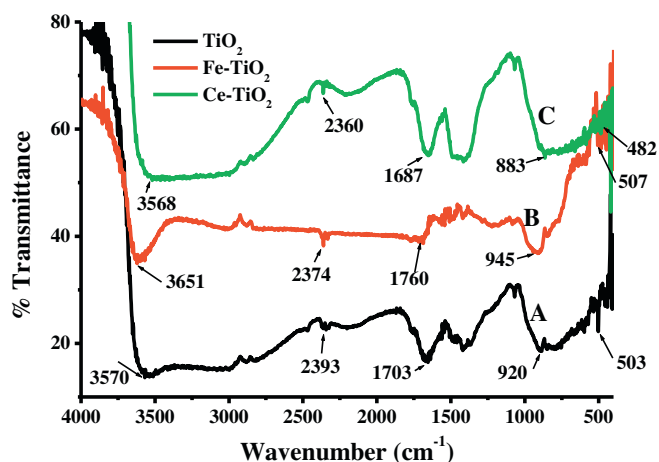
Fig. 4. FTIR spectra of (A) Pure TiO_2, (B) Fe–TiO_2, and (C) Ce–TiO_2 synthesized by sonochemical method.
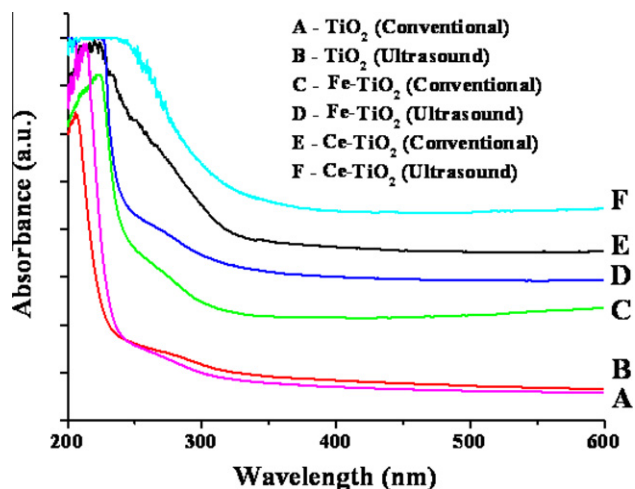
Fig. 5. UV–vis spectra of pure and doped TiO₂ nanoparticles prepared by conventional and sonochemical method.

conventional and sonochemical methods. It is well known that the absorption at wavelength of less than 387 nm is caused by the intrinsic band gap absorption of TiO_2. Usually, metal ion doping affects the light absorption characteristics of TiO_2. The introduction of dopants not only shifts the absorption edge towards the visible region but also increases the absorption of TiO_2 in whole of the visible range (higher wavelength 400–600 nm) [1,2,6,27]. It can be seen from the Fig. 5 that each sample has a broad intense absorption below 400 nm which is the characteristic absorption of TiO_2 corresponding to the excitation of electrons from the valence band to the conduction band in the anatase TiO_2. In the visible region (>400 nm) Ce-doped TiO_2 samples exhibit red shifts of absorption edge and significant enhancement of light absorption at 400–600 nm which is higher than pure TiO_2. The red shift of the absorption spectra could be ascribed to the broad absorption band of transition metals and rare earth elements, and the effect of doping into pure TiO_2 was similar to the influence of adding a photosensitizer to the reaction solution. Further, the enhancement in the absorption could also be due to the adsorption/ deposition of doping elements on TiO_2 particles clearly indicating a decrease in the band gap energy of TiO_2 [44]. This extended absorbance indicates the possible enhancement in the photocatalytic activity of prepared samples. A crystal violet molecule can be degraded into aryl compounds representing the photo oxidation activity. Though, it has been presumed that the doping gives the visible light effect, it is important to note here that the UV light effect is more dominant than the visible light as UV light activated photocatalytic reaction is more pronounced [45].

Fig. 5 also clearly shows the influence of doping and the preparation method on the UV–vis absorption. Modification of TiO_2 with Fe, Ce ions significantly affected the absorption properties of photocatalysts, whereas for pure TiO_2 particles there was no significant increment in the absorption using ultrasound assisted method as compared to the conventional method. However for doped TiO_2 particles, higher absorption was shown by the particles prepared by sonochemical method. For Ce–TiO_2 samples the absorbance in the visible range was increased by 15% as compared to the samples prepared by conventional method.

3.4. TEM analysis and particle size distribution of TiO₂ and doped TiO₂ nanoparticles

Fig. 6 illustrates the transmission electron microscopy (TEM) images of pure TiO_2 (A), Fe doped TiO_2 (B) and Ce doped TiO_2 (C)

nanoparticles prepared by sonochemical method. Spherical TiO_2 particles were formed by the sonochemical method. During ultrasonic irradiation, microjets formed due to the cavitational activity helps to form the resultant inorganic oxide particles with smaller and more uniform particles size. The particle were formed with a fairly narrow size distribution and uniform shape could be observed. The primary particle size of sonochemically synthesized TiO_2, Ce–TiO_2 and Fe–TiO_2 nanoparticles was in the rage of 10–50 nm and the individual particles aggregated to form secondary particles of larger size. Further the particle size of pure TiO_2 (Fig. 6A) is large as compared to the doped TiO_2. The crystallite size decreased because of the doping, which implied that Fe, Ce doping restrained the increase in grain size and refined the crystallite size. Moreover the decrease in the particle size is due to an increase in the microstrain effect. The increase in the microstrain may be because of the metal introduction into the anatase lattice and the associated generation of oxygen vacancies [46]. Nahar et al. [24] used impregnation and calcination method for the preparation of Fe doped TiO_2 nanoparticles and reported that the particle size was in the range of 1–2 μm. In the present study, the particle size is found to be around 10–50 nm, which is significantly lower than that obtained in the work of Nahar et al. [24]. The observed trends can be attributed to the fast kinetics of the ultrasound assisted
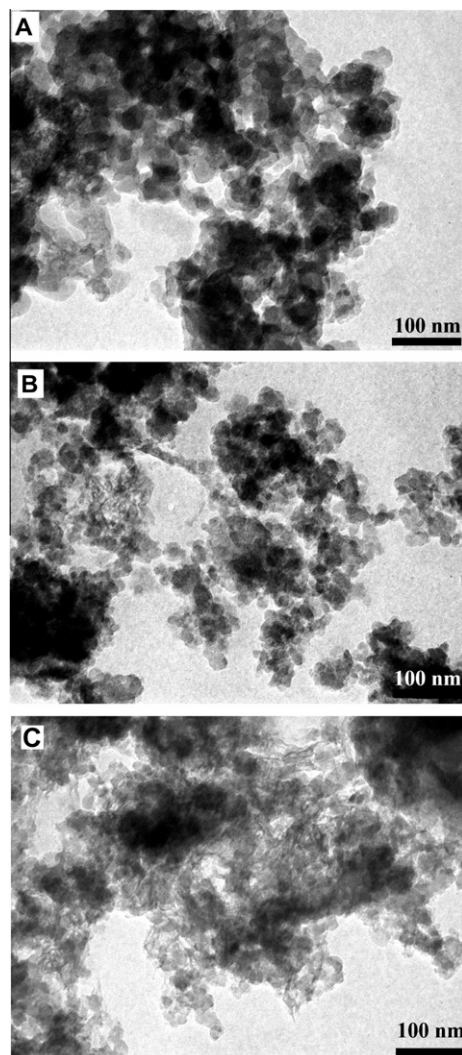
Fig. 6. TEM images of (A) pure TiO₂, (B) Fe doped TiO₂ and (C) Ce doped TiO₂ nanoparticles prepared by sonochemical method.

reaction providing insufficient time for particle nucleation and growth [47].

The particle size distribution of the samples prepared by sonochemical method and conventional method has been depicted in Fig. 7. All the samples prepared by sonochemical method showed smaller particle size whereas for the synthesis using conventional method, the size was found to be larger. The average particle size of undoped TiO_2 prepared by sonochemical method is found to be 197 nm whereas the average particle size of Fe and Ce doped TiO_2 for sonochemical method is observed to be 169 and 157 nm respectively. The average particle size of undoped TiO_2 prepared by conventional method was found to be 298 nm.

3.5. Photocatalytic activity of the catalysts for degradation of dye

The photocatalytic activity of the prepared samples was tested for the degradation of crystal violet dye. The effect of different operating parameters such as effect of preparation method, doping material content, catalyst loading and effect of initial dye concentration on the extent of degradation was investigated and has been discussed in the following sections.

3.5.1. Effect of preparation method and irradiation time

Fig. 8 shows the change in the absorption spectra of crystal violet dye with different irradiation times catalyzed by TiO_2. The aqueous solution of crystal violet dye (30 mg/L) shows a major absorption band at 590 nm. After achieving the equilibrium (soaking time under stirring), the change in the extent of degradation was observed with an increase in the UV irradiation time. With UV irradiation time increasing from 0 to 120 min, the absorption decreased gradually and the peak intensity at 590 nm also decreased. The initial peak intensity (after reaching the adsorption equilibrium) was found to be the maximum at 590 nm as expected. It was also observed that the extent of decrease in the absorption peak was lower at higher treatment times. This may be because of the formation of intermediates and their competitiveness with parent dye molecules in the photocatalytic degradation process. The slow kinetics of dye degradation after certain time limit can also be attributed to the difficulty in converting the N-atoms (N-demethylated products) of dye into oxidized nitrogen compounds [48]. Also, hydroxyl radicals .OH can attack different electron rich sites such as N–C bonds, phenyl rings and the central carbon atom of CV in non-effective way with increased treatment times [49]. To find out the maximum possible degradation, initially the experiments were conducted for 180 min and it was found that there was no appreciable degradation after 120 min irradiation. Hence all the experiments were carried at a constant treatment time as 120 min.

To study the effect of preparation method on the photocatalytic activity of the catalysts prepared by sonochemical and the conventional method, the experiments were conducted for 2% (mol%) of Ce and Fe doped TiO_2 and pure TiO_2. Fig. 9 shows the relative concentration (C/C_o) of dye with UV irradiation time (C_o is the concentration after achieving the adsorption equilibrium) for the initial dye concentration of 30 mg/L and the catalyst loading of 0.2 g/L. It is observed that the degradation of crystal violet increased gradually with UV irradiation time for all the samples. The highest degradation (84%) was achieved with Ce-TiO_2 (US) sample followed by Fe–TiO_2 (US) (77%) and undoped TiO_2 (US) sample gave 71% degradation. The samples prepared by conventional method resulted in 75, 68 and 61% degradation for Ce–TiO_2(CV), Fe–TiO_2(CV) and TiO_2(CV) respectively. Maximum extent of degradation for the Cerium doping can be attributed to the fact that cerium shows the enhanced photo-response in the visible region and the redox pair of cerium (Ce^{3+}/Ce^{4+}) is also important, since cerium could act as an effective electron scavenger to trap the bulk electrons in TiO_2 [13]. The preparation method played an important role in deciding the photoactivity of a catalyst. It was observed that the catalysts prepared by sonochemical method showed higher activity against catalyst prepared by the conventional method, possibly attributed to the higher surface area for the reaction due to the lower particle size of the catalyst achieved with the sonochemical method. The increased high-velocity interparticle collisions among the particles can result in the fragmentation of the TiO_2 particles leading to lower size in the case of sonochemical method. Also ultrasonic irradiation may accelerate the hydrolysis and formation of titania crystals. Further sonication method can evenly disperse the metal ions into the crystal lattice of TiO_2, independent of whether the ions react with Ti–gel or not [36]. This study clearly demonstrates the importance and advantages of sonication in the modification and improvement of the photocatalytic properties of TiO_2 and doped TiO_2 catalysts. After the first set of experiments, as it was observed that all the samples prepared by sonochemical method gives higher degradation than the samples prepared by conventional method, the studies related to the effect of other operating parameters on the degradation process were performed with the catalyst prepared by sonochemical method.
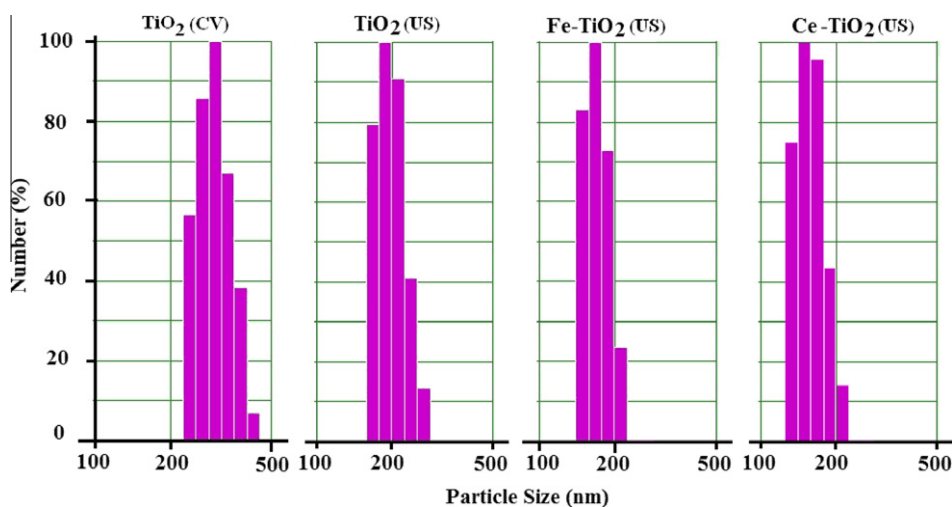
Fig. 7. Particle size distributions of Fe–TiO_2, Ce–TiO_2 and TiO_2 synthesized by sonochemical and conventional method.
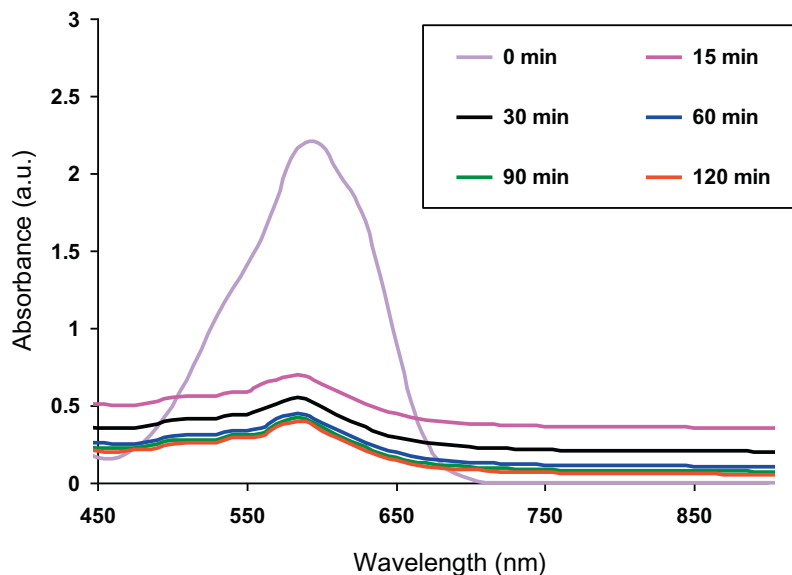
Fig. 8. Change in the absorbance spectra of crystal violet with irradiation time in presence of TiO₂ at dye concentration 30 mg/L.
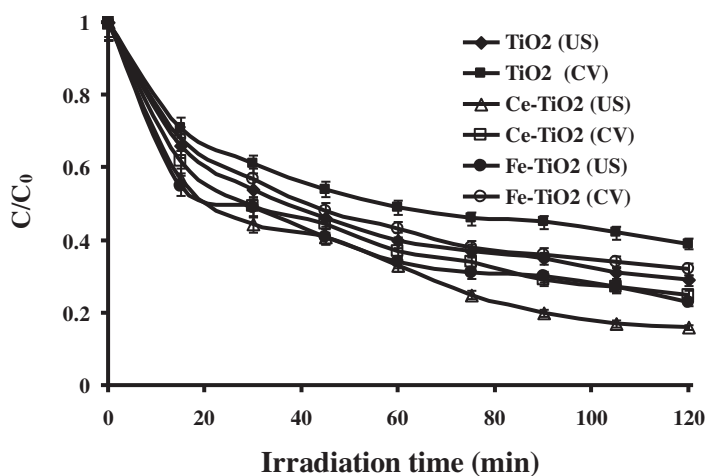
Fig. 9. Degradation vs. time decay curves of crystal violet during the photocatalytic experiments using different catalysts (dye initial concentration = 30 mg/L, pH 6.5 and catalyst dose = 0.2 g/L).

3.5.2. Effect of doping

Fig. 10 shows the variation in the relative concentration of crystal violet dye, C/C_o with UV irradiation time (C_o is the concentration after achieving the adsorption equilibrium) in the presence of cerium doping over the range of 0.4–2 mol%. It can be seen from the figure that the effectiveness of the catalyst strongly depends on the loading of Ce. The photoactivity of the catalyst increased by 10% when the content of cerium doping increased from 0.4 mol% to 0.8 mol%, however further increase resulted in a marginally decreased photoactivity of the catalyst. The observed result can be attributed to the fact that a small amount of cerium can act as a photo-generated electron trap and inhibit the hole–electron recombination [13,22]. On the other hand, the higher dopant content may become the recombination centers for the photo excited electrons, thus reducing the photocatalytic activity. Thus, an optimal dopant concentration is needed for the doping of TiO₂ and based on the present work, 0.8 mol% cerium doping was considered as the optimum doping concentration.

Fig. 11 shows the effect of iron doping concentration on the extent of degradation of crystal violet dye. As doping content of iron increased from 0.4 mol% to 1.2 mol%, the photoacivity of the catalyst increased but beyond 1.2 mol%, the activity decreased with an increase in the iron content. The observed results can be attributed to the fact that the introduction of small quantity of iron in TiO₂ is responsible for a reduction in the photo-generated hole–electron recombination rate. But at higher loadings, iron ions can serve as recombination centers and the activity steadily decreases as also demonstrated in some of the earlier investigations [2,6,24]. Thus, 1.2 mol% iron doping has been considered as the optimum doping concentration.

The high activities of the Fe and Ce doped TiO₂ powders could be attributed to the results of the synergetic effects of doping elements, small crystallite size and good crystallization during the synthesis. In both the cases, it is seen that an excess amount of dopant at the surface of TiO₂ could notably screen the TiO₂ from the UV light and inhibit the interfacial electron and hole to transfer resulting in a low photoactivity. It is observed that the photocatalytic activity of Ce doped TiO₂ is higher than that of Fe doped TiO₂. This may be because when Ce is located in an interstitial site of TiO₂, the electron density of the doped TiO₂ may increase, which
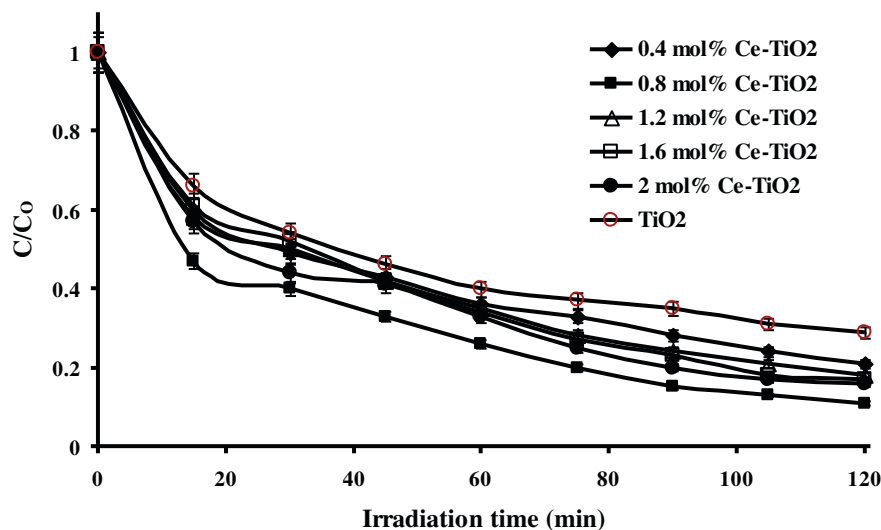
Fig. 10. Effect of cerium doping content on degradation of crystal violet dye (dye initial concentration = 30 mg/L, pH 6.5 and catalyst dose = 0.2 g/L).
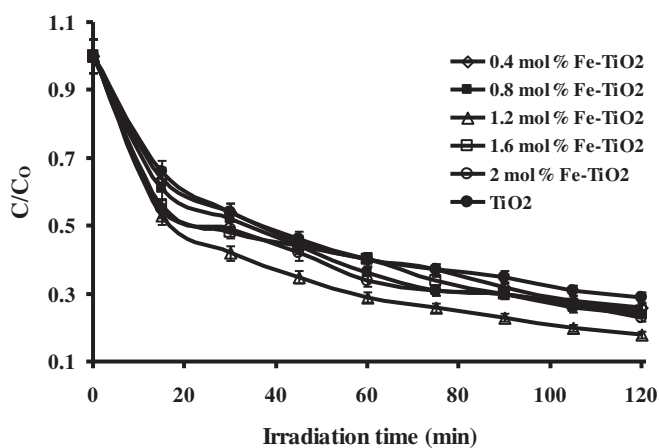
Fig. 11. Effect of iron doping content on degradation of crystal violet dye (dye initial concentration = 30 mg/L, pH 6.5 and catalyst dose = 0.2 g/L).

would increase the photocatalytic activity; while when Fe ions are located in a substitutional site of TiO$_2$, the electron density of the doped TiO$_2$ may have decreased and though TiO$_2$ is an n type semiconductor it may have changed into a p type semiconductor, resulting in decreased photocatalytic activity. The existence of Ce^{4+}, Fe^{3+} in the TiO$_2$ matrix decreases the photocurrent. According to the doping principle, the introduction of Ce^{4+}, Fe^{3+} into the matrix of TiO$_2$ will produce p-type micro regions [47,50], which results into change from n-type to p-type semiconductor. However, Ce 4f level in Ce–TiO$_2$ plays an important role in interfacial charge transfer than Fe 3f level in Fe–TiO$_2$ [22]. Kim et al. [51] reported that TiO$_2$ sample prepared by ultrasound method showed a change in surface area due to reduction in aggregation which is major change in the physical properties. Overall it can be said that the photocatalytic activity of Fe doped TiO$_2$ is lower than that of the Ce doped TiO$_2$ and the amount of doping of Fe required is also larger. Similar results are reported by Li et al. [8] for Be, Mg and Ca doped TiO$_2$ for photocatalytic production of hydrogen. Another reason for the difference in activities of Ce–TiO$_2$ and Fe–TiO$_2$ is that the cationic dye such as crystal violet has different charge in aqueous solution after ionization; so the electrostatic attraction or repulsion occur between the organic dye ions and the surface of catalysts, which may also result in the difference in degradation rates [23].

3.5.3. Effect of catalyst loading

To investigate the effect of catalyst loading on the degradation rate of crystal violet, experiments were conducted for three different catalyst loadings as 0.1, 0.2 and 0.3 g/L, at initial dye concentration of 30 mg/L and at pH 6.5. The obtained results have been given in Fig. 12. It can be seen from the figure that the extent of degradation increased significantly with an increase in the catalyst dosage up to a concentration of 0.2 g/L. For 0.8 mol% Ce–TiO$_2$ sample, 89% degradation was achieved with 0.2 g/L and maximum extent of degradation was observed to be equal to 92% at the catalyst dosage of 0.3 g/L. It was observed that there was no major difference in the degradation efficiencies for 0.2 and 0.3 g/L catalyst loadings; however 0.1 g/L catalyst loading resulted in almost 10% lesser degradation than 0.2 g/L. Similar trend was observed with Fe–TiO$_2$ and pure TiO$_2$ samples. The photodecomposition rates of pollutants are influenced by the active sites and the photoabsorption of the catalyst used in the study. Adequate loading of the catalyst can increase the generation rate of electron/hole pairs for enhancing the degradation of pollutants. At higher loadings, the catalysts may block the light irradiation, and restrain the effective usage of light for photo excitation [7,12,30]. Thus, the results indicate that an optimal dose of 0.2 g/L of the catalysts was most effective to achieve the best degradation results.
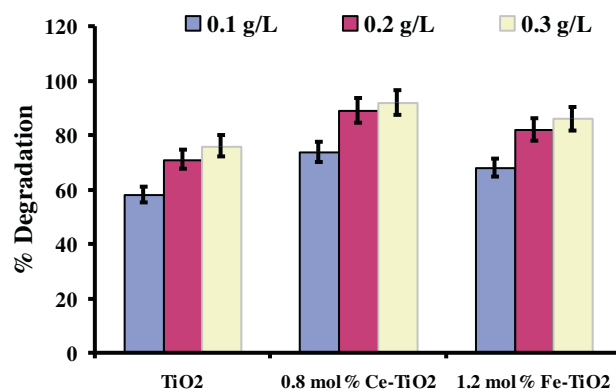
Fig. 12. Effect of catalyst loading on the crystal violet degradation (Dye initial concentration = 30 mg/L, pH 6.5).
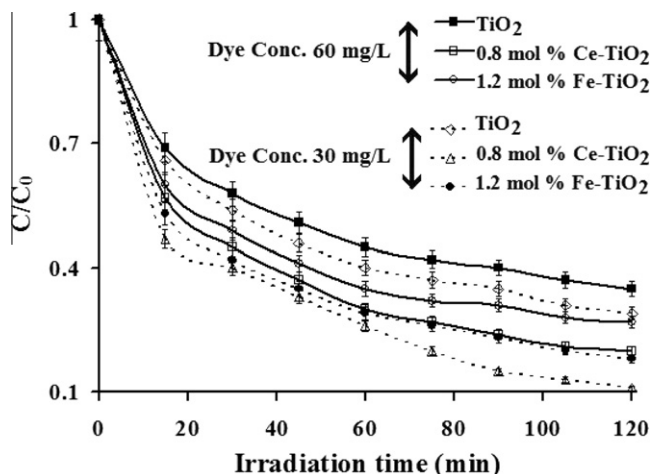
Fig. 13. Effect of initial concentration of crystal violet dye (pH 6.5 and catalyst dose = 0.2 g/L).

Fig. 14. Reaction kinetics for photocatalytic degradation of crystal violet (dye initial concentration = 30 mg/L, pH 6.5 and catalyst dose = 0.2 g/L).

Table 1
Rate constants for first order kinetics.

Catalyst	Rate constant (min^{-1})	R^2 values
Pure TiO_2	0.007	0.962
1.2 mol% Fe–TiO_2	0.010	0.983
0.8 mol% Ce–TiO_2	0.014	0.990

3.5.4. Effect of initial dye concentration

Fig. 13 illustrates the variation in the relative concentration, C/C_o with irradiation time (C_o is the concentration after achieving the adsorption equilibrium) for two initial concentrations of crystal violet dye as 30 and 60 mg/L. The experiments have been conducted at pH of 6.5 and catalyst loading of 0.2 g/L. It can be seen from the figure that the higher the value of initial concentration, lower is the observed degradation rate. This negative effect may be because of the following reasons (i) when the dye concentration increases the amount of dye adsorbed on the catalyst surface increases. The increase in dye concentration will decrease the path length of photons entering the dye solution. In addition to this, at a high dye concentration, a significant amount of UV light may be absorbed by the dye molecules rather than by the catalyst particles and that reduces the efficiency of the catalytic reaction, (ii) the rate of degradation is dependent on the probability of OH**.** radicals formation on the catalyst surface and the probability of OH**.** radicals reacting with dye molecules. But at high dye concentrations the generation of OH**.** radicals on the surface of catalyst is likely to be reduced since active sites are covered by dye ions. Thus the limitation of surface sites for the reaction may control the final extent of dye degradation, (iii) the reduction in the degradation of dye can also be attributed to the filter effect caused by absorption of photon energy by the dye molecules, (iv) the relatively longer chain of crystal violet cannot completely enter the electron-hole, and thus reduces the degradation rate.

The results clearly demonstrated that the photocatalytic oxidation process is promising at low concentrations of the pollutant. This is also true for heterogeneous catalytic systems where the reaction occurs at the interface between two phases. [2,7,12]

3.5.5. Kinetics of the degradation

Kinetics of photocatalytic degradation of crystal violet has also been investigated. The pseudo-first order reaction kinetics can be represented by the following equation

$$-\ln\left(\frac{C}{C_0}\right) = kt \qquad (1)$$

where C is the final concentration (mg/L) of crystal violet after irradiation, C_0 is the initial concentration (mg/L) of crystal violet (after reaching the adsorption equilibrium but prior to irradiation), t is the irradiation time (min) and k is the apparent reaction rate constant (min^{-1}). The kinetic studies have been performed for the sonochemically prepared catalysts with the optimum doping content

for cerium and iron as 0.8 and 1.2 mol% respectively and also comparison has been done with the sonochemically synthesized pure TiO_2. Fig. 14 gives the first-order reaction kinetics for photocatalytic degradation of crystal violet dye for the three catalyst samples. The obtained rate constants have been reported in Table 1. It can be seen that the rate constant for 0.8 mol% Ce–TiO_2 sample was twice as compared to that of pure TiO_2 and for 1.2 mol% Fe–TiO_2 it was 0.010 min^{-1}, which is about 45% more as compared to the pure TiO_2. The results have clearly established the better efficacy of the doped photocatalyst as compared to the pure form of TiO_2.

4. Conclusions

Nano-sized Fe, Ce-doped and undoped TiO_2 particles were synthesized by sonochemical and conventional methods using titanium isopropoxide as a starting material. Catalysts prepared by sonochemical method exhibited higher photocatalytic activity as compared to the catalysts prepared by conventional method. The presence of Fe and Ce in the TiO_2 structure caused a significant absorption shift towards the visible region. An optimum quantity of dopant obtained was 0.8 mol% Ce–TiO_2 and 1.2 mol% Fe–TiO_2 where maximum photoactivity could be observed. Also, an optimal dosage of 0.2 g/L of the photocatalyst was observed whereas lower initial concentration of the dye was favorable for giving higher extents of degradation. The photocatalytic degradation followed first-order kinetics and overall it can be said that crystal violet dye was effectively degraded (more than 85% degradation) within 120 min of UV irradiation.

References

[1] R. Chand, E. Obuchi, K. Katoh, H.N. Luitel, K. Nakano, Enhanced photocatalytic activity of TiO2/SiO2 by the influence of Cu-doping under reducing calcination atmosphere, Catal. Commun. 13 (2011) 49–53.

[2] M. Asiltürk, F. Sayılkan, E. Arpac, Effect of Fe^{3+} ion doping to TiO2 on the photocatalytic degradation of Malachite Green dye under UV and vis-irradiation, J. Photochem. Photobiol. A: Chem. 203 (2009) 64–71.

[3] M. Asilturk, F. Sayılkan, S. Erdemoglu, M. Akarsu, H. Sayılkan, M. Erdemoglu, E. Arpac, Characterization of the hydrothermally synthesized nano- TiO2 crystallite and the photocatalytic degradation of Rhodamine B, J. Hazard. Mater. B129 (2006) 164–170.

[4] S. Rengaraj, X.Z. Li, Enhanced photocatalytic activity of TiO2 by doping with Ag for degradation of 2, 4, 6-trichlorophenol in aqueous suspension, J. Mol. Catal. A: Chem. 243 (2006) 60–67.

[5] F. Wang, K. Zhang, Reduced graphene oxide- TiO2 nanocomposite with high photocatalytic activity for degradation of rhodamine B, J. Mol. Catal. A: Chem. 345 (2010) 101–107.

[6] M. Zhou, J. Yu, B. Cheng, Effects of Fe-doping on the photocatalytic activity of mesoporous TiO2 powders prepared by an ultrasonic method, J. Hazard. Mater. B137 (2006) 1838–1847.

[7] H. Wang, J. Niu, X. Long, Y. He, Sonophotocatalytic degradation of methyl orange by nano-sized Ag/ TiO2 particles in aqueous solutions, Ultrason. Sonochem. 15 (2008) 386–392.

[8] Y. Li, S. Peng, F. Jiang, G. Lu, S. Li, Effect of doping TiO2 with alkaline-earth metal ions on its photocatalytic activity, J. Serb. Chem. Soc. 72 (2007) 393–402.

[9] U.G. Akpan, B.H. Hameed, Enhancement of the photocatalytic activity of TiO2 by doping it with calcium ions, J. Colloid Interface Sci. 357 (2011) 168–178.

[10] H.K. Shon, S. Vigneswaran, J. Kandasamy, M.H. Zareie, J.B. Kim, D.L. Cho, J.H. Kim, Preparation and characterization of titanium dioxide (TiO2) from sludge produced by TiCl4 flocculation with FeCl3, Al2(SO4)3 and Ca(OH)2 coagulant aids in wastewater, Sep. Sci. Technol. 44 (2009) 1525–1543.

[11] Y.H. Peng, G.F. Huang, W.Q. Huang, Visible-light absorption and photocatalytic activity of Cr-doped TiO2 nanocrystal films, Adv. Powder Technol. 23 (2010) 8–12.

[12] M.A. Barakat, H. Schaeffer, G. Hayes, S. Ismat-Shaha, Photocatalytic degradation of 2-chlorophenol by Co-doped TiO2 nanoparticles, App. Catal. B: Environ. 57 (2004) 23–30.

[13] A.M.T. Silva, C.G. Silva, G. Drazić, J.L. Faria, Ce-doped TiO2 for photocatalytic degradation of chlorophenol, Catal. Today 144 (2009) 13–18.

[14] M.A. Rauf, M.A. Meetani, S. Hisaindee, An overview on the photocatalytic degradation of azo dyes in the presence of TiO2 doped with selective transition metals, Desalination 276 (2011) 13–27.

[15] S. Anandan, M. Ashokkumar, Sonochemical synthesis of Au–TiO2 nanoparticles for the sonophotocatalytic degradation of organic pollutants in aqueous environment, Ultrason. Sonochem. 16 (2009) 316–320.

[16] K. Kocí, K. Mateju, L. Obalová, S. Krejčíková, Z. Lacný, D. Plachá, L. Capek, A. Hospodková, O. Solcov, Effect of silver doping on the TiO2 for photocatalytic reduction of CO2, App. Catal. B: Environ. 96 (2010).

[17] Y. Li, C. Xie, S. Peng, G. Lu, S. Li, Eosin Y-sensitized nitrogen-doped TiO2 for efficient visible light photocatalytic hydrogen evolution, J. Mol. Catal. A: Chem. 282 (2008) 117–123.

[18] H.K. Shon, D.L. Cho, S.H. Na, J.B. Kim, H.J. Park, J.H. Kim, Development of a novel method to prepare Fe- and Al-doped TiO2 from wastewater, J. Ind. Eng. Chem. 15 (2009) 476–482.

[19] S. Chang, W. Liu, Surface doping is more beneficial than bulk doping to the photocatalytic activity of vanadium-doped TiO2, App. Catal. B: Environ. 101 (2011) 333–342.

[20] N. Venkatachalam, M. Palanichamy, B. Arabindoo, V. Murugesan, Enhanced photocatalytic degradation of 4-chlorophenol by Zr^{4+} doped nano TiO2, J. Mol. Catal. A: Chem. 266 (2007) 158–165.

[21] A. Zaleska, Doped- TiO2: a review, Recent Patents on Engineering 2 (2008) 157–164.

[22] Z.L. Shi, C. Du, S.H. Yao, Preparation and photocatalytic activity of cerium doped anatase titanium dioxide coated magnetite composite, J. Taiwan Inst. Chem. Eng. 42 (2011) 652–657.

[23] J. Wang, Y. Lv, L. Zhang, B. Liu, R. Jiang, G. Han, R. Xu, X. Zhang, Sonocatalytic degradation of organic dyes and comparison of catalytic activities of CeO2/TiO2, SnO2/TiO2 and ZrO2/ TiO2 composites under ultrasonic irradiation, Ultrason. Sonochem. 17 (2010) 642–648.

[24] M.S. Nahar, K. Hasegawa, S. Kagaya, S. Kuroda, Comparative assessment of the efficiency of Fe-doped TiO2 prepared by two doping methods and photocatalytic degradation of phenol in domestic water suspensions, Sci. Technol. Adv. Mater. 8 (2007) 286–291.

[25] T.K. Ghorai, S.K. Biswas, P. Pramanik, Photooxidation of different organic dyes (RB, MO, TB, and BG) using Fe (III)-doped TiO2 nanophotocatalyst prepared by novel chemical method, Appl. Surf. Sci. 254 (2008) 7498–7504.

[26] N.D. Abazovic, L. Mirenghi, I.A. Jankovic, N. Bibic, D.V. Sojic, B.F. Abramovic, M.I. Comor, Synthesis and characterization of rutile TiO2 nanopowders doped with iron ions, Nanoscale Res. Lett. 4 (2009) 518–525.

[27] C.L. Luu, Q.T. Nguyen, S.T. Ho, Synthesis and characterization of Fe-doped TiO2 photocatalyst by the sol–gel method, Adv. Nat. Sci. Nanosci.: Nanotechnol. 1 (2010) 01–05.

[28] Q.H. Zhang, W.D. Han, Y.J. Hong, J.G. Yu, Photocatalytic reduction of CO2 with H2O on Pt-loaded TiO2 catalyst, Catal. Today 148 (2009) 335–340.

[29] X. Li, R. Xiong, G. Wei, Preparation and photocatalytic activity of nanoglued Sn-doped TiO2, J. Hazard. Mater. 164 (2009) 587–591.

[30] F.I. Kiriakidou, D.I. Kondarides, X.E. Verykios, The effect of operational parameters and TiO2-doping on the photocatalytic degradation of azo-dyes, Catal. Today 54 (1999) 119–130.

[31] S. Liu, X. Chen, A visible light response TiO2 photocatalyst realized by cationic S-doping and its application for phenol degradation, J. Hazard. Mater. 152 (2008) 48–55.

[32] B.N. Narayanan, Z. Yaakob, R. Koodathil, S. Chandralayam, S. Sugunan, F.K. Saidu, V. Malayattil, Photodegradation of methylorange over zirconia doped TiO2 using solar energy, Eur. J. Sci. Res. 28 (2009) 566–571.

[33] X.K. Wang, C. Wang, W.L. Guo, Sonochemical synthesis of nitrogen doped TiO2 at a low temperature, Adv. Mater. Res. 356 (2012) 403–406.

[34] J. Yu, M. Zhou, B. Cheng, H. Yu, X. Zhao, Ultrasonic preparation of mesoporous titanium dioxide nanocrystalline photocatalysts and evaluation of photocatalytic activity, J. Mol. Catal. A: Chem. 227 (2005) 75–80.

[35] X. Chen, S.S. Mao, Titanium dioxide nanomaterials: synthesis, properties, modifications, and applications, Chem. Rev. 107 (2007) 2891–2959.

[36] W. Huang, X. Tang, Y. Wang, Y. Koltypin, A. Gedanken, Selective synthesis of anatase and rutile via ultrasound irradiation, Chem. Commun. 15 (2000) 1415–1416.

[37] J.C. Yu, J. Yu, W. Ho, L. Zhang, Preparation of highly photocatalytic active nano-sized TiO2 particles via ultrasonic irradiation, Chem. Commun. 19 (2001) 1942–1943.

[38] H. Li, G. Liu, S. Chen, Q. Liu, Novel Fe doped mesoporousTiO2 microspheres: Ultrasonic–hydrothermal synthesis, characterization, and photocatalytic properties, Physica E 42 (2010) 1844–1849.

[39] B. Neppolian, Q. Wang, H. Jung, H. Choi, Ultrasonic-assisted sol-gel method of preparation of TiO2 nano-particles: characterization, properties and 4-chlorophenol removal application, Ultrason. Sonochem. 15 (2008) 649–658.

[40] Y. Zhu, H. Li, Y. Koltypin, Y.R. Hacohen, A. Gedanken, Sonochemical synthesis of titania whiskers and nanotubes, Chem. Commun. 24 (2001) 2616–2617.

[41] W. Huang, X. Tang, I. Felner, Y. Koltypin, A. Gedanken, Preparation and characterization of FexOy-TiO2 via sonochemical synthesis, Mater. Res. Bull. 37 (2002) 1721–1735.

[42] Y. Xie, C. Yuan, Visible-light responsive cerium ion modified titania sol and nanocrystallites for X-3B dye photodegradation, Appl. Catal. B: Environ. 46 (2003) 251–259.

[43] S. Liu, X. Chen, Preparation of N-doped visible-light response nanosize TiO2 photocatalyst using the acid-catalyzed hydrolysis method, Chin. J. Catal. 27 (2006) 697–702.

[44] Z. Shi, H. Lai, S. Yao, S. Wang, Photocatalytic Activity of Fe and Ce Co-doped Mesoporous TiO2 Catalyst under UV and Visible Light, J. Chin. Chem. Soc. 59 (2012) 1–8.

[45] J.C.S. Wu, C.H. Chen, A visible-light response vanadium-doped titania nanocatalyst by sol–gel method, J. Photochem. Photobiol. A Chem 163 (2004) 509–515.

[46] M. Popa, E. Indrea, P. Pascuta, V. Cosoveanu, I.C. Popescu, V. Danciu, Fe, Ce, and Cu influence on morpho-structural and photoctalytic properties of TiO2 aerogels, Rev. Roum. Chim. 55 (2010) 369–375.

[47] D.V. Pinjari, A.B. Pandit, Room temperature synthesis of crystalline CeO2 nanopowder: advantage of sonochemical method over conventional method, Ultrason. Sonochem. 18 (2011) 1118–1123.

[48] J. Bandara, V. Nadtochenko, J. Kiwi, C. Pulgarin, Dynamics of oxidant addition as an important parameter in the modelization of dye mineralization (orange II) via advanced oxidation technologies, Water Sci. Technol. 35 (1997) 87–93.

[49] E.G. Janzen, Y. Kotake, R.D. Hinton, Stabilities of the hydroxyl radicals spin adducts of PBN-type spin traps, Free Radical Biol. Med. 12 (1992) 169–173.

[50] P. Yang, C. Lu, N. Hua, Y. Du, Titanium dioxide nanoparticles co-doped with Fe^{3+} and Eu^{3+} ions for photocatalysis, Mater. Lett. 57 (2002) 794–801.

[51] S.Y. Kim, T.S. Chang, C.H. Shin, Enhancing effects of ultrasound treatment on the preparation of TiO2 Photocatalysts, Catal. Lett. 118 (2007) 224–230.

Removal of Brilliant Green from wastewater using conventional and ultrasonically prepared poly(acrylic acid) hydrogel loaded with kaolin clay: A comparative study

Sachin R. Shirsath [a], Anup P. Patil [a], Rohit Patil [d], Jitendra B. Naik [d], Parag R. Gogate [c], Shirish H. Sonawane [b,*]

[a] Department of Chemical Engineering, Sinhgad College of Engineering, Vadgaon (BK), Pune 411041, India
[b] Department of Chemical Engineering, National Institute of Technology, Warangal, AP 506004, India
[c] Chemical Engineering Department, Institute of Chemical Technology, Matunga, Mumbai, India
[d] Chemical Technology Department, North Maharashtra University, Jalgaon, India

ARTICLE INFO

ABSTRACT

The present work deals with the removal of Brilliant Green dye from wastewater using a poly(acrylic acid) hydrogel composite (PAA-K hydrogel) prepared by incorporation of kaoline clay. The composite has been synthesized using ultrasound assisted polymerization process as well as the conventional process, with an objective of showing the better effectiveness of ultrasound assisted synthesis. It has been observed that the hydrogel prepared by ultrasound assisted polymerization process showed better results. The optimum conditions for the removal of dye are pH of 7, temperature of 35 °C, initial dye concentration of 30 mg/L and hydrogel loading of 1 g. The extent of removal of dye increased with an increase in the contact time and initial dye concentration. A pseudo-second-order kinetic model has been developed to explain the adsorption kinetics of dye on the PAA-K hydrogel. Thermodynamic and kinetic parameters indicate that the adsorption process is spontaneous in nature and the PAA-K hydrogel prepared by ultrasound process is a promising adsorbent compared to conventional process. The obtained adsorption data has also been fitted into commonly used adsorption isotherms and it has been found that Freundlich as well as Langmuir adsorption isotherm models fits well to the experimental results.

© 2012 Elsevier B.V. All rights reserved.

1. Introduction

Effluent streams generated by different industries such as textile, tannery, food, printing, pulp and paper, etc. contain dyes as one of the most commonly observed component imparting obnoxious color to the effluent streams [1–3]. Discharge of effluent streams containing dyes into the natural streams is harmful to the aquatic life and also in long run to the human beings. Removal of dyes from wastewaters is a complex problem because of the significant difficulty in treating the dye containing wastewaters using the conventional treatment schemes. In the past, various attempts have been made to develop effective treatment technologies for dye bearing wastewaters, but no single solution has been found to be satisfactory [4]. Different physicochemical processes like adsorption, electro-kinetic coagulation, ion-exchange, membrane filtration, electrochemical oxidation, and photo-catalytic degradation processes have been attempted in treating these wastewaters [5–10]. Each technique has its own limitations such as generation of secondary effluent, hazardous intermediate products and slow rates of degradation. Thus, it is need of time to research into cleaner techniques for the effective removal of dyes from the effluent stream. The present work deals with adsorption of dyes on hydrogel synthesized using ultrasonic irradiations and by conventional technique as adsorption using hydrogel is one of the important approaches for the effective removal of dyes. Hydrogel are superior as compared to other adsorbents due to their characteristic properties such as adsorption–regeneration, economic feasibility and environmental friendly behavior, and hence lot of research is done on the use of hydrogels in pollution control studies. The hydrogels are made of porous structure networks and allow solute diffusion through their structure. They possess ionic functional groups which can be helpful for trapping ionic dyes. The model dye selected in the work is Brilliant Green, which is a odorless cationic dye used for various purposes, e.g. biological stain, dermatological agent, veterinary medicine, and an additive to poultry feed to inhibit propagation of mold, intestinal parasites and fungus [11]. It is also extensively used in textile dying and paper printing. Brilliant Green causes several effects on human beings including irritation to the gastrointestinal tract, nausea and vomiting, irritation to the respiratory tract and irritation to skin [12]. Brilliant Green

* Corresponding author. Tel.: +91 870 2462626.
E-mail address: shirishsonawane09@gmail.com (S.H. Sonawane).

may form hazardous products like nitrogen oxides, and sulfur dioxides due to decomposition on heating [13].

In the past some studies for the removal of dye have been based on the use of hydrogel, a class of cross-linked polymeric materials, which have played an important role in the treatment of wastewater for the removal of different water pollutants like dyes [14–16], phenolic compounds [17], heavy metals [18], ammonia [19], boron [20,21], etc. In addition, hydrogel are extensively used in many fields, such as molecular filters, super absorbents, and contact lenses [22–26]. Mechanical stability of hydrogel is an important issue for their effective use in wastewater treatment. Recently, some attempts have been made to modify the mechanical properties like elasticity and permeability of the gels to adsorb different substances by the incorporation of the clays or inorganic materials, such as montmorillonite, kaolin, mica, bentonite into the polymer networks [27–30]. Many hydrogel composites such as polyacrylamide with bentonites or montmorillonites, polyacrylic acid or poly(N-isopropyacrylamide) with different clays have been synthesized and studied in terms of mechanical properties and swelling behavior [27–32]. Clays as compared to the other adsorbents are natural, abundantly available and inexpensive minerals that have unique structure and high mechanical strength. Clay minerals are good adsorbents for removing contaminants from textile and dye industry wastewater [20,33–37].

Ultrasonic irradiation has been used for intensification/improvement of different physical and chemical processing applications and one of the applications has been in the polymer synthesis through the generation of free radicals and activation of free radical initiators. Ultrasound has been found to be an effective method for the polymerization of monomers and production of hydrogel in the absence of a chemical initiator [38]. Due to the cavitation effects such as formation of micro-jets and turbulence, which are higher in the case of heterogeneous systems [39], uniform particle size distribution of the composite can be obtained. Similarly uniform dispersion of clay into the polymer matrix can be effectively achieved. Further, clay acts as a cross-linking agent and uniform cross-linking can be achieved due to the cavitation effects. During the adsorption studies when the hydrogel is immersed in water for adsorbing the dye molecules from the wastewater, hydrophilic polymer chains of the hydrogel does not dissolve into the aqueous phase because of the uniform cross-linking. The degree of cross-linking in the polymer network structure is critical as it dictates the mechanical strength, swelling ratio, and many other properties of the polymer gel by influencing the molecular weight between cross-links [40].

In the present work, poly(acrylic acid) hydrogel loaded with the Kaolin clay was synthesized using ultrasound induced polymerization and conventional process and the feasibility of these hydrogels for the removal of Brilliant Green (BG) dye has been investigated. The adsorption equilibrium studies were carried out and the effect of various parameters such as pH, temperature, initial dye concentration, quantity of hydrogel and clay loading on the extent of removal of dye has been investigated.

2. Experimental methodology

2.1. Materials

Acrylic acid (AA), ammonium persulfate (APS), sodium dodecyl sulfate (SDS) and Brilliant Green dye (BG) were of analytical grade and procured from M/s CDH, India. Kaolin (China clay) clay was obtained from MD Chemicals Pune, India and used without any further purification. Deionized water was used for dilution in all the experiments.

2.2. Synthesis of poly(acrylic acid)-Kaolin (PAA-K) hydrogel using insitu ultrasound assisted emulsion polymerization and conventional process

PAA-K hydrogel has been synthesized from acrylic acid (monomer), APS (initiator), and SDS (surfactant). Initially, the reactor was flushed using argon to maintain inert atmosphere. In the actual synthesis process, 36 g of acrylic acid with 100 mL water was loaded into the ultrasound polymerization reactor. In other beaker, SDS–kaolin solution was prepared using 0.5 g of SDS and 0.36 g kaolin in 20 mL water (corresponding to 1.0% (wt.%) of acrylic acid). The mixture was then homogeneously mixed using ultrasound bath and added into a polymerization reactor. Then the solution was irradiated for 5 min using ultrasonic horn (Dakshin make, 22 mm probe diameter) operating at 22.5 kHz frequency and rated power of 120 W. The total acoustic power dissipated into the sample was calculated using calorimetric method. The total power dissipated into polymerization reactor was 12.5 W. The objective of using the ultrasonic irradiation was to form uniform small size emulsion droplets which will remain stable and hence, will give uniform final polymer particle size. APS solution was prepared by mixing 0.1 g of APS in 10 mL water and it was added into the reactor as initiator. Reactor temperature was maintained at 60 °C for 30 min. Argon gas was used for blanketing of the polymerization reactor to avoid the contact with atmosphere. The presence of ultrasonic environment in the polymerization reactor assisted the uniform distribution of kaolin platelets through hydrogel network. Another hydrogel containing 2% (wt.%) kaolin was also prepared to study the effect of kaolin loading. Fig. 1a shows the experimental setup for the synthesis of hydrogel by ultrasound assisted method and Fig. 1b shows the schematic representation of the process of the formation of PAA-K hydrogel. Similar procedure was used for conventional synthesis in which the temperature of the polymerization reactor was maintained at 60 °C and the reaction was carried out for 60 min under mechanical stirring instead of using ultrasound probe. In both the preparation methods, the formation of thick solution was initially observed which then transformed into a sticky suspension. However during the ultrasonic synthesis less time was required for the formation of the gel. The reduction in time compared to conventional synthesis is due to the cavitational effect. Further, the rapid micromixing and implosive collapse of bubbles in a liquid solution could have resulted in extremely high temperature which accelerated the reaction.

2.3. Water uptake of hydrogel

To confirm the swelling behavior of synthesized hydrogel, 1 g of PAA-K hydrogel was allowed to swell in 100 mL of deionized water at 30 °C for 3 h. At predetermined time intervals, the hydrogel was taken, wiped with filter paper to remove excess water and was weighed to find the water content [16]. The swelling ratio, S, was calculated using Eq. (1).

$$S = \frac{W_s - W_d}{W_d} \tag{1}$$

where W_s and W_d are the swollen and dry weights of the hydrogel respectively.

2.4. Adsorption of BG dye

The adsorption experiments were carried out in a batch mode to study the effect of different parameters like pH, temperature, initial dye concentration, quantity of hydrogel and clay content on the extent of adsorption. PAA-K hydrogel (1 g) was added to
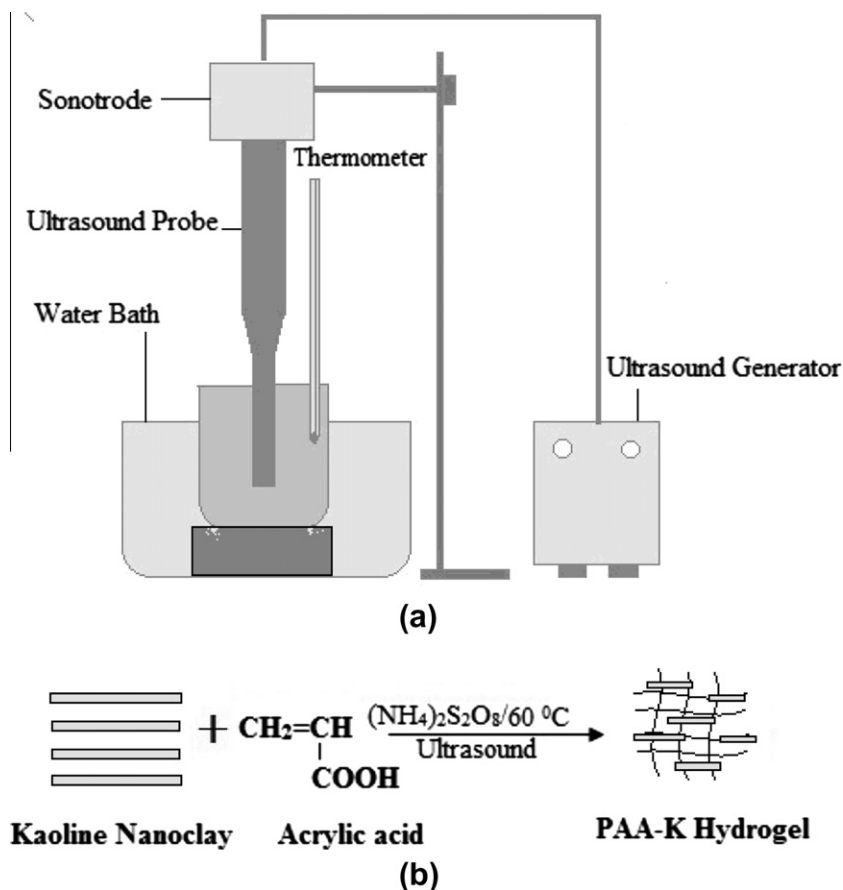
Fig. 1. (a) Experimental set up for synthesis of hydrogel by ultrasound assisted method, (b) schematic representation of the formation of hydrogel.

100 mL of aqueous dye solution of known concentration and pH of the solution was adjusted using buffer solution. The effect of initial BG dye concentration was investigated over the concentration range of 10–50 mg/L. The effect of hydrogel loading was investigated using different quantities of PAA-K hydrogel over the range 0.5–2 g. Temperature was maintained constant throughout the duration of experiments using water bath. The percentage dye removal has been calculated using the following equation:

$$\text{Percentage removal} = (C_0 - C_e)/C_0 \times 100 \qquad (2)$$

where, C_o and C_e are the initial and equilibrium concentrations of BG dye (mg/L).

Amount of dye adsorbed per unit mass of hydrogel (mg/g) has been determined using following equation.

$$q_t = (C_0 - C_t)V/M \qquad (3)$$

where V is volume of the dye solution in L and M is the mass of dry hydrogel in g, t refers to the time of treatment.

2.5. Analysis and characterization

The concentration of Brillient Green (BG) dye was measured using UV–vis spectrophotometer (SHIMADZU 160A model). The wavelength of maximum absorbance (λ_{max}) of BG dye was found to be 624 nm. Deionized water was used as a reference. FTIR Spectra of the hydrogel samples were recorded on Perkin Elmer FTIR spectrometer (Paragon 1000 PC) in the wave number range of 500–4000 cm^{-1} with resolution of 1 cm^{-1}. FTIR of the sample was taken after partially drying the hydrogel in an oven at 60 °C

for 180 min. Transmission electron microscopy (TEM, magnification 750,000×) image was taken on a Philips Tecnai 20 model.

3. Results and discussion

3.1. Morphology of poly(acrylic acid) and nanocomposite hydrogel

With an objective of investigating the efficacy of dispersion of kaolin clay in the PAA hydrogel matrix, transmission electron microscope (TEM) images of the dried PAA-K hydrogel (0.36 g clay) prepared by conventional as well as ultrasound method have been obtained and shown in Fig. 2. Fig. 2a shows the TEM image of poly(acrylic acid). Hydrogel with kaolin prepared by conventional method whereas Fig. 2b gives the image for the ultrasonically prepared hydrogel. The presence of dark-spots in both the figures confirms the occurrence of kaolin clay in the hydrogel matrix however it can be observed in the case of Fig. 2a that the kaolin particles are not uniformly distributed through the hydrogel matrix and aggregation of kaolin particles can be seen at different locations. In contrast, it can be clearly established from the depicted image for the ultrasound assisted synthesis (Fig. 2b) that the clay platelets are substantially exfoliated and dispersed homogeneously throughout the polymer matrix. Thus, fine and homogeneous clay dispersion was achieved in the hydrogel matrix due to the presence of ultrasound. The complete exfoliation of clay platelets and insertion of poly(acrylic acid) chains into the gallery spacing of clay is due to the shear and turbulence effects of the cavitation phenomena occurring during the emulsion polymerization. The particle size of kaolin clay was measured from the TEM images, where the black
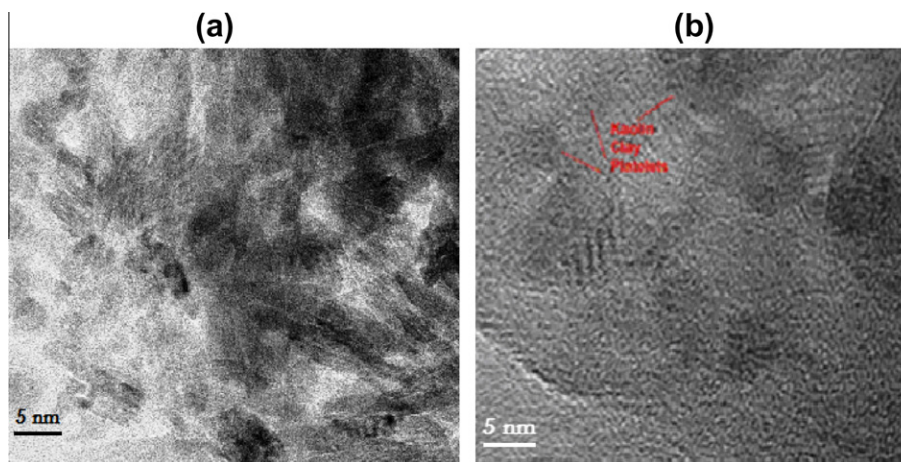
Fig. 2. Transmission electron microscopic images of PAA-K nanocomposite hydrogel (a) conventional method, (b) ultrasound assisted method.

spots in Fig. 2b indicates the presence of clay. The particle size of the kaolin clay was found to be in the range of 20–50 nm.

3.2. Swelling behavior of PAA-K hydrogel

In recent years, considerable efforts have been made to understand the mechanism of water diffusion through hydrogel matrices [20,32,33]. The time dependent swelling behavior of hydrogels has been described by a power-law function [32,33] as shown in Eq. (4).

$$F = M_t/M_s = Kt^n \tag{4}$$

where, F is the fractional uptake at time t, K is a constant depending on the type of the diffusion system, and 'n' is related to the transport mode of the penetrate. M_t and M_s are the mass uptake of water at time t and equilibrium respectively. Eq. (4) is valid for the initial 60% of the fractional uptake. The plot of $\ln(M_t/M_s)$ against $\ln(t)$ depicting the swelling behavior of PAA-K hydrogel synthesized using conventional method and ultrasound assisted method has been shown in Fig. 3. For the diffusion of water in the hydrogel, value of 'n' in Eq. (4) has been found to be 0.39 for hydrogel prepared by conventional method as against 0.87 for the ultrasound assisted method. The diffusion of solvent into a polymer is a combination of two different processes: the diffusion of the solvent into the swollen matrix, and the advancement of the swollen–unswollen boundary as a result of the stress induced in the polymer. When the first mechanism is the rate determining step there is a linear dependency between the solvent uptake and time and the system exhibits Fickian behavior. Also the value of n is a characteristic of the mode of transport of the penetrating molecule and it actually indicates the type of diffusion inside the hydrogel. The values of n for Fickian diffusion and case II transport are 0.5 and 1, respectively whereas for the n value between 0.5 and 1, it is usually described as the non-Fickian diffusion, which is considered the intermediate between Fickian diffusion and case II transport. In the present investigation, from the obtained values of n, we can conclude that for conventionally synthesized hydrogel the Fickian behavior was observed while for ultrasonically synthesized hydrogel non fickian behavior was observed indicating that the advancement of the swollen–unswollen boundary was slower than the diffusion of the solvent in the swollen polymer indicative of zero-order kinetics. As a result, the water uptake increased linearly with the sorption time [10,14,41]. The value of n varied significantly as a result of change in the method of preparation and therefore different diffusion behaviors are expected. Similar type of change of behavior related to diffusion is reported by Li et al. [16] for PAAm/Laponite clay nanocomposite hydrogel as a result of heat treatment to the hydrogel.

3.3. Effect of pH on the responsive adsorption of BG dye

The initial pH of the dye solution is an important parameter, which controls the adsorption process, especially the adsorption capacity. The operating pH of the solution changes the surface charge of the adsorbent, the degree of ionization of the adsorbate molecule and the extent of dissociation of functional groups on the active sites of the adsorbent. The influence of solution pH on the extent of removal of the dye was investigated over the pH range of 4–9 using acidic and basic buffer solutions. The percentage dye removal for the initial dye concentration of 30 mg/L and 1 g hydrogel at different operating pH has been shown in Fig. 4. For both preparation methods it has been observed that the maximum adsorption takes place at pH value of 7. The extent of removal of dye increases with an increase in the pH till an optimum value of 7, beyond which it gradually decreases. The observed results can be attributed to the fact that the pH value affects the structural stability of Brilliant Green molecules [13]. For kaolin, the point of zero charge (ZPC) is 7.0 [11]. Below this range, the kaolin surface acquires positive charge and there would be an

Fig. 3. Plot of $\ln(M_t/M_s)$ against $\ln(t)$ of water in PAA-K hydrogel.
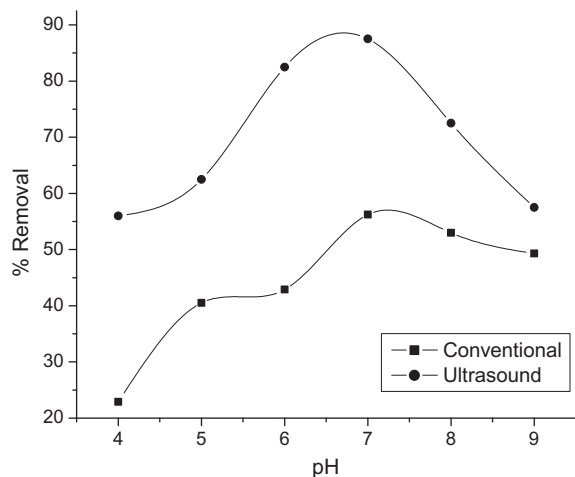
Fig. 4. Effect of pH on adsorption of BG dye on PAA-K hydrogel at 35 °C.

electrostatic repulsion between cationic dye molecules and kaolin. Above a pH of 7, the kaolin particle acquires a negative surface charge. This should lead to higher cationic dye adsorption, however, this behavior has not been observed in the present investigation as seen in Fig. 4. The observed trends can be attributed to the chemical structure of a dye molecule (ionic or molecular) and its behavior under alkaline conditions [34]. Nandi et al. [11] have reported similar existence of the optimum pH of 7 for the removal of Brilliant Green dye from aqueous medium using kaolin. Based on these results, all the further experiments were carried out at pH value of 7.

3.4. Effect of operating temperature on the responsive adsorption of dye

The influence of operating temperature on the adsorption process has been studied at three different temperatures as 15, 25 and 35 °C and the obtained results have been shown in Fig. 5. It can be seen from the figure that the adsorption of the dye increased with an increase in the operating temperature. The maximum extent of removal obtained at 35 °C was 56.24% for the conventional method and 88.3% for ultrasonic method (Fig. 5). The observed results can be attributed to the relaxing of the hydrogel network at higher temperatures, due to which the dye molecules can diffuse more easily through the matrix resulting into more adsorption. However it should be noted that the temperature cannot be increased indefinitely as collapse of hydrogel matrix

may take place due to heat effects. It has been demonstrated that many hydrogel show continuous volume transition with change in the temperature and highly swollen gel network can collapse at high temperatures [17]. Based on these results and related discussion, the operating temperature was fixed at 35 °C for all the further experiments.

3.5. Effect of initial concentration of dye

The effect of initial concentration of dye on the extent of removal has been investigated by varying the initial concentration of BG dye over the range 10–50 mg/L. The solution of dye was mixed with 1 g of PAA-K hydrogel at pH 7 and 35 °C temperature and then equilibrated for 5 h. The obtained results indicate that the dye uptake by hydrogel increases sharply with an increase in the initial dye concentration for both the preparation methods as shown in Fig. 6. The obtained trends can be attributed to the fact that with increasing concentration of BG dye in the initial solution, higher concentration gradient at the hydrogel–solvent interface exists resulting in an enhancement in the BG dye removal rate. Similar results have been reported for the adsorption of metal ions on chitosan-2-acrylamido-2-methyl propane sulfonic acid (AMPS) hydrogel [18]. It is also seen that for the hydrogel prepared by ultrasonic method the extent of removal was increased by almost 30% as compared to conventional method. This may be attributed to the cavitational effects such as formation of micro-jets and

Fig. 5. Effect of temperature on adsorption of BG dye in PAA-K hydrogel at pH 7 for conventional method and ultrasound assisted method.
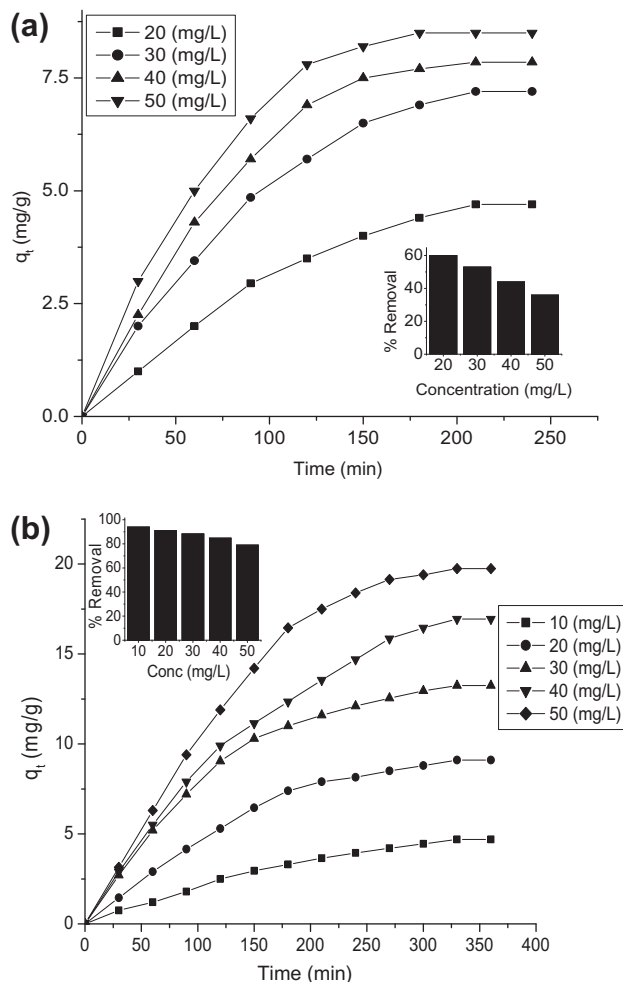
Fig. 6. Effect of initial concentration on adsorption of BG dye in PAA-K hydrogel at pH 7 and 35 °C (a) conventional method, (b) ultrasound assisted method.
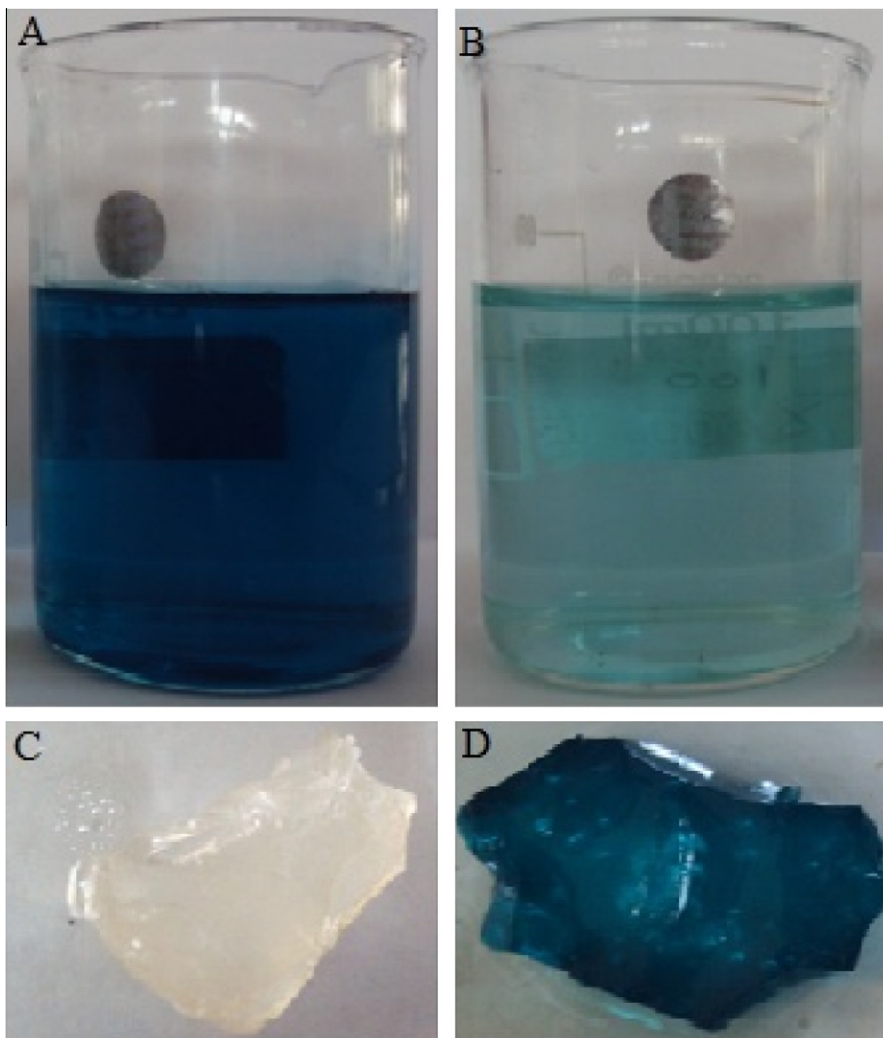
Fig. 7. Colour changes of BG dye and hydrogel before (A, C) and after adsorption (B, D), respectively.

turbulence during polymerization resulting in uniform distribution of kaolin clay throughout the hydrogel matrix. The change in color of both the hydrogel and dye solution before and after the adsorption has been shown in Fig. 7.

3.6. Effect of quantity of hydrogel and kaolin loading

The effect of hydrogel loading on the extent of removal of dye was studied by using different amounts of hydrogel (0.5, 1, 1.5, 2 g) in 100 mL of fixed concentration (30 mg/L) BG dye solution. Fig. 8 shows that the percent removal of the dye increases with an increase in the quantity of hydrogel. The higher dye removal, close to 100%, was reached when 2 g of ultrasonically synthesized hydrogel was used. This indicates that the presence of higher quantity of hydrogel provides large number of active adsorbent sites for removal of enhanced quantum of the pollutant. At the same time when the conventionally synthesized hydrogel was used, 2 g hydrogel was able to remove only 63% dye.

Effect of the clay content on BG adsorption was investigated for PAA-K hydrogel prepared by both methods. For this purpose, PAA-K hydrogel was loaded with two different amounts viz. 0.36 g (1 wt.% of monomer) and 0.72 g (2 wt.% of monomer) of the kaolin clay. The PAA-K hydrogels containing different amounts of kaolin were added to 100 mL solutions of BG dye with different concentrations (10–50 mg/L) at 35 °C in a water bath. The removal effi-
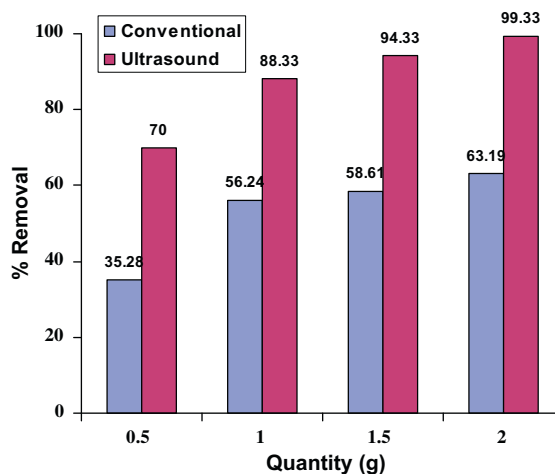
Fig. 8. Effect of initial quantity of PAA-K hydrogel on removal of BG at pH 7 and 35 °C.

ciency (RE%) of the dye by the PAA-K hydrogel containing different amounts of clay has been shown in Fig. 9. Fig. 9a shows the dye removal for conventional method and Fig. 9b shows the same for ultrasound assisted synthesis method. It can be seen from
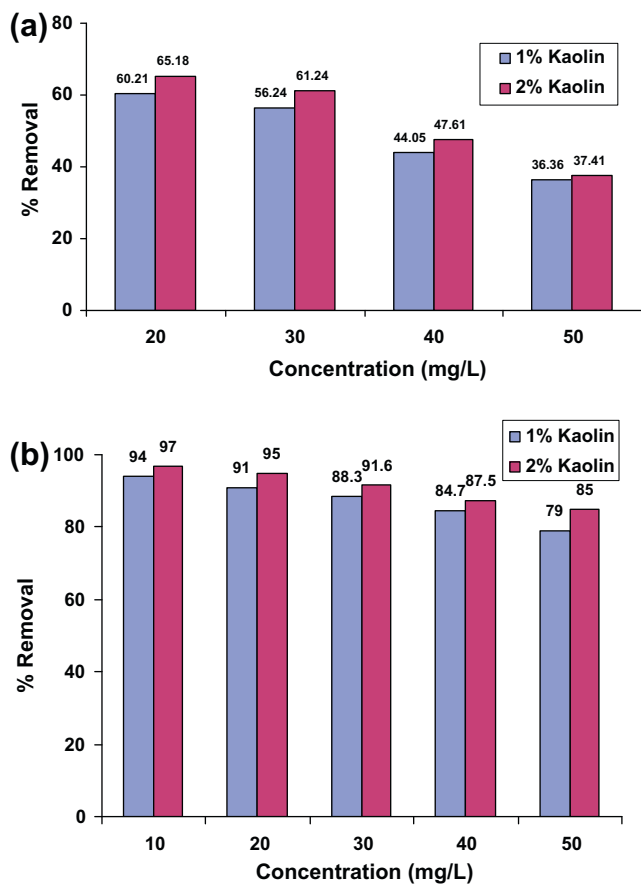
Fig. 9. Effect of clay loading in PAA-K hydrogel for the adsorption of BG dye at pH 7 and 35 °C (a) conventional method, (b) ultrasound assisted method.

both the figures that the dye uptake increases with increasing clay content. The obtained results can be explained on the basis of the fact that enhanced adsorbent active sites are available with an increase in the kaolin content. However there was not a major enhancement in the removal efficiency with the increase in the quantity of kaolin from 1% to 2% (wt.% monomer).

3.7. FTIR study of hydrogel nanocomposite before and after adsorption

The characterization of hydrogel was obtained using FTIR analysis to study the interaction between the dye molecules and the PAA-K hydrogel and to confirm the presence of carboxyl group of acrylic acid. Fig. 10 shows FTIR spectra of PAA-K hydrogel (synthesized by ultrasonic method), before (curve a) and after adsorption
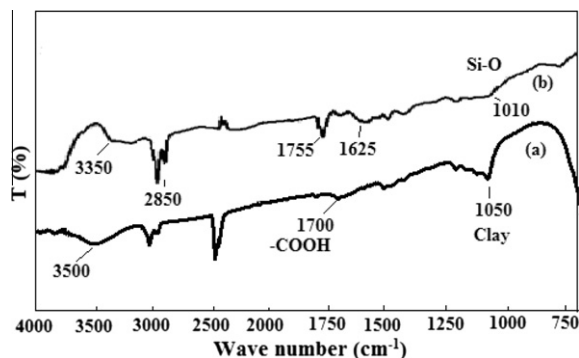
Fig. 10. FTIR spectra of pure PAA-K hydrogel before and after adsorption of BG dye (ultrasound assisted method).

(curve b) of the dye. It can be seen from the spectra that before adsorption, the FTIR spectra of the PAA-K hydrogel shows a peak at 1700 cm^{-1}, which is characteristic peak of the C=O stretching due to the presence of carboxyl groups in poly(acrylic acid). After the adsorption of the dye, the band is shifted to 1625 cm^{-1}. Also, after the adsorption of dye, the FTIR spectra shows a peak at 3350 cm^{-1} which originates due to the formation of hydrogen bond between hydogel and the dye. The presence of band at 1010 cm^{-1} indicates the Si–O stretching vibration of kaolin clay. The presence of band at 3500 cm^{-1} is due to some quantity of moisture in the hydrogel. There are small bands originating at 2850 and 2950 cm^{-1} which are due to the –CH$_3$ groups of the dye molecules.

3.8. Adsorption kinetics and adsorption isotherm models

Based on the studies related to the effect of different operating parameters on the adsorption of BG dye by hydrogel prepared by both the methods it was observed that the hydrogel prepared by ultrasound assisted polymerization process proved to be superior as compared to the hydrogel prepared by conventional method. Therefore for studying the adsorption kinetics the results obtained with hydrogel prepared by ultrasound assisted polymerization process were analyzed in greater details.

In order to find out the rate-controlling step of the adsorption process, it is necessary to establish well defined kinetic models. Pseudo-second-order kinetic model was used to fit the experimental data at different initial concentrations and temperatures. The kinetic rate equation is expressed as follows [42,43].

$$dq/dt = K_2(q_e - q)^2 \tag{5}$$

where, K_2 (g/mg min) is the pseudo second-order rate constant of adsorption. After integrating Eq. (5), the following equation is obtained:

$$t/q = 1/(K_2 q_e^2) + t/q_e \tag{6}$$

The plot of t/q_e against t for the different temperatures gives a characteristic straight line fit as shown in Fig. 11. The obtained values of second-order rate constants K_2 and q_e values are reported in Table 1. The results indicate that the correlation coefficients for the second-order kinetic model were close to 1.0 for all the cases indicating a good fit of the models to the experimental data sets. Therefore, the adsorption of BG dye by the PAA-K hydrogel can be approximated more favorably by the pseudo-second-order model.
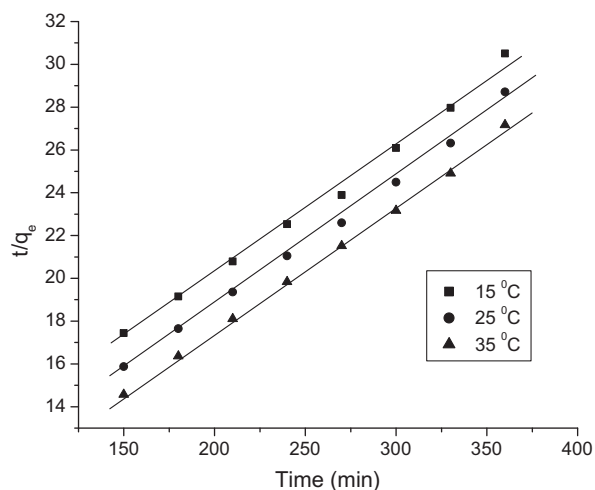
Fig. 11. Adsorption kinetics of BG dye at different temperatures for pseudo-second-order kinetic model.

Table 1
Second-order kinetic constants for the BG adsorption on the PAA-K hydrogel.

Temperature (K)	Pseudo-second-order kinetic constants		
	K_2 (g/mg min) $\times 10^4$	q_e (mg/g)	R^2
288	3.39	17.30	0.98
298	4.12	17.54	0.99
308	5.37	17.85	0.99

Table 2
Langmuir and Freundlich isotherm constants.

Temperature (K)	Langmuir constants		
	Q_m (mg/g)	α	R^2
288	24.90	0.13	0.99
298	25.60	0.20	0.98
308	26.31	0.33	0.98
	Freundlich constants		
	K_F (mg/g)	n	R^2
288	3.82	1.69	0.99
298	4.96	1.85	0.99
308	6.47	1.95	0.98
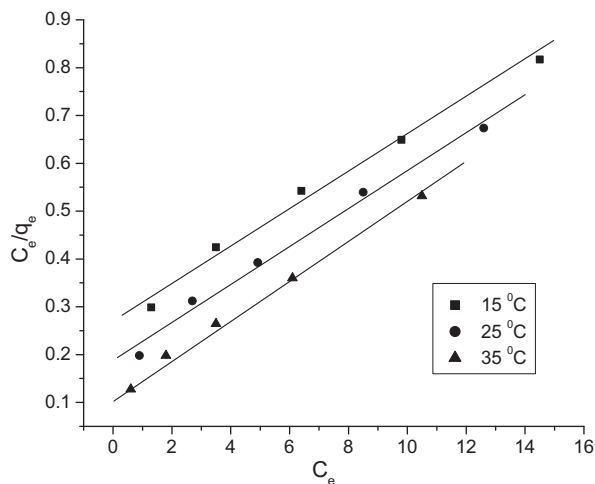
Fig. 12. Plot of C_e/q_e vs C_e for Langmuir isotherm.

Fig. 13. Plot of log q_e vs log C_e for Freundlich isotherm.

There are several isotherm models available for analyzing the experimental data and for describing the equilibrium of adsorption. The more commonly used Langmuir and Freundlich isotherm have been used in this work to determine equilibrium relationships between sorbent and sorbate. The Langmuir equation is given as [43,44].

$$C_e/q_e = 1/(\alpha Q_m) + C_e/Q_m \tag{7}$$

where, C_e (mg/L) is the concentration of the dye solution at equilibrium, q_e (mg/g) is the amount of dye adsorbed at equilibrium, Q_m is the maximum adsorption capacity and α is the Langmuir constant. Q_m and α values were obtained from slope and intercept of the linear plot of C_e/q_e vs C_e (Fig. 12) respectively. The values of Q_m and α are given in Table 2.

Freundlich isotherm is an empirical equation employed to describe heterogeneous systems [43,44]. The Freundlich isotherm is described by equation

$$q_e = K_F \times \log C_e^{(1/n)} \tag{8}$$

Taking log of Eq. (8)

$$\log q_e = \log K_F + (1/n) \log C_e \tag{9}$$

where, K_F and n are the physical constants of the Freundlich adsorption isotherm indicating sorption capacity (mg/g) and intensity respectively. The slope and intercept of the linear plot of log q_e vs log C_e gives the values of n and K_F (Fig. 13). The Freundlich constants are given in Table 2. Values of $1/n$ indicate the type of isotherm to be irreversible ($1/n = 0$), favorable ($0 < 1/n < 1$) or unfavorable ($1/n > 1$). Results showed that n was greater than unity, indicating the dye was adsorbed favorably by the hydrogel at all the temperatures studied. The regression correlation coefficients of both the models were close to 1.0 suggesting that both the isotherms could satisfactorily explain the adsorption of the dye molecules on the hydrogel.

3.9. Evaluation of thermodynamic parameters

Temperature dependence of the adsorption process is associated with several thermodynamic parameters such as Gibbs free energy change ΔG°, standard enthalpy change ΔH° and standard entropy change ΔS°. Thermodynamic considerations of a sorption process are necessary to determine whether the process is spontaneous or not. The value of ΔG° can be determined from the following equation:

$$\Delta G^\circ = -RT \ln K \tag{10}$$

where K is the thermodynamic equilibrium constant.

The effect of temperature on thermodynamic constant is determined by

$$d \ln K/dt = \Delta H^\circ/RT^2 \tag{11}$$

Integrating and rearranging Eq. (11) we get

$$\ln K = -(\Delta H^\circ/RT) + \Delta S^\circ/R \tag{12}$$

and Gibbs free energy is also given by

$$\Delta G^\circ = \Delta H^\circ - T\Delta S^\circ \tag{13}$$

The equilibrium constant K has been determined by plotting $\ln(q_e/C_e)$ versus q_e and extrapolating to zero as shown in Fig. 14 [44,45]. The ΔH° and ΔS° values were calculated from the slope and intercept of linear plot of $\ln K$ versus $1/T$ (Fig. 15). The calculated values of the thermodynamic parameters are reported in Table 3. The negative value of ΔG° indicates that the dye adsorption process is
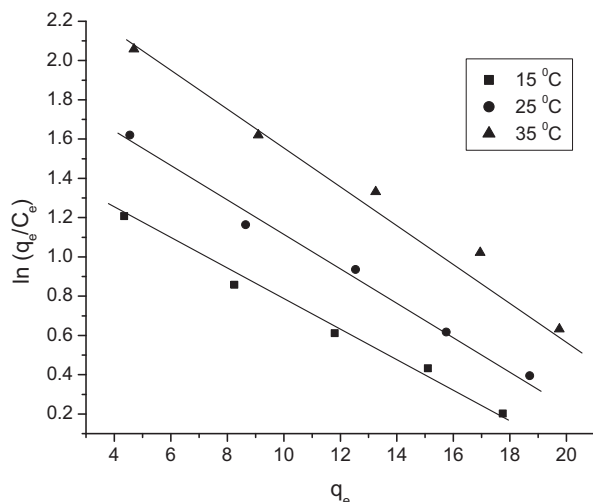
Fig. 14. Plot of ln (q_e/C_e) vs q_e for K values at different temperatures.

$y = -4396.x + 16.7$
$R^2 = 0.998$
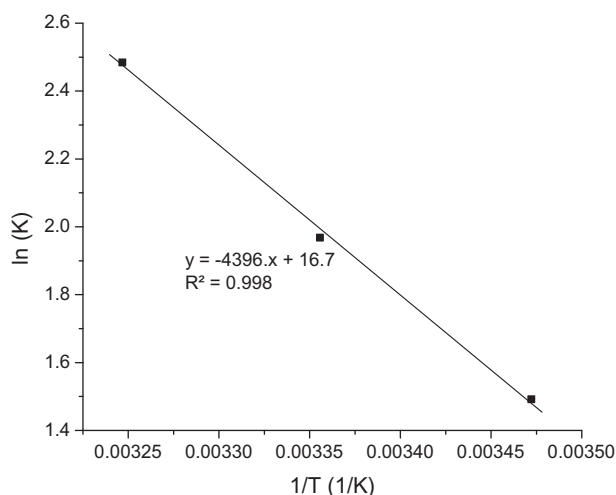
Fig. 15. Plot of ln K vs $1/T$.

Table 3
Thermodynamic parameters of adsorption of dye onto PAA-K hydrogel.

Temperature (K)	ln K	ΔG^o (J/mol)	ΔH^o (J/mol)	ΔS^o (J/mol K)
298	1.49	−3532.61	36,548.34	139.17
308	1.96	−4924.31		
318	2.48	−6315.92		

feasible and positive value of ΔH^o shows that the adsorption process is endothermic in nature.

4. Conclusions

The present work has clearly established the utility of hydrogel synthesized using ultrasound induced polymerization for dye adsorption. The use of ultrasound during polymerization reaction has been shown to uniformly disperse the kaolin clay in the polymer matrix enhancing its adsorption properties considerably for the removal of Brilliant Green from aqueous solution as compared to hydrogel prepared by conventional method. The extent of Brilliant Green removal has been observed to increase with an increase

in pH (till optimum value), temperature, adsorbent and adsorbate concentrations as well as the kaolin clay content in the hydrogel. It has been observed that the maximum BG dye removal by PAA-K hydrogel was achieved for the initial dye concentration of 30 mg/L at a temperature of 35 °C and pH 7. Adsorption kinetics investigation revealed that the pseudo-second-order model fits the experimental data well. Also the Freundlich and Langmuir adsorption isotherm models explain the experimental results satisfactorily. The negative value of ΔG^o indicates the feasibility and spontaneity of the adsorption process and the positive value of ΔH^o indicate the endothermic nature of the adsorption process.

References

[1] V.K. Gupta, I. Ali, M.D. Suhas, Equilibrium uptake and sorption dynamics for the removal of a basic dye (basic red) using low cost adsorbents, J. Colloid Interf. Sci. 265 (2003) 257–264.
[2] K.V. Kumar, V. Ramamurthi, S. Sivanesan, Biosorption of malachite green, a cationic dye onto Pithophora sp., a fresh water alga, Dyes Pigments 69 (2006) 102–107.
[3] R. Ahmad, R. Kumar, Adsorptive removal of congo red dye from aqueous solution using bael shell carbon, Appl. Surf. Sci. 257 (2010) 1628–1633.
[4] G. Moussavi, M. Mahmoudi, Removal of azo and anthraquinone reactive dyes from industrial wastewaters using MgO nanoparticles, J. Hazard. Mater. 168 (2009) 806–812.
[5] V.K. Gupta, M.D. Suhas, Suhas, Application of low-cost adsorbents for dye removal – a review, J. Environ. Manage. 90 (2009) 2313–2342.
[6] J.A. Laszlo, Preparing an ion exchange resin from sugarcane bagasse to remove reactive dye from wastewater, Text. Chem. Color. 28 (1996) 13–17.
[7] A.H. Gemea, I.A. Mansour, R.G. El-Sharkawy, A.B. Zaki, Kinetics and mechanism of the heterogeneous catalyzed oxidative degradation of indigo carmine, J. Mol. Catal.: Chem. 193 (2003) 109–120.
[8] V.L. Grimau, M.C. Gutierrez, Decolorization of simulated reactive dyebath effluents by electrochemical oxidation assisted by UV light, Chemosphere 62 (2006) 106–112.
[9] C. Hachem, F. Bocquillon, O. Zahraa, M. Bouchy, Decolorization of textile industry wastewater by the photocatalytic degradation process, Dyes Pigments 49 (2001) 117–125.
[10] R.L. Cisneros, A.G. Espinoza, M.I. Litter, Photodegradation of an azo dye of the textile industry, Chemosphere 48 (2002) 393–399.
[11] B.K. Nandi, A. Goswami, M.K. Purkait, Adsorption characteristics of Brilliant Green dye on kaolin, J. Hazard. Mater. 161 (2009) 387–395.
[12] A. Mittal, D. Kaur, J. Mittal, Applicability of waste materials-bottom ash and deoiled soya-as adsorbents for the removal and recovery of a hazardous dye, Brilliant Green, J. Colloid Interf. Sci. 326 (2008) 8–17.
[13] V.S. Mane, I.D. Mall, V.C. Shrivastava, Kinetic and equilibrium isotherm studies for the adsorptive removal of Brilliant Green dye from aqueous solution by rice husk ash, J. Environ. Manage. 84 (2007) 390–400.
[14] A.T. Paulino, M.R. Guilherme, A.V. Reis, G.M. Campese, E.C. Muniz, J. Nozaki, Removal of methylene blue dye from an aqueous media using superabsorbent hydrogel supported on modified polysaccharide, J. Colloid Interf. Sci. 301 (2006) 55–62.
[15] S. Li, Removal of crystal violet from aqueous solution by sorption into semi-interpenetrated networks hydrogels constituted of poly(acrylic acid-acrylamide-methacrylate) and amylase, Biores. Technol. 101 (2010) 2197–2202.
[16] P. Li, S. Siddaramaiah, N.H. Kim, S. Heo, J. Lee, Novel PAAm/Laponite clay nanocomposite hydrogels with improved cationic dye adsorption behavior, Composites: Part B 39 (2008) 756–763.
[17] H. El-Hamshary, S. El-Sigeny, M.F. Taleb, N.A. El-Kelesh, Removal of phenolic compounds using (2-hydroxyethyl ethacrylate/acrylamidopyridine) hydrogel prepared by gamma radiation, Sep. Purif. Technol. 57 (2007) 329–337.
[18] Y.H. Gad, Preparation and characterization of poly(2-acrylamido-2-methylpropanesulfonic acid)/Chitosan hydrogel using gamma irradiation and its application in wastewater treatment, Radiat. Phys. Chem. 77 (2008) 1101–1107.
[19] Y. Zheng, A. Wang, Evaluation of ammonium removal using a chitosan-g-poly (acrylic acid)/rectorite hydrogel composite, J. Hazard. Mater. 171 (2009) 671–677.
[20] H. Liu, X. Ye, Q. Li, T. Kim, B. Qing, M. Guo, F. Ge, Z. Wu, K. Lee, Boron adsorption using a new boron-selective hybrid gel and the commercial resin D564, Colloids Surf. A 341 (2009) 118–126.
[21] H. Liu, B. Qing, X. Ye, Q. Li, K. Lee, Z. Wu, Boron adsorption by composite magnetic particles, Chem. Eng. J. 151 (2009) 235–240.

[22] H.B. Bohidar, P. Dubin, Y. Osada, Polymer gels: fundamentals and applications, American Chemical Society, Washington (DC), 2002.

[23] G.V.R. Rao, M.E. Krug, S. Balamurugan, H.F. Xu, Q. Xu, G.P. Lopez, Synthesis and characterization of silica–poly(N-isopropylacrylamide) hybrid membranes: switchable molecular filters, Chem. Mater. 14 (2002) 5075–5080.

[24] M.R. Guilherme, R. Silva, E.M. Girotto, A.F. Rubira, E.C. Muniz, Hydrogels based on PAAm network with PNIPAAm included: hydrophilic–hydrophobic transition measured by the partition of orange II and methylene blue in water, Polymer 44 (2003) 4213–4219.

[25] Y. Liu, J.J. Xie, X.Y. Zhang, Synthesis and properties of the copolymer of acrylamide with 2-acrylamido-2-methylpropanesulfonic acid, J. Appl. Polym. Sci. 90 (2003) 3481–3487.

[26] H.A. Ketelson, D.L. Meadows, R.P. Stone, Dynamic wettability properties of a soft contact lens hydrogel, Colloids Surf B 40 (2005) 1–9.

[27] N.A. Churochkina, S.G. Starodoubtsev, A.R. Khokhlov, Swelling and collapse of the gel composites based on neutral and slightly charged poly(acrylamide) gels containing Namontmorillonite, Polym. Gels Networks 6 (1998) 205–215.

[28] K. Kabiri, Zohuriaan-Mehr, Superabsorbent hydrogel composites, Polym. Adv. Technol. 14 (2003) 438–444.

[29] J. Lin, J. Wu, Z. Yang, M. Pu, Synthesis and properties of poly(acrylic acid)/mica superabsorbent nanocomposite, Macromol. Rapid Commun. 22 (2001) 422–424.

[30] S.G. Starodoubtsev, N.A. Churochkina, A.R. Khokhlov, Hydrogel composites of neutral and slightly charged poly(acrylamide) gels with incorporated bentonite interaction with salt and ionic surfactants, Langmuir 16 (2000) 1529–1534.

[31] J. Wu, J. Lin, M. Zhou, M. Pu, Synthesis and properties of starch-graft polyacrylamide/ clay superabsorbent composite, Macromol. Rapid Commun. 21 (2000) 1032–1034.

[32] Y. Xiang, Z. Peng, D. Chen, A new polymer/clay nano-composite hydrogel with improved response rate and tensile mechanical properties, Eur. Polym. J. 42 (2006) 2125–2132.

[33] S. Karahan, M. Yurdakoc, Y. Seki, K. Yurdakoc, Removal of boron from aqueous solution by clays and modified clays, J. Colloid Interf. Sci. 293 (2006) 36–42.

[34] A.R. Tehrani-Bagha, H. Nikkar, N.M. Mahmoodi, M. Markazi, F.M. Menger, The sorption of cationic dyes onto kaolin: Kinetic, isotherm and thermodynamic studies, Desalination 266 (2011) 274–280.

[35] O. Abdelwahab, Evaluation of the use of loofa activated carbons as potential adsorbents for aqueous solutions containing dye, Desalination 222 (2008) 357–367.

[36] S.H. Sonawane, P.L. Chaudhari, S.A. Ghodke, M.G. Parande, V.M. Bhandari, S. Mishra, R.D. Kulkarni, Ultrasound assisted synthesis of polyacrylic acid–nanoclay nanocomposite and its application in sonosorption studies of malachite green dye, Ultrason. Sonochem. 16 (2009) 351–355.

[37] S. Sonawane, P. Chaudhari, S. Ghodke, S. Ambade, S. Gulig, A. Mirikar, A. Bane, Combined effect of ultrasound and nanoclay on adsorption of phenol, Ultrason. Sonochem. 15 (2008) 1033–1037.

[38] P. Cass, W. Knower, E. Pereeia, N.P. Holmes, T. Hughes, Preparation of hydrogels via ultrasonic polymerization, Ultrason. Sonochem. 17 (2010) 326–332.

[39] P.R. Gogate, V.S. Sutkar, A.B. Pandit, Sonochemical reactors: important design and scale up considerations with a special emphasis on heterogeneous systems, Chem. Eng. J. 166 (2011) 1066–1082.

[40] J.E. Elliott, M. Macdonald, J. Nie, C.N. Bowman, Structure and swelling of poly(acrylic acid) hydrogels: effect of pH, ionic strength, and dilution on the crosslinked polymer structure, Polymer 45 (2004) 1503–1510.

[41] S.J. Kim, K.J. Lee, S.I. Kim, Water sorption of poly(propylene glycol) / poly(acrylic acid) interpenetrating polymer network hydrogels, React. Funct. Polym. 55 (2003) 69–73.

[42] N.M. Mahmoodi, B. Hayati, M. Arami, C. Lan, Adsorption of textile dyes on pine cone from colored wastewater: Kinetic, equilibrium and thermodynamic studies, Desalination 268 (2011) 117–125.

[43] G. Bayramoglu, B. Altintas, M. Arica, Adsorption kinetics and thermodynamic parameters of cationic dyes from aqueous solutions by using a new strong cation-exchange resin, Chem. Eng. J. 152 (2009) 339–346.

[44] O. Aksakal, H. Ucun, Equilibrium, kinetic and thermodynamic studies of the biosorption of textile dye (Reactive Red 195) onto Pinus sylvestris L, J. Hazard. Mater. 181 (2010) 666–672.

[45] R. Gong, S. Zhu, D. Zhang, J. Chen, S. Ni, R. Guan, Adsorption behavior of cationic dyes on citric acid esterifying wheat straw: kinetic and thermodynamic profile, Desalination 230 (2008) 220–228.

CrossMark

Investigation of TiO$_2$ photocatalyst performance for decolorization in the presence of hydrodynamic cavitation as hybrid AOP

Bhaskar Bethi [a], S.H. Sonawane [a,*], G.S. Rohit [a], C.R. Holkar [b], D.V. Pinjari [b], B.A. Bhanvase [c], A.B. Pandit [b]

[a] Department of Chemical Engineering, National Institute of Technology, Warangal 506004, Telangana State, India
[b] Chemical Engineering Department, Institute of Chemical Technology, Matunga, Mumbai, MS, India
[c] Chemical Engineering Department, Laxminarayan Institute of Technology, RTM Nagpur University, Nagpur 440033, MS, India

ABSTRACT

In this article, an acoustic cavitation engineered novel approach for the synthesis of TiO$_2$, cerium and Fe doped TiO$_2$ nanophotocatalysts is reported. The prepared TiO$_2$, cerium and Fe doped TiO$_2$ nanophotocatalysts were characterized by XRD and TEM analysis to evaluate its structure and morphology. Photo catalytic performance of undoped TiO$_2$ catalyst was investigated for the decolorization of crystal violet dye in aqueous solution at pH of 6.5 in the presence of hydro dynamic cavitation. Effect of catalyst doping with Fe and Ce was also studied for the decolorization of crystal violet dye. The results shows that, 0.8% of Fe-doped TiO$_2$ exhibits maximum photocatalytic activity in the decolorization study of crystal violet dye due to the presence of Fe in the TiO$_2$ and it may acts as a fenton reagent. Kinetic studies have also been reported for the hybrid AOP (HAOP) that followed the pseudo first-order reaction kinetics.

© 2015 Elsevier B.V. All rights reserved.

1. Introduction

Dyes are having many applications in different industrial processes such as textile, printing, leather, paint, plastic, food, cosmetics, and pharmaceutical industries [1]. Waste water discharge from these industries containing high concentrations of dyes, high toxicity and intense color causes serious problems on surrounding ecosystem [2]. Many treatment methods are available for the treatment of above mentioned industrial wastewater, such as conventional biological treatment (aerobic and anaerobic), adsorption, coagulation and flocculation. The main drawbacks of these methods are not being able to completely degrade the dye molecules present in the waste water due to the complex and bio recalcitrant nature of the dye molecules. Azo dyes are known to as more non-biodegradable under aerobic biological conditions and these dyes are converted to more hazardous intermediates under anaerobic conditions [3]. Some methods such as coagulation/flocculation and adsorption are physical treatment methods and these methods did not involve chemical transformation and therefore generally transport the waste components from one phase to another phase, that leads to secondary waste pollutant on the environment [4,5]. Therefore, it is necessary to find an effective treatment technology for the degradation of the complex and non-biodegradable

molecules to smaller molecules. For this application, advanced oxidation processes (AOPs) have been employed and evaluated since the 20th century to degrade azo dyes from the wastewater. Among AOPs, electrolysis and photo catalysis are extensively studied [6]. AOPs involve the generation of hydroxyl radicals and complete oxidization of such pollutants including dyes converted into end products, such as CO$_2$, H$_2$O, etc. [7]. Recent literature has indicated that hybridization of different AOPs has been found to be more efficient for the wastewater treatment than individual oxidation process [8,9].

Recently, hydrodynamic and acoustic cavitation has been widely applied as an advanced oxidation technology along with other AOPs for wastewater treatment as a hybrid treatment technique [10–12]. When an aqueous solution is passed through a mechanical constriction, large pressure differentials are generated due to the change in flow geometry. If the pressure of the aqueous solution at the constriction falls below the vapor pressure of the aqueous solution, cavities are formed, and grow and/or subsequently collapse on the recovery of pressure [13]. Sudden collapse of these cavities (occurring in microseconds) yields localized high temperatures and pressures. Water molecules under such extreme conditions undergo thermal dissociation to form hydroxyl radicals, which are powerful oxidants for the complete mineralization of many organic pollutants [14].

---

* Corresponding author.
  E-mail address: shirishsonawane09@gmail.com (S.H. Sonawane).

Researchers have studied photocatalysis extensively among other AOPs as a wastewater treatment method using nano sized and micro sized photocatalysts with doping and/or in pure state.

Among many photocatalysts TiO₂ has been widely studied because of its chemical inertness, strong oxidizing power, and long-term stability against photo and chemical corrosion, suitable band gap energy and electronic and optical properties [15–18]. The main drawbacks which are associated with the use of TiO₂ in waste water treatment are undesirable recombination of electrons and holes, and low efficiency under irradiation in the visible region [20,21]. Scientists are overcome this problem by extending the light absorption range of TiO₂ from UV to visible light and to improve the photocatalytic activity of TiO₂ [22]. Dopants, such as transitional metals can be loaded on to TiO₂ to minimize the recombination of photo-generated electrons and photo-generated holes and also shifts the excitation wavelength from the UV to the visible light spectrum [19–24]. In the past the researchers are used the transition metals (Fe, Al, Ni, Cr, Co, W, V and Zr), metal oxides (Fe_2O_3, Cr_2O_3, CoO_2, $MgO + CaO$ and SiO_2), transition metal ceramics (WO_3, MoO_3, Nb_2O_5, SnO_2 and ZnO) and anionic compounds (C, N, and S) to dope TiO₂ to improve its applicability [25–28]. In the literature very few articles are reported the work on Ce doped TiO₂ catalysts. They reported that the effect of Ce doped TiO₂ catalysts are strongly depends on the various factors, such as the synthesis method and the cerium content [21,29,30]. In this work, the reason for choosing dopants, such as transitional metals was to improve its catalytic activity and to reduce the recombination of photo-generated electrons and photo-generated holes. Rauf [22] has given an overview on the photocatalytic degradation of azo dyes in the presence of TiO₂ doped with selective transition metals. Higher catalytic activity has been reported for the Ce doped TiO₂ materials for photo-degradation of dyes and other pollutants. Cerium oxides have attracted much attention due to the optical and catalytic properties associated with the redox pair of Ce^{3+}/Ce^{4+}. Cerium extends the photo response into the visible region, this can lead to an increase in the charge separation efficiency of surface electron–hole pairs. Earlier there are many reports of Fe doping on TiO₂ to improve its photo catalytic activity among a variety of transitional metals and also Fe on TiO₂ acts as a Fenton reagent (Fe^{2+}) has shown the better degradation performance of organic pollutants than other transition metals. Shirsath et al. [31] synthesized the titanium dioxide nanoparticles doped with Fe and Ce using sonochemical approach. They found that Ce doped TiO₂ exhibits maximum photocatalytic activity followed by Fe-doped TiO₂ and the least activity was for only TiO₂ for the degradation of crystal violet (CV) dye. Narayana et al. [32] have synthesized the pure TiO₂, Fe and Co doped photocatalysts via sol–gel method. From the malachite green decolorization study, they observed that Fe-doped TiO₂ showed highest photocatalytic activity among the other two photocatalysts with 98% decolorization in 2 h. Ramirez et al. [33] have studied the photocatalytic degradation of acid orange 7 (AO7) using Ce-doped TiO₂ slurry and employing solar irradiation. They have observed that AO7 has shown higher decolorization when Ce content in the TiO₂ is about 1.0% (by weight) compared to TiO₂. There is effect of synthesis method on TiO₂ structures and hence on photocatalytic activity. Anatase and rutile are two major phases are present in TiO₂. Composition of these phases varies from 20% to 80%. The anatase phase shows better degradation capability compared to rutile phase of TiO₂. Particle size, surface area, and their calcinations temperature will also adversely affect on the photocatalytic activity of TiO₂. Andronic et al. [34] reported the synthesis of TiO₂ by sol–gel method, the resultant TiO₂ powder having 40% anatase and 60% rutile was shown the degradation of methyl orange up to 37% in 30 min of UV irradiation. Samira et al. [35] reported the crystal violet degradation of initial concentration:

5×10^{-5} mol/L, using nanoanatase TiO2 having anatase and rutile phases in the ratio of 3:1 was shown the degradation rate greater than 99.5% on UV illumination for 45 min. It was also confirmed in the recent literature that ultrasound assisted synthesis of TiO₂ has shown the better decolorization performance than the conventional synthesis technique [31]. The ultrasound assisted synthesis technique able to produce the very small size (nanometer range) TiO₂ particles having more specific surface area which is able to adsorb the large quantity of dye molecules on active sites of the catalyst leads to better decolorization.

Some of the articles have reported the wastewater treatment technique based on photocatalysis combined with cavitation technique as hybrid AOP. Very few articles were found on HC/UV and HC/UV/TiO₂ combination, for dyes decolorization and other organic pollutants (pesticides, pharmaceutical compounds). Though literature reports are found on US/UV/TiO₂ combination, but scale up of waste water treatment using ultrasound cavitation is not effective solution [30]. It requires more energy compared to hydrodynamic cavitation. It can possible to scale up the waste water treatment using HC due to the production of more cavitation yield, less cost of operation, cheap design. It was confirmed that HC is potentially suitable for scale up issues in waste water treatment based on cavitation. Kalumuck [36] reported the degradation of p-nitrophenol in wastewater using hydrodynamic cavitation in a re-circulatory pipe flow. It has been reported that the hydrodynamic cavitation has shown about 20 times more rate of degradation compared to the ultrasonic horn and the oxidation efficiency is almost 25 times more for the hydrodynamic cavitating jets. Sivakumar and Pandit [37] studied the applicability of hydrodynamic cavitation for the degradation of Rhodamine B dye solution, they reported that hydrodynamic cavitation was much more energy efficient compared to acoustic cavitation. Hydrodynamic cavitation unit using multiple hole orifice plates has been reported to give cavitational yields (extent of degradation per unit energy supplied), which are two times higher than the best acoustic cavitation device.

Wang et al. [38] have studied the decolorization of an azo dye, C.I. reactive red 2 (RR2) using TiO₂ photocatalysis coupled with water jet cavitation. Bagal et al. [39] have studied the degradation of diclofenac a pharmaceutical drug in wastewater samples using a combined approach of hydrodynamic cavitation and heterogeneous photocatalysis. They found that the degradation of diclofenac is about 95% with 76% reduction in TOC value. Although there are many studies reported in the literature on doped TiO₂ with Fe and Ce as a photocatalysts for the degradation of various dyes, none of the studies to the best of our knowledge, have been reported in the literature on combination of hydrodynamic cavitation and doped photocatalysis. The novelty of this research is to study the doped TiO₂ photocatalysts with the combination of hydrodynamic cavitation for the treatment of dye waste water to know the effect of doped photocatalyst.

The present work reports the ultrasonic assisted synthesis of TiO₂, Fe-doped TiO₂, Ce-doped TiO₂ nanophotocatalysts. Prepared photo catalysts have been used for the degradation of crystal violet (CV) dye in the presence of hydrodynamic cavitation combined with photo catalysis.

2. Materials and methods

2.1. Materials

For the synthesis of pure TiO₂, Fe–TiO₂, and Ce–TiO₂ chemicals namely Titanium Tetra isopropoxide (TTIP) were obtained from Spectrochem Pvt. Ltd. Mumbai, India. Cerium nitrate and ferric nitrate were obtained from S.D. Fine Chemicals Ltd., Mumbai, India. Sodium hydroxide, methanol and acetone were procured

from Molychem Ltd., Mumbai, India. For the decolorization study, crystal violet dye ($C_{25}N_3H_{30}Cl$) was procured from Sisco Research Laboratories Pvt. Ltd. Mumbai, India. All the chemicals procured were of analytical grade and were used as obtained from the supplier.

2.2. Experimental setup

The experimental setup of hydrodynamic cavitation coupled with photocatalytic reactor is shown in Fig. 1. This set up includes a tank of 5 L volume along with UV light assembly inside the tank. The setup is arranged in a closed loop manner, which includes a feed tank, positive displacement pump (power = 1.1 kW), pressure gauges and valves. Cooling jacket is provided to the feed tank in order to control temperature. Suction side of the pump is connected to the bottom side of the feed tank and the discharge line from the pump branches into two lines. The main line consists of a circular venturi and second line is the bypass line. In the present study, circular venturi with 2 mm throat diameter is used as a cavitating device. Geometrical dimensions of circular venturi are shown in Fig. 2. A bypass line is provided to control the flow through the main lines. Control valves and pressure gauges are provided at appropriate places to control the flow rate through the lines containing the cavitating device (venturi) and to measure the fluid pressures respectively. Alternatively, variable frequency drive (VFD) is also provided to control the motor rpm such that the flow through the main line can be controlled directly by changing the number of piston stroke per minute of the positive displacement pump, while keeping bypass line closed. The material of construction of the entire system except cavitating device is stainless steel (SS-316), whereas cavitating device, circular venturi is made up of brass. Portable assembly, made up of quartz, containing high pressure mercury vapor lamp (125 W) with cooling jacket, is placed centrally in the feed tank for the UV–visible irradiation.

2.3. Analytical procedure

The crystal violet dye samples were collected for every interval and analyzed using UV–Vis Spectrophotometer to observe a change in the absorbance value of crystal violet dye with respect to time at a maximum wavelength (λ_{max}) of 590 nm. The concentration of crystal violet dye was then calculated using the calibration curve prepared for crystal violet dye.

2.4. Synthesis of pure TiO_2 and doped TiO_2 nanophotocatalysts

In a typical synthesis procedure, sonochemical technique [31,40] was used to prepare the pure TiO_2 nanophotocatalyst. The synthesis procedure begins with 10 mL of titanium isopropoxide (TTIP) mixed with 2 mL acetone and 2 mL methanol in a 250 mL beaker (ultrasound reactor). The reactor was placed in a constant temperature bath and the sonication was carried in the presence of ultrasonic irradiation using an ultrasonic horn (Dakshin ultrasonic probe sonicator, 22 kHz operating frequency, 130 W power supply). 50 mL sodium hydroxide solution was added drop wise into the ultrasound reactor. During the addition of sodium hydroxide solution to the above mixture, a white precipitate was formed. After the addition of 50 mL of sodium hydroxide solution, the mixture was further sonicated for 30 min. After 30 min of irradiation the solution was kept undisturbed for settling of the precipitate. The resulting precipitate was filtered, dried and calcined at 200 °C for 2 h.

Procedure used for the synthesis of pure TiO_2 [31,40] has been used for the synthesis of Fe-doped TiO_2, and Ce-doped TiO_2, including the addition of ferric nitrate and cerium nitrate carried out individually for the synthesis of Fe doped TiO_2 and Ce-doped TiO_2 nanophotocatalyst with molar ratios of 0.8 and 1.6 (mol%) of Fe to TiO_2 and Ce to TiO_2 respectively. Schematic experimental setup for the synthesis of undoped and doped TiO_2 nanoparticles is shown in the Fig. 3. Typical method for the synthesis of Fe–TiO_2 and Ce–TiO_2 is shown in the Fig. 4. The same method was adopted for the synthesis of Ce–TiO_2 except the addition of ferric nitrate, in the place of ferric nitrate; cerium nitrate was added to synthesize Ce–TiO_2 nanophotocatalyst.

2.5. Characterization

Pure TiO_2, Fe–TiO_2, Ce–TiO_2 nanophotocatalysts prepared through acoustic cavitation technique was characterized by using powder X-ray diffractometer (Phillips PW 1800, range is 6–80°
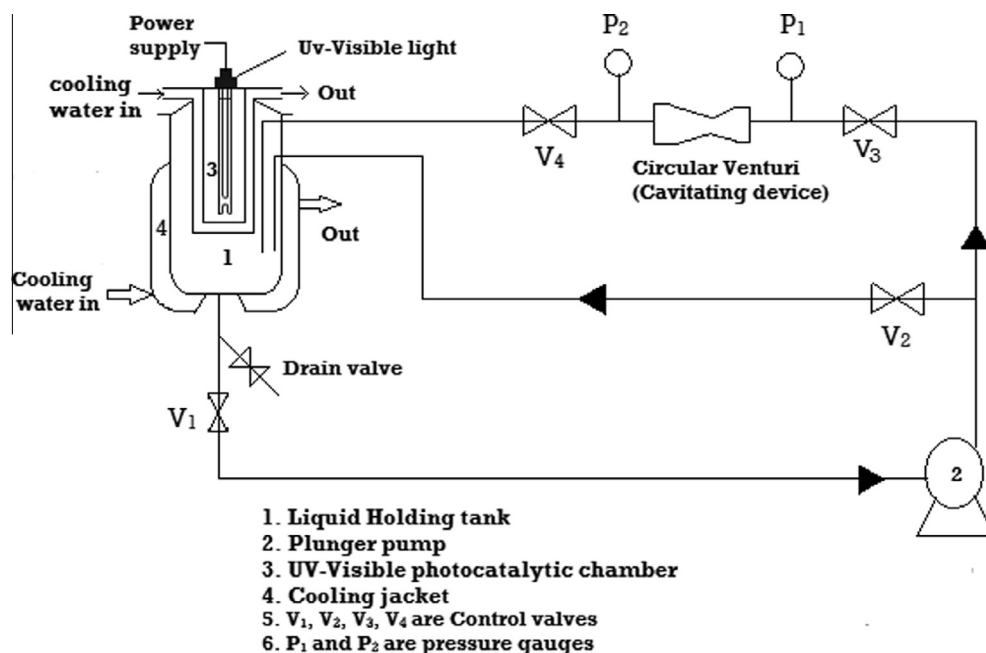
Fig. 1. Hydrodynamic cavitation set up with UV–Vis photocatalysis system.

Convergent angle = 22°

Divergent angle = 6°
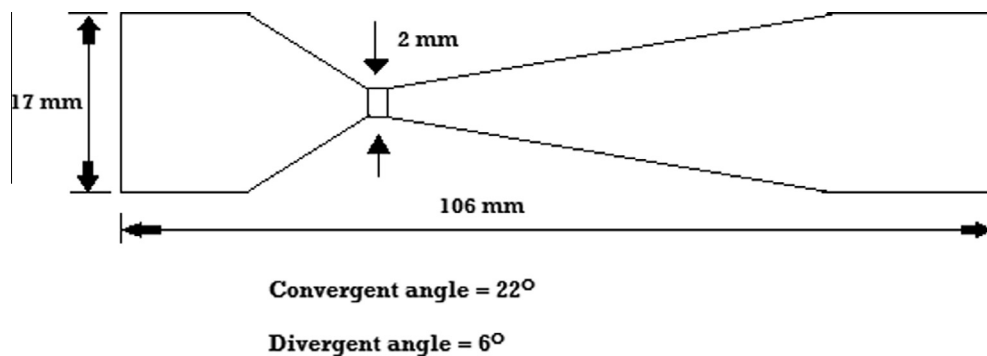
Fig. 2. Geometrical dimensions of cavitating device (circular venturi).
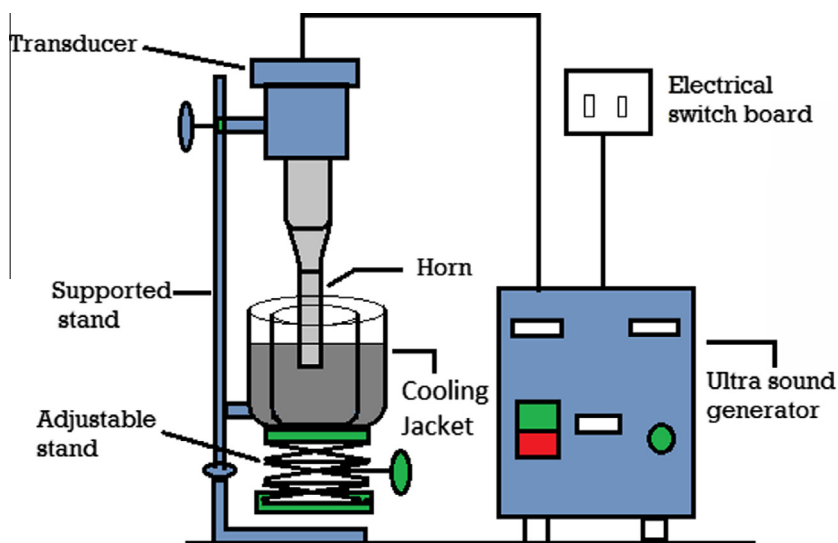
Fig. 3. Experimental setup for synthesis of undoped and doped TiO$_2$ nanoparticles.
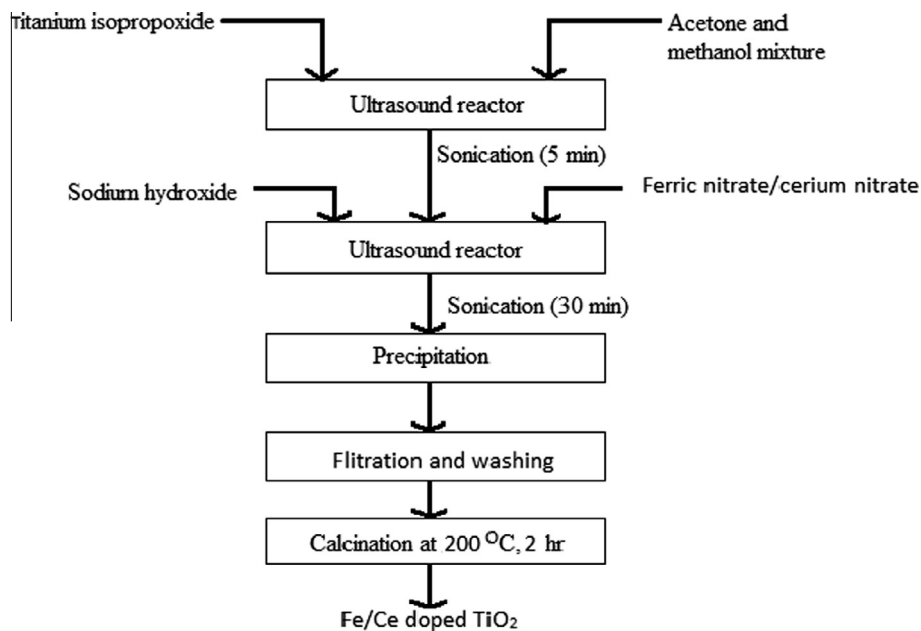
Fig. 4. Method for synthesis of Fe–TiO$_2$.

2θ). The morphology and particle size of these three photocatalysts were characterized by transmission electron microscopy (TEM, H-7650 accelerating voltage of 120 kV).

3. Results and discussion

3.1. XRD analysis of doped and undoped TiO_2 nanoparticles prepared by sonochemical method

Powder X-ray diffraction (XRD) was used for identification of the particles size, crystal structures. TiO_2 powder prepared by sonochemical approach and calcined at 200 °C was used in X-ray powder diffraction (XRD) analysis to characterize the particles structure and crystal size. XRD pattern of ultrasonically prepared TiO_2 powder samples is shown in the Fig. 5. As observed from the XRD pattern of TiO_2, the peaks are generated at $2\theta = 27.5°$, 30°, 42°, 48°, 54°, 62° and 72° confirms the TiO_2 powder was predominantly crystalline in nature with anatase as a major phase. Among the other peaks in XRD pattern of TiO_2, the initial peaks which are generated between the 2θ range of 25⁻30° such as 27.5° and 30° are the prominent peaks with high intensity, which is used to determine crystallite size. These high intensity peaks indicated that the crystalline phase of anatase TiO_2 was successfully formed.

The XRD patterns of 0.8% Fe-doped TiO_2 powder prepared by sononochemical approach and calcined at 200 °C showed the main peaks at $2\theta = 25.8°$, 36.9°, 48.1°, 54.1° and 62.4°. These peaks are corresponding to the anatase crystalline phase (which is photocatalytically active). The XRD pattern of Fe–TiO_2 also showed the peak at 34.4°, the peak which is generated at this angle was assigned to the presence of Fe in hematite form in TiO_2 [41,26]. Similarly the XRD patterns of Ce-doped TiO_2 for 0.8% Fe–TiO_2 showed the generation of main peaks at $2\theta = 30°$, 37.4°, 47.8°, 54.5° and 62.7° again related to the anatase crystalline phase.

It is also observed that the XRD patterns of Ce doped TiO_2 showed the presence of good intensity peaks at 30° and 30.6°. These peaks intensity are assigned to cerium titanate – $Ce_xTi_{1-x}O_2$ [21,42]. Thus, one can observe in the case of XRD pattern of ultrasonically prepared Ce doped TiO_2 consists of peak at $2\theta = 30°$, this peak corresponding to the presence of cerium as a separate cubic CeO_2, or as cerium titanate in the TiO_2 phase [31].
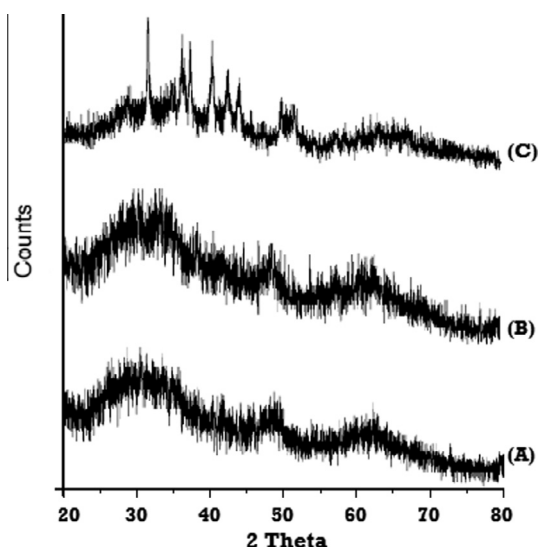
Fig. 5. XRD pattern of Ce-doped TiO_2, Fe-doped TiO_2 and undoped TiO_2 powder prepared by sonochemical method [(A) TiO_2, (B) Fe–TiO_2, (C) Ce–TiO_2].

From the XRD patterns of pure TiO_2, Fe–TiO_2 and Ce–TiO_2, the crystallite sizes of the synthesized TiO_2, Fe–TiO_2 and Ce–TiO_2 nanoparticles were estimated using Scherrer equation [43]:

$$d = \frac{k\lambda}{\beta \cos \theta} \tag{1}$$

where

'd' is crystallite size in nanometer,
'k' is shape factor constant, which is 0.89,
'β' is the full width at half maximum (FWHM) in radian,
'λ' is the wave length of the X-ray which is 1.540598 nm for Cu target Kα radiation and
'θ' is the Bragg diffraction angle.

By using the above data the estimated crystalline sizes for pure TiO_2, Fe–TiO_2 and Ce–TiO_2 are shown in Table 1. In detail, the initial observed peak at $2\theta = 27.5°$, 27.8° and 26.5° for TiO_2, Fe–TiO_2, and Ce–TiO_2 respectively and the full width of maximum intensity for all three photocatalysts are 0.016711.

3.2. TEM analysis and particle size distribution of TiO_2 and doped TiO_2 nanoparticles

Transmission electron microscope (TEM) was used to study the crystal structure, morphology, shapes and particle size. Figs. 6–8 shows the typical transmission electron microscopic images of TiO_2, 1.6 mol% of Fe–TiO_2 and 1.6 mol% of Ce–TiO_2 calcined at 200 °C for 2 h. TEM images indicates that the particles of TiO_2, Fe-doped TiO_2, and Ce–TiO_2 are relatively uniform and are very small in size (<100 nm). It could be clearly interpreted that, the crystal growth formation has not occurred in the three photocatalysts synthesized in this work and shows uniform doping of Fe and Ce on TiO_2. The main reason for the desegregation of crystals is due to the presence of ultrasonic irradiation while synthesis of photocatalysts. During the ultrasonic irradiation, number of micro jets are formed due to the cavitational activity [31], these micro jets avoid the interaction between crystals which are formed during synthesis and also breakdown the crystals into smaller size. This phenomenon helps to reduce the agglomeration of particles hence the smaller and more uniform particles size and uniform shape could be observed.

One can observe from the studies of TEM on pure TiO_2, Fe–TiO_2 and Ce–TiO_2 prepared by various synthesis techniques reported in the literature, tells that all the techniques other than ultrasonic assisted synthesis result into the generation of enormous agglomerated crystalline phase, non-uniform and large crystalline sizes.

3.3. Decolorization of CV through HC alone

In a typical experimental procedure, 50 mg/L of crystal violet (CV) dye were used for the preparation of 5 L crystal violet dye stock solution. The following operating conditions such as constant temperature (35 °C), constant pressure (5 kg/cm² pump discharge pressure to the cavitating device) and normal solution pH 6.5 were used for the study of CV degradation. In this study, experiments were carried out at pH of 6.5, which is the solution pH of the crystal violet dye. A reason for keeping constant pH is reported as follows.

Table 1
Estimated crystalline sizes of photocatalysts prepared by sonochemical method.

Type of photocatalyst	2θ	β	Particles size (nm)
Pure TiO_2	27.5	0.016711	84.47
Fe-TiO_2	27.8	0.016711	84.21
Ce-TiO_2	26.5	0.016711	84.32
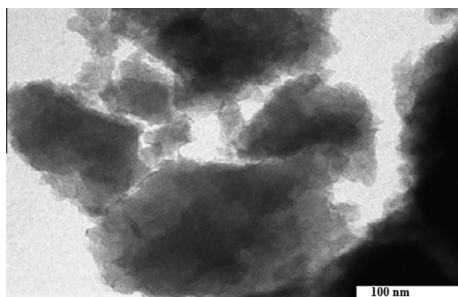
Fig. 6. TEM image of pure TiO$_2$.
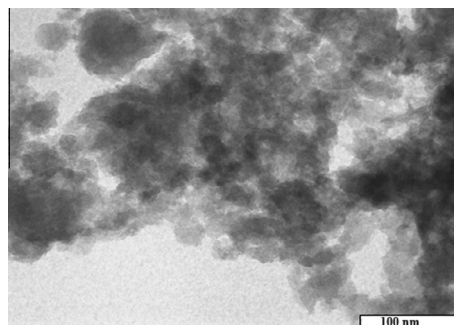
Fig. 8. TEM image of 1.6 mol% of Ce doped-TiO$_2$.

The crystal violet dye solution at different pH values shows different colors and unstable. But at pH 6.5 it has remains in a blue violet color with an absorbance maximum at 590 nm, this is the natural color state of the crystal violet dye. Angeloni et al. [37] reported that at pH 1.0, the CV dye is yellow color with absorption maxima at 420 nm and 620 nm and CV gradually changes its color by increasing the acidity of the aqueous solution, being blue–green at pH 2–5. The different colors are a result of the different charged states of the dye molecule. In the yellow form, all three nitrogen atoms carry a positive charge, of which two are protonated. At neutral pH, both extra protons are lost to the solution, leaving only one of the nitrogen atoms positive charged [37]. In alkaline solutions, nucleophilic hydroxyl ions attack the electrophilic central carbon to produce the colorless triphenylmethanol or carbinol form of the dye. Suhail et al. [44] studied the effect of pH = 11 and pH = 12 on crystal violet dye but they did not consider this pH value because at pH = 11 turning color of crystal violet from violet to pale yellow, and this shows that the dye molecule structure is convert from case of saline formula to OH$^-$ within pH = 11 therefore, the dyes is deposited at the bottom reaction vessel at this pH. The primary decolorization of synthetic waste water (crystal violet dye solution) in HC was performed by pumping of liquid solution through the cavitation device (circular venturi). Samples were taken for every 30 min over the time span of 90 min of experiment and analyzed for the UV absorbance for finding out the percentage decolorization of crystal violet dye in aqueous solution. Fig. 9 shows the extent of CV decolorization from the analysis of UV–Vis absorption spectra of crystal violet dye decolorization as a function of time. Concentration of CV decolorized in the presence of HC alone as a function of time was shown in the Fig. 10. It has been observed that crystal violet dye was decolorized up to ~45% when HC alone was alone used for 90 min.

The hydrodynamic characteristic of the cavitating device (circular Venturi) has been studied by measuring the flow rate in main line. The calculated CV for a circular venturi at an inlet pressure of 5 kg/cm^2 is 0.15 (CV = 0.15) according to the following equation [10,45]:
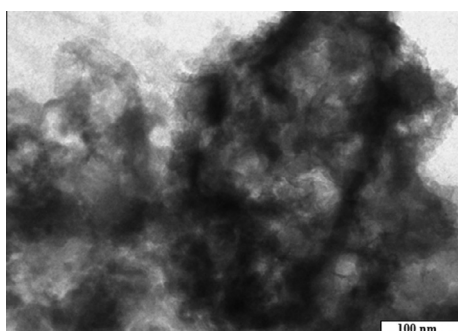
Fig. 7. TEM image of 1.6 mol% of Fe doped-TiO$_2$.
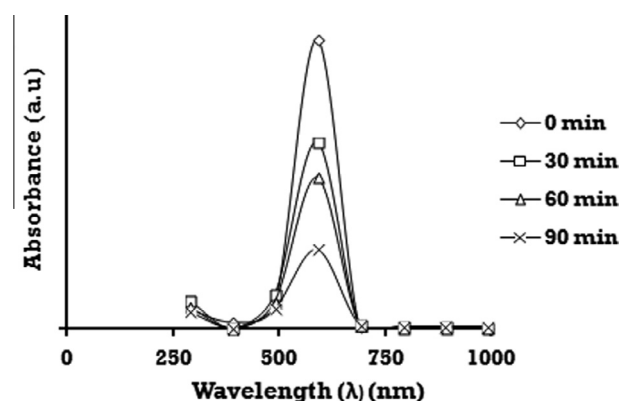
Fig. 9. Identification of CV decolorization from UV–Vis absorption spectra analysis [HC alone].

$$CV = \frac{P_2 - P_v}{\frac{1}{2}\rho v_0^2} \qquad (2)$$

where

P_2 = fully recovered downstream pressure in kg/cm^2.
P_v = vapor pressure of the dye solution in kg/cm^2.
ρ = density of the dye solution in kg/m^{-3}.
v_0 = velocity of the dye solution at the throat of the cavitating constriction in m/s.

3.4. Effect of Fe–TiO$_2$ on CV decolorization

In a typical experimental study, UV photocatalysis has been coupled with hydrodynamic cavitation (HC) to make a hybrid advanced oxidation process (HAOP) for studying the synergy of the decolorization of crystal violet dye solution. In a typical hybrid AOP, 5 L of crystal violet dye solution consisting of 50 mg/L of dye and 0.6 g/L of 0.8% Fe–TiO$_2$ were used to study the decolorization rate of crystal violet dye at it's solution pH of 6.5. Samples were taken, filtered and tested using the UV spectrophotometry, after every 30 min interval in the total decolorization time of 90 min. similar procedure was followed for 1.6% of Fe–TiO$_2$ for finding out the decolorization rate of crystal violet dye following HAOP. It was observed that, 0.8% Fe–TiO$_2$ showed the extent of decolorization to 98%. Whereas 1.6% of Fe–TiO$_2$ showed the decolorization of 85% in 90 min of treatment.

Shirsath et al. [31] reported that, as doping content of iron on TiO$_2$ increased from 0.4 mol% to 1.2 mol%, the photocatalytic activity of the Fe doped TiO$_2$ increased but above 1.2 mol%, the photocatalytic activity of Fe doped TiO$_2$ decreased with an increase in the iron content. They also reported that small quantity of iron in TiO$_2$ is responsible for a reduction in the photo-generated hole–
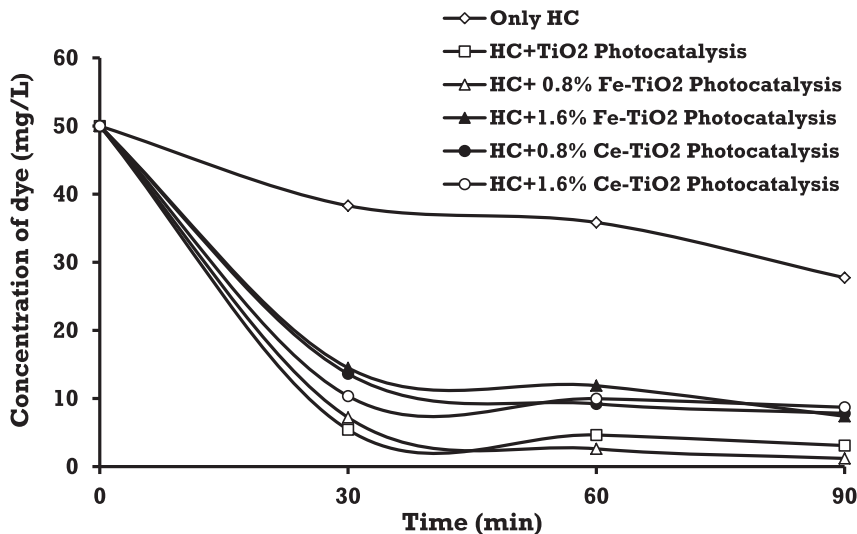
Fig. 10. Concentation of CV decolorized with respect to time [at pH = 6.5, inlet pressure = 5 bar, temperature = 35 °C, initial dye concentration 50 mg/L].

electron recombination rate. But at higher loadings, iron ions can serve as recombination centers and the photocatalytic activity of Fe doped TiO_2 decreases. This phenomenon is also demonstrated in some of the earlier investigations [2,6,24]. The results obtained with Fe doped TiO_2 and HC work was also matches with the results obtained by Shirsath et al. [31], in brief discussion, in this work doping has been carried out between 0 and 1.6 mol% i.e. doping with 0.8 and 1.6 mol% has been carried out. The doping of 0.8 mol% gives the maximum decolorization of 98%, whereas 1.6 mol% shows the reduction in decolorization. Doping with 1.6 mol% shown in reduction in decolorization has been reconfirmed from the results obtained by Shirsath et al. [31]. Thus, in this study 0.8 mol% iron doping on TiO_2 has been considered as the optimum doping concentration for the decolorization of crystal violet dye.

3.5. Effect of Ce–TiO$_2$ on CV decolorization

In this method, the prepared Ce–TiO_2 nanophotocatalyst with different doping percentages of 0.8% and 1.6% (Ce:TiO_2 mol%) was used for the decolorization studies of crystal violet dye. Each

photocatalyst having 0.6 g/L of catalysts loading were tried for the decolorization studies. All the remaining parameters such as pH, dye concentration, volume of dye solution, temperature and pressure are kept constant throughout the process and were same as before. From the results, 0.8% Ce–TiO_2 showed the decolorization of ~84%. Whereas, 1.6% of Ce–TiO_2 showed the decolorization of ~82%. It was observed that the Ce doped TiO_2 did not show a significant effect on the degradation of crystal violet dye compared to the Fe doped TiO_2. It has been observed that crystal violet dye decoloration increased as the Ce content increased in the Ce-doped TiO_2 catalyst up to 1.0% i.e. 0.8% of Ce content. The increase in Ce loading may be attributed the photocatalytic activity of Ce doped TiO_2 by trapping of electrons in cerium sites with their subsequent transfer to the absorbed O_2 [30]. However, if the doping of Ce amount is continued to increase from 1.0% to 3.0%, then excess Ce dopant may introduce the indirect recombination of electrons and holes to reduce the photocatalytic activity, leading to a significant decrease in decolorization [25,30]. It has been observed that the degradation efficiency was higher when Ce content was below or equal to 1.0% in the TiO_2 catalyst and achieved 84% color removal after 90 min of treatment. While, the
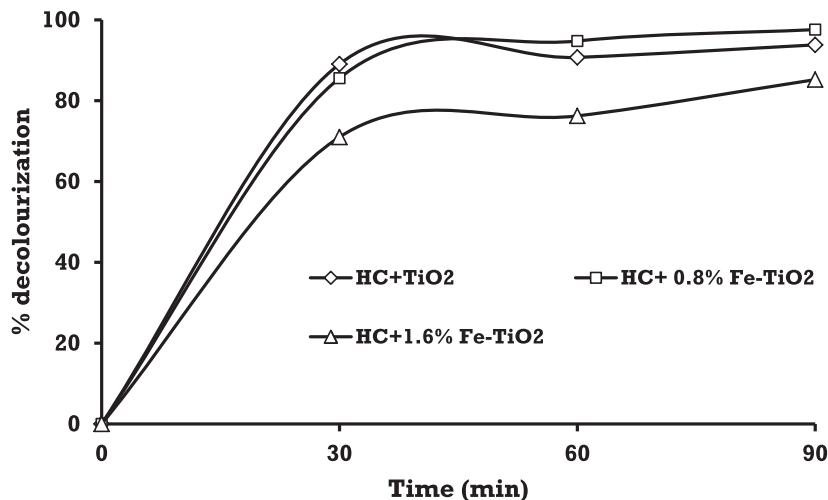
Fig. 11a. Percentage decolorization of CV dye in HC combined with pure TiO_2 and Fe doped TiO_2 [at pH = 6.5, inlet pressure = 5 bar, temperature = 35 °C, initial dye concentration 50 mg/L].
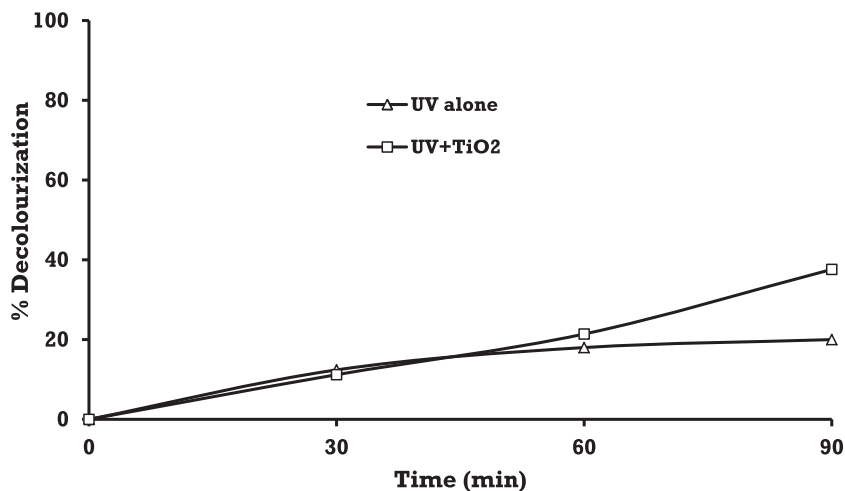
Fig. 11b. Percentage decolorization of CV dye in photolytic and photocatalytic processes [at pH = 6.5, inlet pressure = 5 bar, temperature = 35 °C, initial dye concentration 50 mg/L].
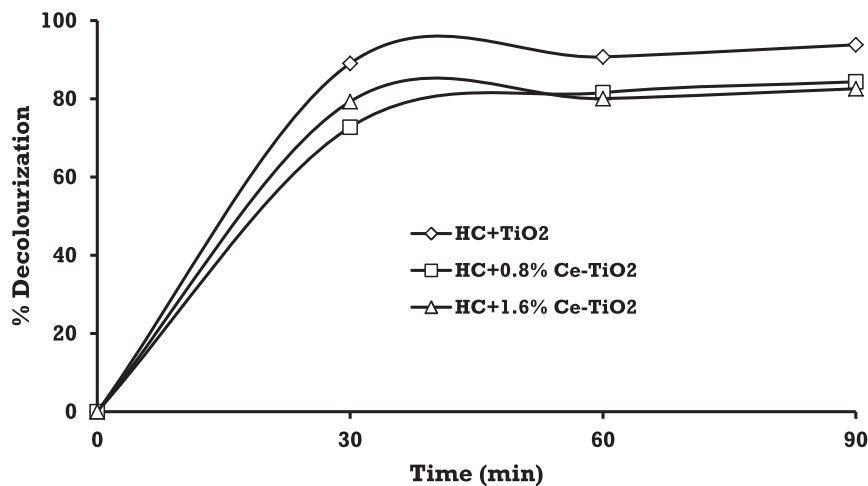
Fig. 11c. Percentage decolorization of CV dye in HC combined with Ce–TiO$_2$ [at pH = 6.5, inlet pressure = 5 bar, temperature = 35 °C, initial dye concentration 50 mg/L].
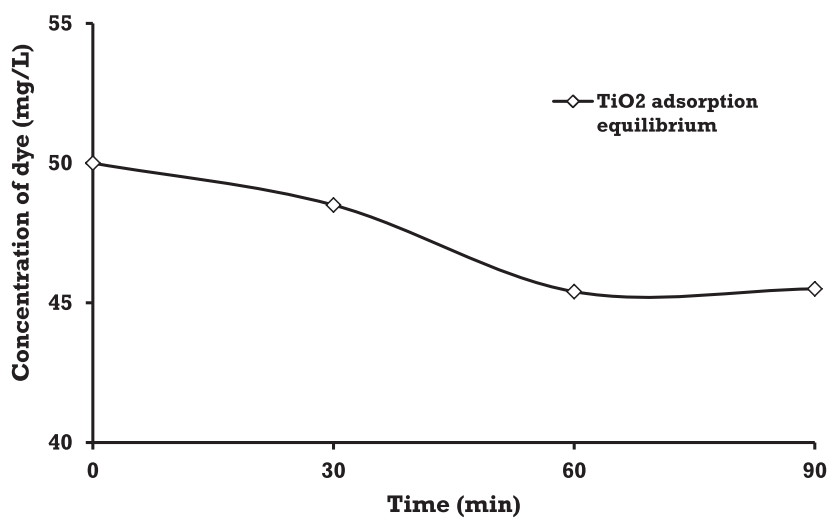
Fig. 12. Adsorption behavior of pure TiO$_2$ as a function of time.

decolorization efficiency was lower when Ce content was 1.6%, achieved 82% of color removal at the same time. This effect has been also observed in other reports [25, 30, and 31]. The results obtained in this work was also matches with the results obtained by the Ramirez et al. [33]. They have been studied the acid orange 7 (AO7) decolorization using Ce doped TiO_2 photocatalysts and reported lower photocatalytic activity for Ce doped TiO_2 than the pure TiO_2. Hence, in this study 0.8 mol% of Ce doping on TiO_2 has been considered as optimum loading concentration for decourization of crystal violet dye.

3.6. Effect of undoped TiO_2 on CV decolorization

To understand the effect of undoped TiO_2, 0.6 g/L of undoped TiO_2 were used for the decolorization of crystal violet dye at its normal pH (6.5) using HAOP. From the UV–Vis absorption spectra, it was observed that the crystal violet dye has been decolorized up to 94% when TiO_2 used along with HC. It has been observed that the undoped TiO_2 shown higher decolorization rate than 1.6% Fe–TiO_2, Ce–TiO_2 and 0.8% Ce–TiO_2. However shows less decolorization than 0.8% Fe–TiO_2. Graphical representation of percentage decolorization of CV dye in various systems was shown in the Fig. 11a–c.

3.7. Comparison of adsorption, photolytic, photo catalytic, HC+ photo catalytic processes

Initially, a study on adsorption equilibrium for TiO_2 surface has been established in 1 L of crystal violet dye solution. Further, we have evaluated the time required for achieving the adsorption equilibrium as well as the maximum amount of CV dye adsorbed onto the TiO_2 surface. This was attempted under agitation prior

to carry out the actual experiments. Initially the crystal violet dye mixture was taken in a 1 L beaker and agitation was carried out with magnetic stirrer for 90 min in the dark environment to establish the equilibrium adsorption characteristics of undoped TiO_2. With the above procedure a maximum of 9% of crystal violet dye was adsorbed on to the TiO_2 (0.6 g/L loading) surface and adsorption equilibrium was obtained within 60 min of contact time. The equilibrium adsorption stage has been evaluated from the Fig. 12 contains a plot of concentration of CV dye Vs time. It has been observed from Fig. 12 the adsorption behavior of undoped TiO_2 after 60 min has shows no reduction in concentration of the CV dye with extended time of contact.

Degradation of CV dye in photolytic process due to the generation of hydroxyl radicals by the dissociation of water molecules under UV irradiations. During the photolytic process, crystal violet dye decolorized up to 20%. Hence in photocatalytic process, the generation of hydroxyl radicals is more as compared to photolytic process, in this process, crystal violet dye has been decolorized up to 37.6%. It was observed that the maximum extent of decolorization of 94% was obtained using combined HC/UV + TiO_2 process, whereas, 44.5% and 37.6% of decolorization was obtained in HC and UV + TiO_2 alone respectively. The extent of decolorization in hybrid process has been attained due to generation of greater hydroxyl radical compared to individual operating processes (HC alone or UV + TiO_2 alone).

Synergetic effect of combined processes has been evaluated on the basis of reaction rate constant data of single and combined process. The synergetic index of the HC combined with TiO_2 photocatalysis has been calculated to evaluate the efficiency of the combined process of HC and TiO_2 photocatalysis to compare with individual process (HC and TiO_2 photocatalysis alone). The synergetic index (f) of HC combined with TiO_2 photocatalysis has been calculated by using the following equation shows synergetic effect of hybrid AOP:

$$f_{(HC+TiO_2\ photocatalysis)} = \frac{k_{(HC+TiO_2\ photocatalysis)}}{k_{(HC)} + k_{(TiO_2\ photocatalysis)}}$$
$$= \frac{0.0275}{0.003 + 0.0048}$$
$$= 3.52 \qquad (3)$$

3.8. Rate kinetics of CV decolorization

The degradation of organic pollutants in hydrodynamic cavitation will be occur by the generation of ·OH radicals and also

Table 2
Reaction rate constants (k) of CV degradation in different systems [at pH = 6.5, inlet pressure = 5 bar, temperature = 35 °C, initial dye concentration 50 mg/L].

Method	k Value (min^{-1})	Synergetic coefficient
UV alone	0.0029	–
UV + TiO_2	0.0048	–
HC	0.003	–
HC + TiO_2	0.0275	3.52
HC + TiO_2 + 0.8% Fe	0.0332	–
HC + TiO_2 + 1.6% Fe	0.017	–
HC + TiO_2 + 0.8% Ce	0.0289	–
HC + TiO_2 + 1.6% Ce	0.0302	–
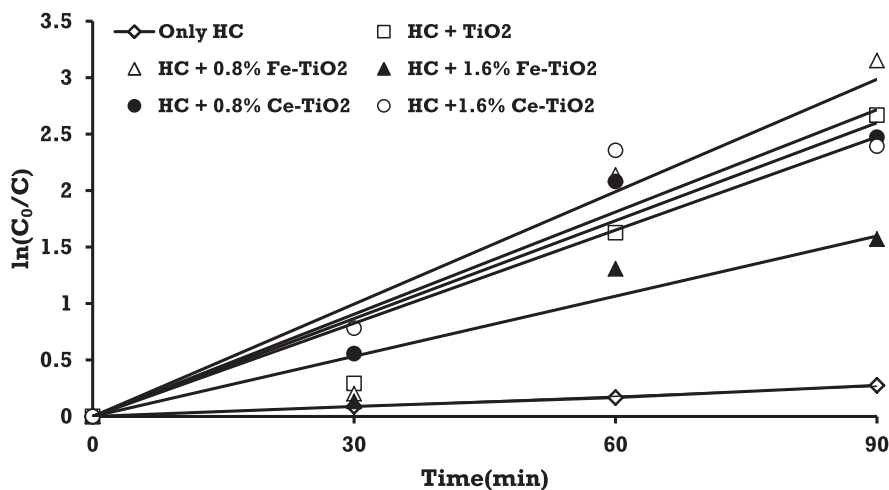
Fig. 13. Pseudo first order reaction kinetics of CV decolorization in HC and its combination with photocatalysis.
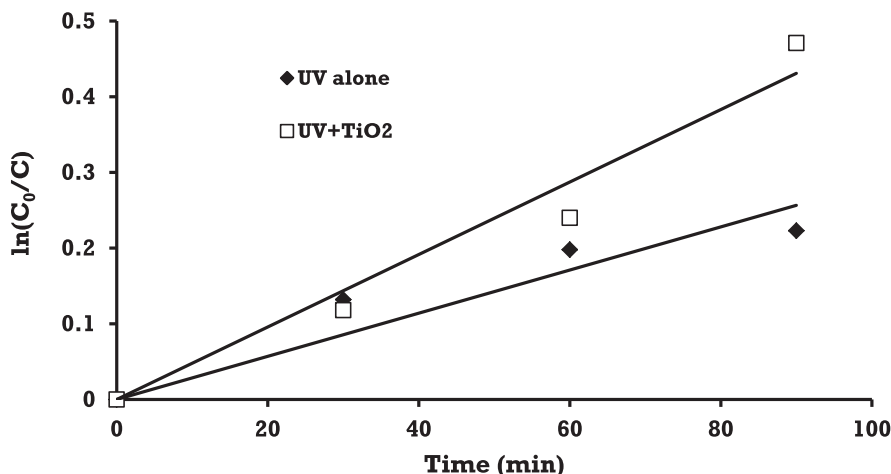
Fig. 14. Pseudo first order reaction kinetics of CV decolorization in photolytic and photocatalysis.

possibly due to the breakage of chromophore. These $^\cdot$OH radicals are rapidly react with CV dye, which is present at the interface of the cavities and the waste water. Most of the investigators reported that the degradation reactions of many organic pollutants in advanced oxidation processes followed a pseudo first order reaction. The rate constants of degradation reaction of CV dye has been calculated using the following equation:

$$\ln\left(\frac{C_0}{C}\right) = k \times t \tag{4}$$

where 'C' is the concentration of dye molecules present in mol/L, 'k' is the rate constant in min^{-1} and 't' is the time in minutes.

The kinetic mechanism for decolorization of CV dye using hydrodynamic cavitation coupled with photocatalysis followed a first order reaction as confirmed by the plot of $\ln\left(\frac{C_0}{C}\right)$ vs. time (t). The plot of $\ln\left(\frac{C_0}{C}\right)$ vs. time (t) is a straight line and it passes through the origin. Reaction rate constants (k) of CV decolorization in different systems (HC alone and HC + photocatalysis) has been reported in Table 2. Pseudo reaction kinetics of CV decolorization in various systems was shown in the Figs. 13 and 14.

4. Conclusion

From this work, it has been concluded that, a novel synthesis technique was successfully implemented for the production of undoped and doped TiO_2 nanophotocatalysts. Photocatalysts prepared by sonochemical technique has shown good and uniform doping on TiO_2 and confirms the crystalline nature, when it is calcined at 200 °C. Approximately half of the CV dye in aqueous solution has been decolorized when the HC is used alone. Whereas, further decolorization has been achieved when hybrid technique (HC + photocatalysis) was used. In the hybrid technique, 0.8% Fe-doped TiO_2 photocatalyst has shown the maximum decolorization about 98% than other photocatalysts such as Ce-TiO_2 and pure TiO_2.

Acknowledgment

References

[1] Y. Anjaneyulu, N. Sreedhara Chary, D. Samuel Suman Raj, Decolourization of industrial effluents available methods and emerging technologies a review, Rev. Environ. Sci. Biotechnol. 4 (2005) 245–273.

[2] U.G. Akpan, B.H. Hameed, Parameters affecting the photocatalytic degradation of dyes using TiO_2-based photocatalysts: a review, J. Hazard. Mater. 170 (2009) 520–529.

[3] G.L. Baughman, E.J. Weber, Transformation of dyes and related compounds in anoxic sediments: kinetics and products, Environ. Sci. Technol. 28 (1994) 267–276.

[4] S. Papic, D. Vujevic, N. Koprivanac, D.S. Inko, Decolorisation and mineralization of commercial reactive dyes by using homogeneous and heterogeneous Fenton and UV/Fenton processes, J. Hazard. Mater. 164 (2009) 1137–1145.

[5] M.S. Lucas, J.A. Peres, Decolorization of the azo dye reactive Black 5 by Fenton and photo-Fenton oxidation, Dyes Pigm. 71 (2006) 236–244.

[6] S. Velazquez-Peña, C. Sáez, P. Cañizares, I. Linares-Hernández, V. Martínez-Miranda, C. Barrera-Díaz, M.A. Rodrigo, Production of oxidants via electrolysis of carbonate solutions with conductive-diamond anodes, Chem. Eng. J. 230 (2013) 272–278.

[7] Y.G. Adewuyi, Sonochemistry in environmental remediation. 2. Heterogeneous sonophotocatalytic oxidation processes for the treatment of pollutants in water, Environ. Sci. Technol. 39 (2005) 8557–8570.

[8] J. Chen, M. Liu, J. Zhang, X. Ying, L. Jin, Photocatalytic degradation of organic wastes by electrochemically assisted TiO_2 photocatalytic system, J. Environ. Manage. 70 (2004) 43–47.

[9] F. Parolin, U.M. Nascimento, E.B. Azevedo, Microwave-enhanced UV/H_2O_2 degradation of an azo dye (tartrazine): optimization, colour removal, mineralization and ecotoxity, Environ. Technol. 34 (2013) 1247–1253.

[10] K.M. Kalumuck, G.L. Chahine, The use of cavitating jets to oxidize organic compounds in water, J. Fluids Eng. Trans. ASME 122 (2000) 465–470.

[11] X. Wang, J. Wang, P. Guo, W. Guo, C. Wang, Degradation of Rhodamine B in aqueous solution by using swirling jet-induced cavitation combined with H_2O_2, J. Hazard. Mater. 169 (2009) 486–491.

[12] X. Wang, J. Jia, Y. Wang, Electrochemical degradation of reactive dye in the presence of water jet cavitation, Ultrason. Sonochem. 17 (2010) 515–520.

[13] K.S. Suslick, M.M. Mdleleni, J.T. Ries, Chemistry induced by hydrodynamic cavitation, J. Am. Chem. Soc. 119 (1997) 9303–9304.

[14] P.R. Gogate, A.B. Pandit, Engineering design methods for cavitation reactors II: hydrodynamic cavitation, AIChE J. 46 (2000) 1641–1649.

[15] M. Zhou, J. Yu, B. Cheng, Effects of Fe-doping on the photocatalytic activity of mesoporous TiO_2 powders prepared by an ultrasonic method, J. Hazard. Mater. B137 (2006) 1838–1847.

[16] H. Wang, J. Niu, X. Long, Y. He, Sonophotocatalytic degradation of methyl orange by nano-sized Ag/TiO_2 particles in aqueous solutions, Ultrason. Sonochem. 15 (2008) 386–392.

[17] Y. Li, S. Peng, F. Jiang, G. Lu, S. Li, Effect of doping TiO_2 with alkaline-earth metal ions on its photocatalytic activity, J. Serb. Chem. Soc. 72 (2007) 393–402.

[18] U.G. Akpan, B.H. Hameed, Enhancement of the photocatalytic activity of TiO_2 by doping it with calcium ions, J. Colloid Interface Sci. 357 (2011) 168–178.

[19] Y.H. Peng, G.F. Huang, W.Q. Huang, Visible-light absorption and photocatalytic activity of Cr-doped TiO_2 nanocrystal films, Adv. Powder Technol. 23 (2010) 8–12.

[20] M.A. Barakat, H. Schaeffer, G. Hayes, S. Ismat-Shaha, Photocatalytic degradation of 2-chlorophenol by Co-doped TiO_2 nanoparticles, Appl. Catal. B: Environ. 57 (2004) 23–30.

[21] A.M.T. Silva, C.G. Silva, G. Drazic, J.L. Faria, Ce-doped TiO_2 for photocatalytic degradation of chlorophenol, Catal. Today 144 (2009) 13–18.

[22] M.A. Rauf, M.A. Meetani, S. Hisaindee, An overview on the photocatalytic degradation of azo dyes in the presence of TiO_2 doped with selective transition metals, Desalination 276 (2011) 13–27.

[23] K. Koci, K. Mateju, L. Obalova, S. Krejcikova, Z. Lacny, D. Placha, L. Capek, A. Hospodkova, O. Solcov, Effect of silver doping on the TiO_2 for photocatalytic reduction of CO_2, Appl. Catal. B: Environ. 96 (2010) 239–244.

[24] Y. Li, C. Xie, S. Peng, G. Lu, S. Li, Eosin Y-sensitized nitrogen-doped TiO_2 for efficient visible light photocatalytic hydrogen evolution, J. Mol. Catal. A: Chem. 282 (2008) 117–123.

[25] M. Asilturk, F. Sayılkan, E. Arpac, Effect of Fe^{3+} ion doping to TiO_2 on the photocatalytic degradation of Malachite Green dye under UV and visirradiation, J. Photochem. Photobiol. A: Chem. 203 (2009) 64–71.

[26] H.K. Shon, D.L. Cho, S.H. Na, J.B. Kim, H.J. Park, J.H. Kim, Development of a novel method to prepare Fe- and Al-doped TiO_2 from wastewater, J. Ind. Eng. Chem. 15 (2009) 476–482.

[27] S. Chang, W. Liu, Surface doping is more beneficial than bulk doping to the photocatalytic activity of vanadium-doped TiO_2, Appl. Catal. B: Environ. 101 (2011) 333–342.

[28] N. Venkatachalam, M. Palanichamy, B. Arabindoo, V. Murugesan, Enhanced photocatalytic degradation of 4-chlorophenol by Zr^{4+} doped nano TiO_2, J. Mol. Catal. A: Chem. 266 (2007) 158–165.

[29] Z.L. Shi, C. Du, S.H. Yao, Preparation and photocatalytic activity of cerium doped anatase titanium dioxide coated magnetite composite, J. Taiwan Inst. Chem. Eng. 42 (2011) 652–657.

[30] J. Wang, Y. Lv, L. Zhang, B. Liu, R. Jiang, G. Han, R. Xu, X. Zhang, Sonocatalytic degradation of organic dyes and comparison of catalytic activities of CeO_2/TiO_2, SnO_2/TiO_2 and ZrO_2/TiO_2 composites under ultrasonic irradiation, Ultrason. Sonochem. 17 (2010) 642–648.

[31] S.R. Shirsath, D.V. Pinjari, P.R. Gogate, S.H. Sonawane, A.B. Pandit, Ultrasound assisted synthesis of doped TiO_2 nano-particles: characterization and comparison of effectiveness for photocatalytic oxidation of dyestuff effluent, Ultrason. Sonochem. 20 (2013) 277–286.

[32] R.L. Narayana, M. Matheswaran, A.A. Aziz, P. Saravanan, Photocatalytic decolourization of basic green dye by pure and Fe, Co doped TiO_2 under daylight illumination, Desalination 269 (2011) 249–253.

[33] R.J. Ramirez, J.V. Sanchez, S.S. Martinez, Solar assisted degradation of acid orange 7 textile dye in aqueous solutions by Ce-doped TiO_2, Mex. J. Sci. Res. 1 (2012) 42–55.

[34] L. Andronic, D. Andrasi, A. Enesca, M. Visa, A. Duta, The influence of titanium dioxide phase composition on dyes photocatalysis, J. Sol–Gel. Sci. Technol. 58 (2011) 201–208.

[35] S. Samira, P. Akash Raja, C. Mohan, J.M. Modak, Photocatalytic degradation of crystal violet (C.I. basic violet 3) on nano TiO_2 containing anatase and rutile phases (3:1), J. Thermodyn. Catal. 3 (2012).

[36] M. Sivakumar, A.B. Pandit, Wastewater treatment: a novel energy efficient hydrodynamic cavitational technique, Ultrason. Sonochem. 9 (2002) 123–131.

[37] L. Angeloni, G. Smulevich, M.P. Marzocchi, Resonance Raman spectrum of crystal violet, J. Raman Spectrosc. 8 (1979) 305–310.

[38] X. Wang, J. Jia, Y. Wang, Degradation of C.I. reactive red 2 through photocatalysis coupled with water jet cavitation, J. Hazard. Mater. 185 (2011) 315–321.

[39] M.V. Bagal, P.R. Gogate, Degradation of diclofenac sodium using combined processes based on hydrodynamic cavitation and heterogeneous photocatalysis, Ultrason. Sonochem. 21 (2014) 1035–1043.

[40] I.H. Perez, A.M. Maubert, L. Rendón, P. Santiago, H.H. Hernández, L. Díaz Arceo, V. Garibay Febles, E.P. González, L. González-Reyes, Ultrasonic synthesis: structural, optical and electrical correlation of TiO_2 nanoparticles, Int. J. Electrochem. Sci. 7 (2012) 8832–8847.

[41] H.K. Shon, S. Vigneswaran, J. Kandasamy, M.H. Zareie, J.B. Kim, D.L. Cho, J.H. Kim, Preparation and characterization of titanium dioxide (TiO_2) from sludge produced by $TiCl_4$ flocculation with $FeCl_3$, $Al_2(SO_4)_3$ and $Ca(OH)_2$ coagulant aids in wastewater, Sep. Sci. Technol. 44 (2009) 1525–1543.

[42] Y. Xie, C. Yuan, Visible-light responsive cerium ion modified titania sol and nanocrystallites for X-3B dye photodegradation, Appl. Catal. B: Environ. 46 (2003) 251–259.

[43] S.T. Hayle, G.G. Gonfa, Synthesis and characterization of titanium oxide nanomaterials using sol–gel method, Am. J. Nanosci. Nanotechnol. 2 (2014) 1–7.

[44] F.S.A. Suhail, M.S. Mashkour, D. Saeb, The study on photo degradation of crystal violet by polarographic technique, Int. J. Basic Appl. Sci. 15 (2015) 12–21.

[45] P. Senthil Kumar, M. Siva Kumar, A.B. Pandit, Experimental quantification of chemical effects of hydrodynamic cavitation, Chem. Eng. Sci. 55 (2000) 1633–1639.

Accepted Manuscript

Title: Nanomaterials based Advanced Oxidation Processes for Waste Water Treatment: A review

Author: Bhaskar Bethi Shirish H. Sonawane Bharat A. Bhanvase Sarang Gumfekar
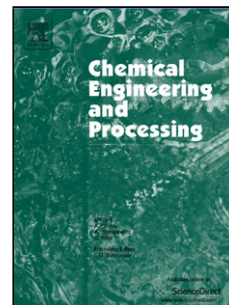
Please cite this article as: Bhaskar Bethi, Shirish H.Sonawane, Bharat A.Bhanvase, Sarang Gumfekar, Nanomaterials based Advanced Oxidation Processes for Waste Water Treatment: A review, Chemical Engineering and Processing http://dx.doi.org/10.1016/j.cep.2016.08.016

Nanomaterials based Advanced Oxidation Processes for Waste Water Treatment: A review

Bhaskar Bethi[a], Shirish H. Sonawane[a]*, Bharat A. Bhanvase[b], Sarang Gumfekar[c]

[a]Department of Chemical Engineering, National institute of Technology, Warangal-506004, Telangana state, India.

[b]Chemical Engineering Department, Laxminarayan Insitutite of Technology, Rashtrasant Tukadoji Maharaj Nagpur University, Nagpur-440033, Maharashtra, India

[c]Chemical and Materials Engineering Department,University of Alberta, Edmonton, Canada

* Corresponding Author

E-mail: shirish@nitw.ac.in

Tel: . 0870-2462626

Research Highlights

- Nanomaterials based single advanced oxidation processes for wastewater treatment.

- Nanomaterials based hybrid advanced oxidation processes for wastewater treatment.

- Current status of work on hybrid nanomaterials as heterogeneous photocatalysts.

- Process Intensification of nanostructured materials in waste water oxidation.

- Mechanistic aspects of various advanced oxidation processes.

Abstract

Over the past decades advanced oxidation processes (AOPs) in wastewater treatment established a great deal of attention of the researchers. AOP's are one of the promising advanced technologies used to destroy the total organic content, toxic pollutants etc. Number of attempts has been made from the past two decades on the waste water treatment using various advanced oxidation treatment techniques. The main objective of this review article is to provide the quick reference for researchers and academicians in the area of wastewater treatment using nanomaterials conjunction with various AOP's and/or hybrid AOP's. This review article mainly focused on (1) the nanomaterials assisted individual and hybrid advanced oxidation processes for treatment of various industrial effluents or model effluents, (2) the current status of work in the area of hybrid nanomaterials as heterogeneous catalysts combined with AOPs and hybrid advanced oxidation processes.

Keywords: Waste water treatment; Nanoparticles; Nanocatalyst; Advanced oxidation process (AOP); Photo catalysis; Hybrid systems

Contents

1. Introduction

Today the entire world is facing drinking water scarcity due to the contamination of ground water and the discharge of untreated or partially treated industrial waste water. Potable water demand is increasing day by day due to expontial growth of population and it's become severe problem to be solved for sustainable society needs [1]. So far the chemical manufacturing industries are depends on the conventional waste water treatment techniques such as chemical oxidation, biological treatment, electrochemical decomposition, photo catalytic, physical and physico-chemical treatment. Among these treatment methods, few of them utilizes chemicals (catalyst, intiators etc) to decompose the organic contaminates in the water. Recovery of such chemicals after treatment of waste water is another issue need to be addressed. Conventional treatment methods are reported to be inefficient as some contaminants found in wastewater are recalcitrant to some degree [2]. A novel advanced treatment method is needed to destroy the organic contents in the waste water. In the past two decades research has been progressed on the waste water treatment using advanced oxidation processes. Few studies attempted the step of using nano particles as an effective adsorbents and catalysts instead of micro meter size particles in the waste water treatment with the AOP's. Number of articles found related to the application of nanoparticles in the advanced oxidation processes (AOP's) for waste water treatment. AOP's generate extremely reactive ·OH radicals that are responsible for the degradation of pollutents spotted in the wastewater. These ·OH radicals attack the organic molecules rapidly and non-selectively. AOP's can be called as versatile technologies due to the production of hydroxyl radicals by various alternative ways. AOP's can generate the less toxic intermediate products during the degradation of organic pollutants. As compared to conventional treatment techniques AOPs are more efficient and capable of degrading recalcitrant organic pollutants. Interestingly, few specific AOPs can also operate on natural light source (sun light) rather than using artificial light sources (UV, Visble, Mercury etc.). AOP's such as ozonation (O_3), ozone combined with

hydrogen peroxide (O_3/H_2O_2) and UV irradiation (O_3/UV) or both ($O_3/H_2O_2/UV$), ozone combined with catalysts ($O_3/catalysts$), UV/H_2O_2, Fenton, photo-Fenton processes (Fe^{2+}/H_2O_2 and $Fe^{2+}/H_2O_2/UV$), the ultrasonic cavitation process and photo catalysis have been successfully used for wastewater treatment. Significant research has been done in the area of water purification using nanomaterials and it was concluded that nanomaterials are able to remove the pollutants and germs efficiently. Nanomaterials such as nanoparticles, nanomembrane and nanopowder has been successfully used for the detection and removal of various chemicals and biological substances which includes the metals such as mercury, nickel, cadmium, lead, copper and zinc etc, algae, organics, bacteria, viruses, nutrients, cyanide and antibiotics. Appropriate attempts have been made for using advanced nanotechnology in water purification for making potable water. Nanotechnology, is the deliberate manipulation of matter at size scales of less than 100 nm, holds the promise of creating new materials and devices which take advantage of unique phenomena realized at those length scales [3]. Generally the high surface area to volume/mass ratios of nanomaterials will greatly improve the adsorption properties of sorbent materials. Recent studies on waste water treatment using nanotechnology has reported many nanomaterials in the literature, which includes the semiconductors, nanoclay, nanocatalyst, nanoclusters, nanorods, nano composites, the reported nanoparticles are mainly TiO_2 [4], [5] and [7], palladium, Fe_3O_4 [6], cerium oxide [8], magnetic chitosan [9]. Few researchers are also attempted waste water treatment using nanocomposites made up of two or more different materials such as $CoxFe_3-xO_4$, $CoFe_2O_4$ magnetic nanoparticles, $BiAg_xO_y$ (bismuth silver oxide, BSO).

In this report, we have classified the important nanoparticles which are useful for the degradation of organic matter in waste water. Such as, (1) Dendrite polymers, (2) Metal oxide nanoparticles, (3) Zeolites, (4) Carbonbased nanomaterials [10]. Following are the different

types of nanomaterials that have been used for removal/degradation of organic speices in waste water.

1.1 Dendrite polymers

Polymeric dendrimers are random hyper branched polymers. Dendrigraft polymers and dendrons will come under the catageory of dendrite polymers. They mainly consist of a spherical macromolecules nature and composed of dense shell morphology with crosslinking sites and terminal groups that ultimately produce a properly defined structure [11]. Dendrimers can be produce in differenct structures notably cone, sphere, and disc type consists of 2 to 20 nm size range. Different dendrimer structures can be produce by the reaction between too many dendrons consists of multi-functional properties. Scientists have been synthesized approximately one hundred different dendrimer families based on the various compositions and several chemical surface modifications [12], [13] and [14]. The organics pollutents and heavy metals can be removed using dendrimers as adsorbents. The interior shell of the dendrimers exhibits the hydrophobic nature for the adsorption of organic pollutents. Whereas the outside shell of dendrimers is made up of hydroxyl- or amine-terminated functional groups for adsorption of heavy metals. Cu(II) ions from aqueous solutions has been removed using the ultrafiltration enhanced dendron and poly (amidoamine) dendrimers with ethylene diamine as a core and terminal amine groups [15]. Dendritic polymers are efficient adsorbents for recovering toxic metal ions, radio nuclide and organic solutes from water [16]. With these features dendritic polymers are became popularized in the application of water purification [17]. Without loss of solubility, the poly (amidoamine) dendrimer (PAMAM) incorporated silver nanocomposites has shown the excellent antimicrobial activity against *S. aureus, P. aeruginosa* and *E. coli* [18]. Rether and Schuster has studied the influence of ammonia, tri-ethanol amine or tartrate as representative ligands on the retention of Ni(II), Zn(II), and Cu(II) in aqueous solutions of

benzoylthiourea modified PAMAM dendrimer (PAMAM) at different pH values in the range of 5-9 [19]. Jiangand Gao have reported the competitive removal of metal ions of different initial concentrations such as Ni, Cr, Pb, Zn and Cu by PAMAM-SBA-15 and EDTA modified PAMAM-SBA-15 inorganic–organic hybrid materials. In their study organic groups were functionalized onto the mesoporous inorganic materials [20].

1.2 Metal/Metal oxide containing nanoparticles for waste water treatment.

Silver, gold, palladium metal nanoparticles have been widely studied for the wastewater treatment. Nano size silver such as colloidal silver, spun silver are typically having 10 to 200 nm in size range consists of high surface area and strong antimicrobial properties. Ag (I) and silver nanomaterial acts as an antimicrobial agent to in-activate the coli form microbes found in the wastewater [21]. Gold nanoparticles impregnated palladium has been used to destroy the trichloroethane (TCE) from groundwater. Gold nanoparticles impregnated palladium catalyst was shown the 2,200 times better than palladium catalyst alone as reported by Tobiszewski [22]. Metal oxide nanoparticles such as TiO_2, ZnO and CeO_2 have been widely used for the degradation of organic pollutants in aqueous streams. Due to high surface area and better photolytic properties [23], metal oxide nanoparicles considered as good photocatalysts for water purification. MgO and magnesium (Mg) nanoparticles are used to destroy/adsorb biocides against gram-positive and gram- negative bacteria such as *Escherichia coli* and *Bacillus megaterium*and bacterial spores (*Bacillus subtillus*) [24]. Application of nano TiO_2 and Cu_2O electrodes in electrocatalytic oxidation process was shown the efficient oxidation of organic pollutants and higher COD removal rate was reported [25]. High biocidal activity was observed towards the *Escherichia coli* and *Staphylococcusaureus* using silver- SiO_2 nanocomposite with crosslinked chitosan as an upper layer [26]. Ferrites and iron minerals, such as akaganeite, feroxyhyte, ferrihydrite, goethite, hematite, lepidocrocite, maghemite and magnetite have been utilized in adsorption processes for wastewater treatment [27]. Oxides of Iron and titanium are

good sorbents for the removal of metal contaminants from their sources. Pd/Fe_3O_4 nanocomposite catalyst has been applied for de-halogenation in wastewater treatment process [6].

1.3 Zeolites

Mostly zeolite nanoparticles have been produced by using introduction of pulsed laser on the zeolite LTA microparticles or by hydrothermal activation of fly ash. Laser-induced fragmentation of Zeolites LTA microparticles generates the zeolite nanoparticles. Zeolites have an effective ion exchange property. Zeolites have been widely used as an ion exchange media for water purification and also an effective sorbents for the removal of metallic ions from the wastewater. Zeolites employed widely for the removal of Cr(III), Ni(II), Zn(II), Cu(II) and Cd(II) heavy metals from the wastewater sources of electroplating industry and acid mines [28].

1.4 Carbon-based nanoparticles

Nanoparticles based on the carbon materials used as potential sorbents for organic solutes in aqueous solutions due to its unique advantage of high surface area and sorption capacity and selectivity. Notable cabon based nanoparticles are Fullerenes, carbon nanotubes, nano size diamonds and nano size wires. Carbon nanomaterials exhibit extreme properties such as, excellent thermal, electrical conductivity, stable, limited reactivity and strong antioxidants [29]. Enhanced colloidal stability of CNTs was achieved by the surface modification of CNTs with acid was successfully employed for the removal of Cr (VI) [9]. Multi walled CNTs have been employed to study the nature of adsorption towards the binary contaminants in aqueous media such as 2, 4, 6- trichlorophenol and Cu(II) metal ion [30]. Chitosan nano particles show enhanced absorption capacities for the acid dyes removal [31].

2. Individual AOP's involving Nanomaterials

Advanced oxidation processes (AOP's) have received the increasing attention towards the research and development of wastewater treatment technologies over the last two decades. These processes (e.g., cavitation, photocatalytic oxidation, Fenton, ozonation) have been applied successfully for the degradation of recalcitrant organic pollutants at laboratory scale. Homogeneous and heterogeneous advanced oxidation processes (AOP's) have been investigated well in advance in the area of wastewater treatment. To activate the AOP's, ultraviolet (UV) or visible light, different oxidants (O_2, H_2O_2, O_3), catalysts (TiO_2) are necessary. During the activation process, AOP's able to generate hydroxyl radicals ($\cdot OH$) reactive with organic compounds in the presence of dissolved oxygen of aqueous media. Among various industrial pollutants, printing, paper and dyeing are the major environmental polluting industries due to the extensive use of organic colors during the production process. Presence of organic colorants in aquatic bodies restricts the absorption and reflection of sunlight, and increases the toxicity concentration ultimately creates the problems to the aquatic life. Efficient AOP's can be used to obtain the complete mineralization of organic dyes. Many studies demonstrated the behavior of various AOP's towards the successful degradation of dye pollutants in aqueous media. Photo-catalytic advanced oxidation process initiates the complex chain reactions and it may produce the colourless organic intermediates. Some times these intermediates are more toxic than the parent compound. Total mineralization of the pollutant is the main objective of the advanced oxidation processes. Over the past decades, many research studies have been utilized the micro sized catalysts in photocacatlytic advanced oxidation process for the degradation of organic compounds, only few research studies have been utilizes nanomaterials as nanophotocatlysts in AOP's for the treatment of wastewater [9] and [25]. This study is aiming to review the nanomaterials assisted AOP's that are used for degradation of different organic pollutants in waste water.

2.1. Visible/UV light assisted Nanomaterials as a Photocatalyst:

Over the past two decades, nanocrystalline TiO_2 has been widely used as a photocatalyst for organic pollutent degradation from the wastewater [32], [33], [34] and [35]. Identification of intermediate products and formation of end products in the photocatalysis have been investigated in the earlier literature [36], [37], [38] and [39]. Around 70% of literature is available on photocatalysis for wastewater treatment used TiO_2 as a photocatalyst. Among them, very few studies have attempted the use of doped TiO_2 nanophotocatlysts for the treatment of wasterwater. The TiO_2 photocatalyst consist of wide bandgap (3.2 eV) and can be called as a semiconductor, corresponding to radiation in the near UV range is one of the advantage compared to other semiconductor photocatalysts. When, the UV light is irradiated on the TiO_2 surface, and then TiO_2 get excited and generates pairs of electrons and holes in the conduction and valence band. The positive hole will adsorb the surrounding water molecules and get oxidize to form a hydroxyl radical. The generartion of hydroxyl radical seems to be cyclic process and intiates the series of reactions on the TiO_2 surface as reported in **Fig. 1**. Both the photocatalyst and light source is necessary to intiate the photocatalytic oxidation reaction for the degradation of organic pollutants in the wastewater.

The possible utilization of visible light/sunlight for intiating the photocatalytic reaction has recently drawn an attention due to the utilization of UV energy is more expensive and hazardous. However, we have been discussed in brief about the articles that are reported the UV/Visible induced nanomaterials as a photocatalysts. Nogueira and Jardim demonstrated how the photobleaching of dyes could be achieved by sunlight irradiation using TiO_2 as photocatalyst [40]. Reeves et al. [41] proposed the use of high intensity sunlight for the degradation of textile dyes and non-biodegradable biological stains from wastewater. However, out of the total UV energy released from the sun, only < 5% of UVenergy reaching the surface of the earth. This UV energy is insufficient to obtain the significant photocatalytic degradation rates for the organic pollutants

in the wastewaters. Serpone's group was studied further using visible light as an energy source for photo-oxidation of dye in water system such as degradation of erythrosine and rhodamine B dye [42] and [43], and malachite green dye [44]. Many of the dyes and other organic pollutants during the degradation can generate toxic intermediates which may be hazards to environment. Degaradation of dyes may produce the intermediates, that can be substructures of parent molecules and these have been reported as carcinogenic and toxic components [45]. Ao et al. [46] studied the decolorization of anthraquinonic dye acid blue 80 using sol–gel TiO_2 thin film in the presence of photocatalytic oxidation process. Obtained results explained that formation of TiO_2 thin films at lower temperature calcination show effective decolorization in the UV region. Where as, the modified TiO_2 thin film by Cr ion implantation, shows that the light absorption was shited from UV to the visible range. Modified TiO_2 thin film by Cr ion was acted as a solar photocatalyst for the decolorization of dye for treatment of textile effluent. Zhu et al. [47] reported the crosslinked chitosan/nano-CdS composite catalyst has been employed to decolorize the Congo Red (CR) dye as model pollutant under visible light irradiation. Effect of catalyst loading, initial concentration of dye, and pH of the solution and reaction kinetics has been studied. Shukla et al. [48] investigated the phenolic compound degradation in the presence of aqueous solution using TiO_2, ZnO as a photocatalyst and persulphate as an additional radicals producing agent in the presence of UV–Vis light. It was observed that ZnO shown higher photocatalytic degradation of phenol than TiO_2 in the presence of simulated solar light. Lu et al. [49] has studied the degradation of azo dye in aqueous solutions using commercial TiO_2 nanoparticles as a photocatalyst immobilized on the inner wall of the glass reactors mounted with 8 W UV light. In this study UV light was illuminated for 4 h for the degradation of azo dye. Gao et al. [50] have prepared new photocatalyst composite i.e.Er^{3+}:$YAlO_3$/Fe-doped TiO_2–ZnO composite using ultrasound assisted and liquid boiling method. It has been reported that with an addition of luminescence agent such as Er^{3+}:$YAlO_3$ can convert the visible light present in the

solar radiations into UV light that make up the requirement of energy for the process of photocatalysitc degration using TiO_2–ZnO composite phototcatalyst. Therefore, it has been further reported that the novel Er^{3+}:$YAlO_3$/Fe-doped TiO_2–ZnO composite photocatalyst is found superior for the degradation of candidate dye compared to Fe-doped TiO_2-ZnO photocatalyst. Bansal et al. [51] studied the photocatalytic activity of TiO_2 – P25 Degussa, ZnO/TiO_2 composite towards the degradation of Acid orange 7 as a model pollutant. The results were compared with TiO_2 – P25 Degussa. ZnO/TiO_2 shows promising photocatalytic activity and shows 12% higher rate of decolorisation of the dye than that of TiO_2 – P25 Degussa. Shi et al. [52] was prepared the immobilizing Er^{3+}:$YAlO_3$/TiO_2 on the surface of the spherical shaped activated carbon as a support. Er^{3+}:$YAlO_3$/TiO_2 photocatalyst was also employed to study its photodegradation performance for methyl orange (MO) dye under visible light irradiation using LED lamp (λ >400 nm). Elamin et al. [53] have been synthesized the nanostructured ZnO materials such as nanotubes and nanosheets through the hydro-thermal route. The performance of both the phtocatalysts towards the degradation of Methyl Orange has been evaluated by using UV light (λ =253.7 nm). The obtained results concluded that ZnO nanosheets exhibited effective degradation of MO compared to nanotubes. Such result was obtained due to nanosheets attributed high surface area than the nanotubes. Pompermayer et al. [54] have studied the environmental assessment of ZnO nanophotocatalysts synthesis via six different procedures. The corresponding ZnO nanophotocatalysts have been investigated for Rhodamine B dye degradation, and they concluded that degradation rate of the Rhodamine B dye increased up to 30 times. Booshehri et al. [55] investigated the disinfection of *Escherichia coli* under visible light (λ > 420 nm) and Ag/$BiVO_4$ composites. An impregnated silver nanoparticle with the $BiVO_4$ was shown the enhanced photocatalytic activity and total disinfection of the *Escherichia coli* cells over 3 h of study. Barakat et al. [56] reported the illuminated TiO_2 catalyst was tested for the cyanide and Cu (II) ions removal form wastewater. Both free and complex cyanide have

12

been destroyed under TiO_2 with UV irradiation of 100 W. It was confirmed that photocatalytic process possesses excellent conversion of organic species in to CO_2 and nitrogen than conventional cyanide wastwater treatment processes. Muruganandham et al. [57] evaluated the performance of 30 nm particles size TiO_2-P25 (Degussa) photocatalyst under UV-A light irradiation (365 nm) for the degradation of Reactive Orange 4 (RO4). RO4 dye was completely decolourised and degraded within the period of 80 min and 180 min respectively under the optimum conditions. Dai et al. [58] studied the methyl orange photodegradation in aqueous solution by mesostructured Titania nanoparticles in the presence of UV irradiation. They are reported that 98 % MO is degraded with the use of 1.0 g/L mesostructured Titania catalyst suspension (pH 2.0) after 45 min irradiation. Tu et al. [59] reported the preparation of Fe-doped TiO_2 nanotube arrays using template-based liquid phase deposition method and its photocatalytic acticities were examined by the degradation of methylene blue dye under visible light. It was reported that the Fe doped TiO_2 nanotube arrays photocatalyst shows better photocatalytic activities under visible light irradiation.

Liu et al. [60] synthesized the TiO_2 nanotubes–polyurethane nanocomposite photocatalyst and applied for photocatalytic degradation of Rhodamine B. The prepared composite can be reused further as they act as heterogeneous phase catalyst. Wang et al. [61] studied the photodegradation of methylene blue in aqueous solutions using various photocatalysts, including TiO_2, CNT (Carbon nanotube)–TiO_2, Au–TiO_2, and Au–CNT–TiO_2 composites. Liu et al. [62] was tested the Fe doped TiO_2 nanophotocatalyst for the removal of chlorophenols from aqueous solution. The Fe/TiO_2 nanophotocatalyst was exhibited better dechlorination and effeicent oxidation of 2,4-DCP (2,4-dicholorophenol) under UV irradiation. Cui et al. [63] synthesized the γ -Fe_2O_3@SiO_2@TiO_2–Ag nanocomposites with a core–shell structure using a hydrothermal method and a sol–gel method. Photocatalytic activity of the γ-Fe_2O_3@SiO_2@TiO_2–Ag was examined under UV irradiation for the degradation of methyl orange dye solution. It was found

13

that γ -Fe_2O_3@SiO_2@TiO_2–Ag nanocomposites exhibited better photocatalytic degradation rate compared to pure TiO_2. They are reported that γ -Fe_2O_3@SiO_2@TiO_2–Ag and TiO_2 decomposed 84% and 49% of the methyl orange respectively over 1 h of UV irradiation. Sowbhagya et al. [64] have synthesized the nano-structured Se-doped ZnO photocatalyst by electrochemical method. The photocatalytic activity of the Se-doped ZnO nanoparticles was studied by the kinetics of degradation of Indigo carmine dye. The degradation efficiency of Se-doped ZnO was found to be 96 %. Wei et al. [65] carried out the series of iron-doping on to anatase TiO_2 nanotubes (Fe/TiO_2 NTs) under ultrasonic assisted sol-hydrothermal process. Photocatalytic activity of Fe/TiO_2 NTs have been studied in the presence of visible light for the degradation of candidate dye i.e. reactive brilliant red X-3B dye in aqueous solution. The dimensions of the used TiO_2NTs have been found to be 20 nm to 100 nm in length.

Cheng et al. [66] performed the comparison of nanosized ZnO with TiO_2 in presence of UVC radiation for the removal of *E. coli* from wastewater at different concentration of nanosized ZnO and TiO_2. It was reported that the nanosized ZnO is superior in the removal of *E.coli* than nanosized TiO_2. Behnajady et al. [67] employed the liquid impregnation (LI) and photo-deposition (PD) method for the synthesis of silver doped TiO_2 nanoparticles. Photocatalytic degradation of C.I. Acid Red 88 (AR 88) monoazo dye has been tested by silver doped TiO_2 using 15 W UV lamp as a photo source. The obtained result reveals the fact that silver doped TiO_2 is better than undoped TiO_2 interms of photocatalytic degradation of AR 88. Sathish kumar et al. [68] reported the preparation of magnetic $CoFe_2O_4$ and $CoFe_2O_4$/TiO_2 nanophotocatalysts by a co-precipitation method and the photocatalytic degradation of Reactive Red 120 (RR 120) were studied by varying its initial concentration and the amount of nanocatalyst loading in order to attain a maximum degradation. Doh et al. [69] developed the photocatalytic TiO_2 nanofibers by using electro spinning method for the treatment of organic compounds. To increase the photocatalytic activity and effective surface area, TiO_2 nanoparticles particles were coated on the

TiO_2 nanofibers by using sol–gel method. The degradation rate with composite TiO_2 was significantly higher than of TiO_2 nanofibers and that of TiO_2 nanoparticles by the sol–gel method.

Wong et al. [70] synthesized the copper-doped TiO_2 nanocatalysts by photo-deposition and sol–gel methods. They found that, 1% of Cu doped TiO_2 was sufficient for good photocatalytic activity. Whereas more than 1% Cu doping on TiO_2 apparently decreases the photocatalytic activity. They reported that 1% of Cu doped TiO_2 removed 100 % color and 99% of total organic carbon (TOC) over 150 min of photocatalytic reaction. Abbad et al. [71] reported the synthesis of titanium dioxide (TiO_2) nanophotocatalyst using sol-gel technique. The prepared photocatalyst was employed to degrade the chlorophenols of concentration ranges from 50 to 150 mg/L under direct solar radiation. Chlorophenols that are degraded in their study includes 2 chlorophenol (2-CP), 2, 4-dichlorophenol (2,4-DCP) and 2, 4,6-trichlorophenol (2,4,6-TCP). The obtained results concluded that 50 mgl/L of 2-CP, 2,4-DCP and 2,4,6-TCP can be degrade up to 99, 98 and 92 % receptively over 90 min of irradiation time at pH 6. Shao et al. [72] performed the preparation of $ZnFe_2O_4@ZnO$ nanophotocatalysts with enhanced photocatalytic activity using solvothermal method. The photocatalytic degradation of Methylene Blue (MB) was carried out under UV irradiation. It has been reported that the core–shell $ZnFe_2O_4@ZnO$ nanophotocatalyst have superior photocatalytic activity than neat ZnO. Liang et al. [73] developed the novel $Bi_2S_3/Bi_2O_2CO_3$ heterojunction photocatalysts. The photocatalytic activities of $Bi_2S_3/Bi_2O_2CO_3$ were examined by degrading Rhodamine B (RhB) under visible light and sunlight irradiation. They concluded that 5 mol % $Bi_2S_3/Bi_2O_2CO_3$ heterojunction photocatalyst exhibited the best photocatalytic activity (30 min under visible light, $\lambda > 400$ nm). Khataee et al. [74] was studied the degradation of C.I. Basic Red 46 in a batch photocatalytic reactor. In this study TiO_2 nanoparticles immobilized on glass beads and 30 W UV-C lamp was used. He has also developed an artificial neural network model (ANN) to predict in advance about

15

photocatalytic decolorization behavior of BR 46 solution. Deatiled photocatalytic nanoparticles used in the single AOP's has shown in **Table 1.**

3. Hybrid advanced oxidation processes involving Nanomaterials:

A combination of different AOP's have been found to be more efficient for wastewater treatment due to the high degree of energy efficiency and generation of higher quantum of hydroxyl radicals as compared to individual oxidation process. Global treatment of wastewater can be achive with hybrid AOP's. Combination of various AOP's such as $UV/O_3/H_2O_2$, photo-Fenton processes combined with ultrasound cavitation and other non-photochemical AOP's has been studied more. As well as, combination of AOP's with conventional wastewater treatment methods, mainly biological oxidation was also investigated for the treatment of wastewater. Various combination techniques have been investigated and reported in the literature for the wastewater treatment [102], [103], [104], [105] and [106]. Combination of individual AOP's (Hybrid processes) can be applied to increase the mineralization efficiency of the organic compounds. This article also presents an overview of recent work on removal of different kinds of toxic pollutants from wastewater, including aromatic compounds, dyes, pharmaceutical compounds and pesticides using hybrid advanced oxidation processes such as combination of photo-fenton with nanophotocatalyst, combination of UV/O_3 with nanophotocatalyst, sonophotocatalytic degradation, sono-fenton catalytic processes, hydrodynamic cavitation based AOP's involving nanomaterials etc.

Chen et al. [107] reported the $Co–TiO_2/Oxon/Photo$ process for the degradation of Rhodamine B. Effect of pH, [Oxon]/[RhB] molar ratio and catalyst concentration have been studied to found the extent of degradation of Rhodamine B. Bobu et al. [108] synthesized the modified laponite clay-embeded Fe nanocomposite (Fe-Lap-RD) and investigated its Photocatalytic activity towards the degradation of ciprofloxacin (CFX) medicine. Fe-Lap-RD acts as a

heterogeneous photocatalyst and hydrogen peroxide used as additional radical producing agent as well as oxidizing agent. Narendra Kumar et al. [109] have studied the degradation of non-biodegradable H-acid dye using TiO_2 in the presence of UV, UV/H_2O_2, $UV/H_2O_2/Fe^{2+}$ (photo-Fenton process), UV/TiO_2 and $UV/H_2O_2/TiO_2$ systems. They have optimized the amount of catalyst addition, effect of H-acid concentration, contact time, effect of pH in order to obtain the maximum degradation in all AOP's. The order of COD reduction in the above systems is followed as $UV/H_2O_2/TiO_2$> photo-Fenton > UV/TiO_2> UV/H_2O_2>UV. Sivasankaran et al. [110] have studied the hybrid methods like ultrasound+ (NiO/Pd, Pd/C, Pd + NiO/C), hydrogen peroxide etc., on the degradation of Congo red.

Cavitation based hybrid AOPs have been widely investigated for wastewater treatment applications, but the main focus lies on the use of ultrasonically induced cavitational process which have limitation to scale up [111] and [112]. Research has been progressed on development of efficient hybrid systems for waste water treatment using cavitation coupled with various advanced oxidation processes such as UV photocatalysis, addition of H_2O_2, cavitation coupled with photo Fenton etc. the recent literature on waste water treatment using photocatalysis and cavitation coupled with photocatalysis has been reported here.

Some of the recent studies show that ZnO doping on graphene oxide can be used as photocatalyst for waste water treatment due to its improved photocatalytic activity. Behnajady et al. [113] have studied the degradation of Malachite Green (MG) dye in the presence of ultrasonic waves (US), ultraviolet (UV) radiation and UV/H_2O_2 processes. They are concluded that $US/UV/H_2O_2$ process was the most effective process for degradation of MG from aqueous solution and it is 1.15 times more than UV/H_2O_2 process. In UV/US process the degradation of MG from aqueous solution is 1.93 and 8.29 times more than US and UV processes but it is limited for only practical aplication. Behnajady et al. [114] studied the degradation of malachite green (MG) in the aqueous media using ultrasonic bath. They were also investigated the effect of

different operational parameters on degradation of MG dye such as MG concentration, power density, temperature, mechanical agitation and addition of EtOH, 2-PrOH and iso-BuOH.

Talebian et al. [115] studied the degradation of chrome intra orange G (C.I. 18745) azo dye by ZnO nanoparticles as catalyst under UV light irradiation. They are also investigated the degradation rates of orange G dye in sonolysis, sonocatalysis, photocatalysis and sonophotocatalysis. Chakma et al. [116] have studied the ultrasound assisted decolorization/degradation of acid red 14 (azo dye) using sonochemically prepared Fe^{3+} doped ZnO. They have preapred 2 wt % Fe^{3+} doped ZnO nanoparticle by ultrasound assisted (20 kHz) method. Degradation studies were carried out using sonolysis, photocatalysis and sono–photocatalysis processes. Among these processes, sono–photocatlytic process is highly effective with maximum decolorization of 82 % with an initial dye concentration of 20 ppm. Further the sonophotocatalysis process reported to have $1.4 - 1.6$ higher reaction rates with Fe doped ZnO than pure ZnO. Salehi et al. [117] have studied the photolysis and sonophotocatalysis for the degradation of methylene blue dye pollutant over TiO_2 nanopowders. Based on the obtained results they have concluded that the basic pH of the dye solution shows the better degradation of dye. And also higher degradation percentage obtained with higher UV power and lower initial concentration of dye. Sathishkumar et al. [118] has synthesized the TiO_2 nanophotocatalyst for the enhanced photo catalytic degradation of Acid Blue 113 (AB113). The sonolytic, sonocatalytic and sonophotocatalytic degradation of AB 113 was carried out by a 42 kHz sonicator. Shirsath et al. [119] have synthesized the titanium dioxide nanoparticles doped with Fe and Ce using sonochemical approach. TEM image of Ce doped TiO_2 was shown in **Fig. 2** and TEM image of pure TiO_2 was shown in **Fig. 3**. Ultrasond cavitation technique has been used for the study of photocatalytic degradation of crystal violet dye in aqueous solution in the presence of UV light. It was observed that sonochemically prepared catalysts exhibit higher photocatalytic activity than conventional synthesis. The Ce-doped TiO_2 shows better photocatalytic activity

than Fe-doped TiO$_2$ and TiO$_2$. Schematic diagram for the synthesis of nanoparticles using sonochemical technique (ultrasound) has been shown in **Fig. 4**. It can also be used for the removal of organic pollutants by employing UV lamp in the ultrasonic reactor. Addition of catalyst in to the said ractor makes the sonophotocatalysis. Deatiled nanomaterials used in the hybrid AOP's has shown in **Table 2.**

4. Process intenensification using nanostructured materials for wastewater treatment

Process intensification mainly relates to the design and development of new apparatuses and new methods that are expected to improve the quality and quantity of the product compared to past. Intensification of process drastically reduces the size of the plant equipment, energy consumption, or waste generation, which may result into cheaper and sustainable technologies.

Process intensification only involves engineering methods and equipment. In fact, improvements attained in existing technology through development of a new chemical route or a change in composition of a catalyst, that do not qualify as process intensification. Process intensification mainly classified in to 2 categories based on the equipment and methods.Process-intensifying equipment, includes novel reactors, and intensive mixing, heat-transfer and mass-transfer devices

Process-intensifying methods, includes new or hybrid separations, integration of reaction and separation, heat exchange, or phase transition. Intensification of oxidation of organic pollutants in wastewater using process-intensifying equipments and methods has been studied well over the past. But we have been found very narrow literature on Process Intensification-effects resulting from application of nano-structured materials in wastewater oxidation. However, very few studies have been investigated the intensification of wastewater oxidation through nanostrucured materials.

Van Gerven et al. [135] made a good review on intensification of photocatalytic processes; their investigation mainly depends upon the Comparison of different photoreactor configurations.

19

Zhang et al. [136] fabricated a hybrid material (Fe^0-CNTs) to use as a micro-electrolysis in the remediation of contaminated water. Fe^0-CNTs exhibited high efficiency in the degradation of methylene blue (MB). They have been intensified the gradual reduction of absorption band over time denoting the concentration of aromatic intermediates. It indicating the effectiveness in degradation aromatic intermediates.

Behnajady et al. [137] studied the intensification of azo dye removal rate in the presence of immobilized TiO$_2$ nanoparticles and inorganic anions under UV-C Irradiation. The obtained result in their study indicates that the addition of NO3$^-$ and HCO3$^-$ ions intensifies the removal rate of AR17. They have been observed the significant synergitic effect while the combination of NO3$^-$ and HCO3$^-$ ions were studied; under the optimized RSM conditions percentage removal of AR17 was more than the sum of the percentage removal when these ions are used individually.

Wu et al. [138] studied the intensification effects of Pickering emulsions on photocatalytic degradation of nitrobenzene. ZnO nanoparticles modified with 3 wt % modifying agent shows best results in degradation of nitrobenzene. It was found that adopting the scheme of Pickering emulsion stabilized by the modified ZnO nanoparticles could effectively intensify the photocatalytic degradation of organic contaminants in wastewater treatment. Pinho et al. [139] were tested the commercial multi-walled carbon nanotubes as catalysts in wet peroxide oxidation of phenol. Experiments were carried out under the following intensified conditions such as, phenol concentration = 4.5 g L^{-1}, hydrogen peroxide concentration = 25 g L^{-1}, catalyst load = 2.5 g L^{-1}, pH 3.5, T = 353 K and 24 h. Catalytic experiments shows complete removal of phenol is achieved when using some of the carbon nanotubes (Sigma- Aldrich 1, Nanocyl (NC) and Sigma- Aldrich 2), together with a remarkable total organic carbon removal (77, 69 and 67%, respectively). Hu et al. [140] intensified the removal of nitrobenzene from aqueous solution using nano-zero valent iron (nZVI)/Granular Activated Carbon Composite. The involvement of

GAC improved the dispersion of nZVI greatly and intensified the removal of NB from aqueous solution with less dissolved iron after Fenton-like reaction, as GAC in the composite performed as both a reactive support in iron-rich phase and a catalyst promoter on ·OH generation, and there were iron–carbon microelectrolysis effects to promote electrons transfer efficiency to enhance Fe(III)/Fe(II) regeneration and cycles.

Ribeiro et al. [141] assess the intensification of magnetic graphitic nanocomposite (MGNC) as a high per-formance catalyst in catalytic wet peroxide oxidation (CWPO) of 4-Nitrophenol. The incorporation of Fe_3O_4 nanoparticles in a graphitic structure during the synthesis of MGNC was found to be enhancing the catalytic activity in CWPO when compared to Fe3O4, due to increased adsorptive interactions between the surface of the catalyst and the pollutant molecules. Complete removal of 4-Nitrophenol (4-NP) is obtained after 4 h of operations.

Further materialize the potential of nanomaterials for the intensification of oxidation of organic pollutants in waste water, research needs to focus on developing novel nanomaterials that are less energy-intensive. Systematic studies of the fate of nanoparticles in the environment, which can be used to predict the fate of similar nanoparticles, need to be intensified since studying each nanoparticle/nanocomposite is onerous and almost impossible.

5. Mechanistic aspects of AOP's:

The mechanism of AOP's ultimately leads to the generation of highly reactive hydroxyl radicals (OH•), these radicals are highly oxidative with organic pollutants in the wastewater. Hydroxyl radicals mostly prefer the electrons from the surrounding electron-rich organic compounds may leads to the complete degradation of organic pollutants. The oxidation potential of hydroxyl radical is reported around 2.33 V, which is more than the chemical oxidants such as H_2O_2 or $KMnO_4$. The overview of mechanistic aspects of OH• radical generation in various AOP's includes photo and nano photo chemical AOP's have been reported here.

Non-photochemical methods:

Non-photochemical AOP's able to generate the hydroxyl radicals without using light energy. From the literature, few non-photochemical AOP's have been found in wastewater treatment. The mechanistic procedure involved for the hydroxyl radical generation in such AOP's has been discussed here.

1). Ozonation

2). Wet peroxide ozonation (O_3/H_2O_2)

3). Catalytic ozonation

4). Fenton based wet peroxidation (H_2O_2/Fe^{2+})

1). Ozonation

Ozone is one of the highly oxidative agents for the oxidation of chemicals among pure oxygen and air. Ozone can also produce the oxidative redicals in the wastewater. Attacking of ozone molecules on •OH radicals surrounded by organic pollutants may leads to the degradation of pollutants. The typical reaction mechanism involved in ozonation was reported as [142].

$$3O_3 + OH^- + H^+ \rightarrow 2\bullet OH + 4O_2 \quad (1)$$
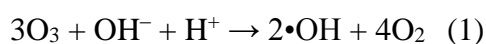
2). Wet peroxide ozonation (O_3/H_2O_2)

It has been reported that faster decomposition of ozone can be made by the addition of hydrogen peroxide to ozone leads to thefaster generation of •OH radicals:

$$2O_3 + H_2O_2 \rightarrow 2 \bullet OH + 3O_2 \quad (2)$$
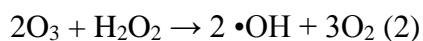
The proposed reaction may continues as described above and •OH radicals are produced [143].

3). Catalytic ozonation

Normally heterogeneous or homogeneous phase catalysts can be use to to improve the ozonation reactions for the efficient degradation of organic pollutants. Several metal oxides have been proposed for catalytic ozonation process such as Fe_2O_3, Al_2O_3, MnO_2, CeO_2, TiO_2 and ZnO. The

reaction mechanism for the degradation of various organic pollutants is remained unclear in most of the catalysts.

4). Fenton system (H_2O_2/Fe^{2+})

The Fenton process was reported by Fenton for maleic acid oxidation. Later, scientists have carried out many researches on application of fenton as a catalyst for the oxidation of various organic pollutants in wastewater [144]. Some of the researchs have also used the other chemical oxidants in conjuction with fenton process to enhance the degradation rate. The raction mechanism for the combined process of fenton and hydrogen peroxide is like.

$Fe^{2+} + H_2O_2 \rightarrow Fe^{3+} + OH^- + \bullet OH$ (3)
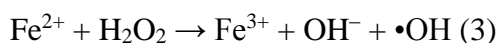
Presence of extra amount of hydrogen peroxide leads to the oxidization of Fe (II) to Fe(III) in a fraction of minutes. It was reported that, hydroxyl radicals can be generate by decomposition of hydrogen peroxide by Fe (III) according to the following reactions:

$Fe^{3+} + H_2O_2 \leftrightarrow H^+ + Fe—OOH^{2+}$ (4)

$Fe—OOH^{2+} \rightarrow HO_2 + Fe^{2+}$ (5)

$Fe^{2+} + H_2O_2 \rightarrow Fe^{3+} + OH^- + \bullet OH$ (6)
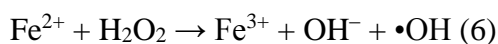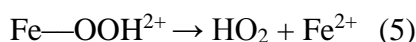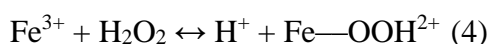
Photochemical methods:

Non-photochemical based treatment techniques suh as ozonationand wet peroxide oxidation does not meet the completely mineralization of organic pollutants [143]. Some of the non-photochemical AOP's can generate more toxic intermediates than the initial parent compound. Complete destruction of organic compounds can be achieved by combining UV radiation with other non-photochemical AOP's. Most of the UV lamps exhibit UV energy in the wavelengthof 200-300 nm range. Due to direct photolysis, organic molecules can be excited upon the absorption of UV energy and generate the hydroxyl radicals. Equations (14-19) describe the main pathways and the role of hydrated electron and hydrogen radical in producing other radicals leading to oxidation products.

23

$$H_2O \xrightarrow{h\nu} HO^{\cdot} + H^{\cdot} + e^{-}_{aq} \quad (7)$$

$$e^{-}_{aq} + O_2 \rightarrow O^{-}_2 \quad (8)$$

$$e^{-}_{aq} + H^+ \rightarrow H\bullet \quad (9)$$

$$H\bullet + O_2 \rightarrow HO_2\bullet \quad (10)$$

$$O_2 \overset{H+}{\leftrightarrow} HO_2\bullet \quad (11)$$

$$HO_2\bullet + RH \rightarrow oxidation\ products \quad (12)$$
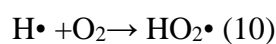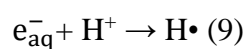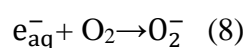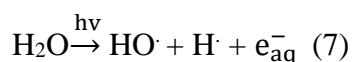
Some of the photo chemical based AOP's have also been discussed here.

1). $O_3/H_2O_2/UV$

2). Photo-Fenton system

3). Photocatalytc system (UV/TiO$_2$)

1). Ozone–hydrogen peroxide–UV radiation (O₃/H₂O₂/UV)

Decomposition rate of ozone can be improved by the supplement of H_2O_2 to the O_3/UV process. Enhanced decomposition of ozone ultimately increased the rate of hydroxyl radical's production. Addition of hydrogen peroxide to some of the AOP's is cost effective, when the organic pollutant possesses low absorption of energy from the UV light irradiation.

2). Photo-Fenton system

When the Fe^{3+} ions and H_2O_2 exposed to UV irradiation, H_2O_2 will be decompose under photocatalytic activity of Fe^{3+} ions leads to the generation of •OH and Fe^{2+} ions. It was observed that Fe $(OH)^{2+}$ complex has been formed at pH 3.

$$Fe^{3+} + H_2O \rightarrow Fe(OH)^{2+} + H^+ \quad (13)$$

$$Fe(OH)^{2+} \leftrightarrow Fe^{3+} + OH^- \quad (14)$$

$$Fe(OH)^{2+} \xrightarrow{h\nu} Fe^{2+} + \bullet OH \quad (15)$$
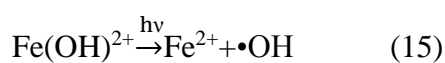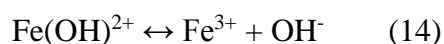
3). Photocatalytic system (UV/TiO₂)

Under UV or visible light irradiation irradiation appropriated semiconductor material may be excited by photons and produce two pairs of electron and holes in the conduction and valence band respectively. Generated charge carriers will initiate the reduction or oxidation reactions respectively. At the surface of the TiO_2 particle these may react with absorbed species [145].

$$e^- + O_2 \rightarrow \bullet O^-_2 \quad (16)$$

$$h^+ + A^- \rightarrow \bullet^. A \quad (17)$$

$$h^+ + OH^- \rightarrow \bullet OH \quad (18)$$

$$\bullet OH + RH \rightarrow \bullet RHOH \quad (19)$$

$$\bullet OH + RH \rightarrow \bullet R + H_2O \quad (20)$$

$$h^+ + RH \rightarrow \bullet RH^+ \quad (21)$$

$$H_2O + h^+ \rightarrow \bullet OH + H^+ \quad (22)$$
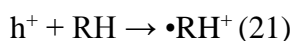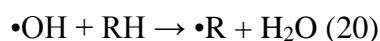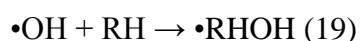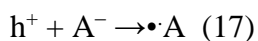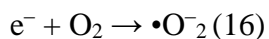
6. Current trends and future prospectus:

Earlier, researches have been mainly focused on conventional or traditional systems for wastewater treatment. Researchers have followed these conventional treatment techniques up to 1990's. Later they shifted to AOP's such as photocatalysis, ozonation, etc. Most of the research works have been carried out in wastewater treatment using TiO_2 based photocatalytic AOP and also most of the work carried out with micro sized photocatalysts. Now the current trend is the researchers using AOP's conjunction with nanotechnology for water and wastewater treatment is gaining momentum globally. The unique properties of nanomaterials and their convergence with AOP's present great opportunities to revolutionize water and wastewater treatment. The combined methods of nanomaterials involving AOP's are one of the advanced wastewater treatment technique to remove contaminants from wastewater or convert pollutants into more degradable compounds. Although many nanomaterials assisted AOP's reported in this review are in the laboratory research stage and some are tested at pilot scale.

There may be future prospects for implementation of Hydrodynamic cavitation and ultrasonic treatment as an AOP on commercial scale and pilot scale respectively, that could promote the production of more hydroxyl radicals. A promising future for these AOP's waits. Nanomaterials assisted these AOP's may become applicable on an industrial scale when every effectiveness factor is optimized and different processes are combined (hybrid system) to eliminate some of the drawbacks associated with the individual techniques to achieve maximum efficiency with minimum energy input. To reach this goal in particular, more efforts are required to handle some key problems, such as the development of novel catalytic materials (which can be operate in visible spectra region or solar based). Furthermore, the amount of $\cdot OH$ produced is an important parameter, but more research work has to be carry out in this direction.

Acknowledgments:

References

[1]. S. T. Akar, R. Uysal, Chem. Eng. J. 162 (2010) 591-598.

[2]. J. O. H. N. Bergendahl, J. A. M. E. S. O Shaughnessy, International Business and Education Conference, A Focus on Water Management, Worcester Polytechnic Institute, 2004.

[3]. D.K. Tiwari, J. Behari. P. Sen, World Appl. Sci. J. 3 (2008) 417-433.

[4]. C. Kormann, D.W. Bahnemann, M.R. Hoffmann, Environ. Sci. Technol. 25 (1991) 494– 500.

[5]. F. Zhang, J. Zhao, T. Shen, H. Hidaka, E. Pelizzetti, N. Serpone, Appl. Catal. B: Environ. 15 (1998) 147–156.

[6]. H. Hildebrand, K. Mackenzie, F.D. Kopinke, Appl. Catal. B- Environ. 91 (2009) 389-396.

[7]. S. Tangestaninejad, M. Moghadam, V. Mirkhani, I. Mohammadpoor-Baltork, H. Salavati, Ultrason. Sonochem. 15 (2008) 815–822.

[8]. S.R. Shirsath, D.V. Pinjari, P.R. Gogate, S.H. Sonawane, A.B. Pandit, Ultrason. Sonochem. 20 (2013) 277–286.

[9]. B. Geng, Z. Jin, T. Li, X. Qi, Chemosphere, 75 (2009) 825-830.

[10]. P. K. Tyagi, R. Singh, S. Vats, D. Kumar, S. Tyagi, International Conference on Nanotechnology and Chemical Engineering (ICNCS'2012), December 21-22, Bangkok (Thailand), (2012).

[11]. J.M.J. Frechet, D.A. Tomalia, Dendrimers and other dendritic polymers, New York, Wiley and Sons, 2001.

[12]. A.W. Bosman, H.M. Janssen, E.W. Meijer, Chem. Rev. 99 (1999) 1665- 1688.

[13]. M. Fischer, F. Vogtle, Dendrimers: from design to application: a progress report, Angew. Chem. Intl. Ed. Engl. 38 (1999) 884-905.

[14]. D.A. Tomalia, I. Majoros, J. Macro Sci. 43 (2003) 411-477.

[15]. M.S. Diallo, S. Christie, P. Swaminathan, J.H. Johnson, W.A. Goddard, Environ. Sci. Technol. 39 (2005) 1366-1377.

[16]. M. Aorkas, D. Tsiourvas, C.M. Paleos, Chem. Mater. 14 (2003) 2844-2847.

[17]. M.F. Ottaviani, P. Favuzza, M. Bigazzi, N.J. Turro, S. Jockusch, D.A. Tomalia, Langmuir, 19 (2000) 7368-7372.

[18]. D.K. Tiwari, J. Behari, P. Sen, World Applied Sciences Journal, 3 (2008) 417-433.

[19]. A. Rether and M. Schuster, React. Funct. Polym. 57 (2003) 13–21.

[20]. J. Gao, X. Luan, J. Wang, B. Wang, K. Li, Y. Li, P. Kang, G. Han, Desalination, 268 (2011) 68–75.

[21]. P. Jain, T. Pradeep, Biotech. Bioeng. 90 (2005) 59-63.

[22]. M. Tobiszewski, J. Namieśnik, Environ. Sci. Pollution Res. 19 (2012) 1994–2006.

[23]. S. J. Klaine, P.J.J. Alvarez, G.E. Batley, T.E. Fernandes, R.D. Handy, D.Y. Lyon, S. Mahendra, M.J. McLaughlin, J.R. Lead, Environ. Toxicol. Chem. 27 (2008) 1825- 1851.

[24]. P.K. Stoimenov, R.L. Klinger, G.L. Marchin, K.J. Klabunde, Langmuir, 18 (2002) 6679- 6686.

[25]. J.H. Chang, T.J. Yang, C.H. Tung, J. Hazard. Mater. 163 (2009) 152- 157.

[26]. N. Mei, L. Xuguang, D. Jinming, J. Husheng, W. Liqiao, X. Bingshe, Carbohyd. Polym.78 (2009) 54-59.

[27]. L. Brittany, V. Carino, J. Kuo, L. Leong, R. Ganesh, Adsorption of organic Compounds to metal oxide nanoparticles, Conference presentation is part of: General Environmental 2006.

[28]. A.E. Alvarez, A.G. Sanchez, X. Querol, Water Res. 37 (2003) 4855- 4862.

[29]. S.N. Schierz, H. Zanker, Environ. Pollut. 157 (2009) 1088-1094.

[30]. G.C. Chen, X.Q. Shan, Y.S. Wang, B. Wen, Z.G. Pei, Y.N. Xie, T. Liu, J.J.Pignatello, Water Research, 43 (2009) 2409-2418.

[31]. W.H. Chewing, Y.S. Szeto, G. McKay, Bioresource. Technol. 100 (2009) 1143-1148.

[32]. C.Y. Hsiao, C.L. Lee, D.F. Ollis, J. Catal. 82 (1983) 418– 423.

[33]. D.F. Ollis, E. Pelizzetti, N. Serpone, Photocatalysis: Fundamentals and Applications, Wiley/Interscience, New York. (1989). 603–637.

[34]. M. Gratzel, N. Serpone, E. Pelizzetti, Photocatalysis: Fundamentals and Applications. Wiley/ Interscience, New York. (1989) 123–157.

[35]. C.S. Turchi, D.F. Ollis, J. Catal. 122 (1990) 178–192.

[36]. W.A. Jacoby, M.T. Nimlos, D.M. Blake, R.D. Noble, C.A. Koval, Environ. Sci. Technol. 28 (1994) 1661–1668.

[37]. J.T. Spadaro, L. Isabelle, V. Renganathan, Environ. Sci. Technol. 28 (1994) 1389– 1393.

[38]. C. Kormann, D.W. Bahnemann, M.R. Hoffmann, Environ. Sci. Technol. 25 (1991) 494– 500.

[39]. J.E. Cavanagh, H.S. Weinberg, A. Gold, G. Sangaiah, D. Marbury, W.H. Glaze, T.W. Collette, S.D. Richardson, A.D. Thurston, J. Environ. Sci. Technol. 26 (1992) 1658–1662.

[40]. R.F.P. Nogueira, W.F. Jardim, J. Chem. Edu. 70 (1993) 861–862.

[41]. P. Reeves, R. Ohlhausen, D. Sloan, K. Pamplin, T. Scoggins, C. Clark, B. Hutchinson, D. Green, Solar Energy. 48 (1992) 413–420.

[42]. F. Zhang, J. Zhao, L. Zang, T. Shen, H. Hidaka, E. Pelizzetti, N. Serpone, J. Mol. Catal. A: Chem. 120 (1997) 173– 178.

[43]. F. Zhang, J. Zhao, T. Shen, H. Hidaka, E. Pelizzetti, N. Serpone, Appl. Catal. B: Environ. 15 (1998) 147–156.

[44]. J. Zhao, K. Wu, T. Wu, H. Hidaka, N. Serpone, J. Chem. Soc. Faraday Trans. 94 (1998) 673–676.

[45]. L.M. Games, R.A. Hites, Anal. Chem. 49 (1977) 1433–1440.

[46]. C.H. Ao, M.K.H. Leung, R. C.W. Lam, D. Y.C. Leung, L.L.P. Vrijmoed , W.C. Yam, S.P. Ng, Chem. Eng. J. 129 (2007) 153–159.

[47]. H. Zhu, R. Jiang, L. Xiao, Y. Chang, Y. Guan, X. Li, G. Zeng, J. Hazard. Mater. 169 (2009) 933–940.

[48]. P. R. Shukla, S. Wang, H. M. Ang, M. O. Tade, Sep. Purif. Technol. 70 (2010) 338–344.

[49]. P.J. Lu, C.W. Chien, T.S. Chen, J.M. Chern, Chem. Eng. J. 163 (2010) 28–34.

[50]. J. Gao, X. Luan, J. Wang, B. Wang, K. Li, Y. Li, P. Kang, G. Han, Desalination. 268 , (2011) 68–75.

[51]. P. Bansal, A. Dhir, N. Tejoprakash, D. Sud, Indian J. Chem. 50 (2011) 991-995.

[52]. D.S. Shi, J,B, Zhang, L,L, Gao, Y,L, Wang, D,D, Zhou, Transactions of Nonferrous Metals Society of China. 22 (2012) 2477-2483

[53]. N. Elamin, A. Elsanousi, J. Appl. Ind. Sci. 1 (2013) 32-35.

[54]. N. B. Pompermayer, M. B. Porto, E. F. Souza, World Acad. Sci. Eng. Technol. 7 (2013) 1878-1883.

[55]. A. Y. Booshehri, S. C. Goh, J. Hong, R. Jiang, R. Xu, J. Mater. Chem. A. 2 (2014) 6209-6217.

[56]. M.A. Barakat, Y.T. Chen, C.P. Huang, Appl. Catal. B: Environ. 53 (2004) 13–20.

[57]. M. Muruganandham, M. Swaminathan, Dyes and Pigments. 68 (2006) 133-142.

[58]. K. Dai, H. Chen, T. Peng, D. Ke, H. Yi, Chemosphere. 69 (2007) 1361–1367.

[59]. Y. Tu, S. Huang, J. Sang, X. Zou, Mater. Res. Bull. 45 (2010) 224–229.

[60]. P. Liu, H. Liu, G. Liu, K. Yao, W. Lv, Appl. Surf. Sci. 258 (2012) 9593– 9598.

[61]. H. Wang, S. Dong, Y. Chang, J. L. Faria, J. Hazard. Mater. 230 (2012) 235-236.

[62]. L. Liu, F. Chen, F. Yang, Y.S. Chen, J. Crittenden, Chemical Engineering Journal. (2012) 189– 195

[63]. B. Cui, H. Peng, H. Xia, X. Guo, H. Guo, Sep. Purif. Technol. 103 (2013) 251–257.

[64]. Sowbhagya, A. Sannaiah, Am. Chem. Sci. J. 4 (2014) 616-637.

[65]. X. Wei, H. Wang, G. Zhu, J. Chen, L. Zhu, Ceram. Inter. 39 (2013) 4009–4016.

[66]. Z. Cheng, K. Ting, Y. Tao, A. Goh, X. Yin, Sustain. Environ. Res. 20 (2010) 281-286.

[67]. M.A. Behnajady, N. Modirshahla, M. Shokri, B. Rad, Global Nest J. 10 (2008) 1-7.

[68]. P. Sathishkumar, R. V. Mangalaraja, S. Anandan, M. Ashokkumar, Chem. Eng. J. 220 (2013) 302–310.

[69]. S. J. Doh, C. Kim, S. Lee, S. Lee, H. Kim, J. Hazard. Mater. 154 (2008) 118–127.

[70]. R. S. K. Wong, J. Feng, X. Hu, P. L. Yue, J. Environ. Sci. Health A - Toxic/Hazard. Subst. Environ. Eng. 39 (2004) 2583–2595.

[71]. M. M. Ba-Abbad, A. A. H. Kadhum, A. B. Mohamad, M. S. Takriff, K. Sopian, Int. J. Electrochem. Sci. 7 (2012) 4871 – 4888.

[72]. R. Shao, L. Sun, L. Tang, Z. Chen, Chem. Eng. J. 217 (2013) 185–191.

[73]. N. Liang, J. Zai, M. Xu, Q. Zhu, X. Wei, X. Qian, J. Mater. Chem. A. 2 (2014) 4208–4216.

[74]. A.R. Khataee, Environ. Technol. 30 (2009) 1155–1168.

[75]. J. Moon, C. Y. Yun, K.-W. Chung, M. S. Kang, Jongheop Yi, Catal. Today. 87 (2003) 77–86.

[76]. R. Suarez-Parra, I. Hernandez-Perez, M.E. Rinon, S. Lopez-Ayala, M.C. Roldan-Ahumada, Solar Energ. Mater. Sol. C. 76 (2003) 189–199.

[77]. J. C. Yu, W. Ho, J. Yu, H. Yip, P. Wong, J. Zhao, Environ. Sci. Technol. 39 (2005) 1175-1179.

[78]. F. Peng, H. Wang, H. Yu, S. Chen, Mater. Res. Bull. 41 (2006) 2123–2129.

[79]. S. Min, F. Wang, Y. Han, Journal of Material Science. 42 (2007) 9966–9972

[80]. N. Venkatachalam, M. Palanichamy, Banumathi Arabindoo, V. Murugesan, J. Mol. Catal. A: Chem. 266 (2007) 158–165.

[81]. H. Wang, C. Xie, W. Zhang, S. Cai, Z. Yang, Y. Gui, J. Hazard. Mater. 141 (2007) 645–652.

[82]. S. Tangestaninejad, M. Moghadam, V. Mirkhani, I. Mohammadpoor-Baltork, H. Salavati, Ultrason. Sonochem. 15 (2008) 815–822.

[83]. H. R. Pouretedal, A. Norozi, M. H. Keshavarz, A. Semnani, J. Hazard. Mater. 162 (2009) 674–681.

[84]. X. Wang, H. Zhao, X. Quan, Y. Zhao, S. Chen, J. Hazard. Mater. 166 (2009) 547–552.

[85]. A.R. Khataee, M.N. Pons, O. Zahraa, J. Hazard. Mater. 168 (2009) 451–457.

[86]. M. Pelaez, A. A. de la Cruz, E. Stathatos, P. Falaras, D. D. Dionysiou, Catal. Today. 144 (2009) 19–25.

[87]. J. Wang, Y. Xie, Z. Zhang, J. Li, X. Chen, L. Zhang, R. Xu, X. Zhang, Solar Energ. Mater. Sol. C. 93 (2009) 355–361.

[88]. C. T. Hsieh, W. S. Fan, W. Y. Chen, J. Y. Lin, Sep. Purif. Technol. 67 (2009) 312–318.

[89]. K. M. Joshi, V. S. Shrivastava, Appl. Nanosci. 1 (2011) 147–155.

[90]. M. Zhu, P. Chen, M. Liu, ACS Nano. 5 (2011) 4529–4536.

[91]. M. Muslim, M. A. Habib, A. J. Mahmood, T. S. A. Islam, I. M. I. Ismail, Inter. Nano Lett. 2 (2012) 1-9.

[92]. C. Zhao, Y. Yang, Z. Zhang, Open J. Appl. Sci. 2 (2012) 86-92.

[93]. W. Shi, Y. Yan, X. Yan, Chem. Eng. J. 215 (2013) 740–746.

[94]. Y. Ruzmanova, M. Ustundas, M. Stoller, A. Chianese, Chem. Eng. Trans. The Italian Asso. Chem. Eng. 32 (2013) 2233-2238.

[95]. Z. Ali, S. T. Hussain, M. N. Chaudhry, S. A. Batool, T. Mahmood, Inter. J. Phys. Sci. 8 (2013) 1201-1208.

[96]. Z. Ali, M. N. Chaudhry, S. T. Hussain, S. A. Batool, S. M. Abbas, N. Ahmad, N. Ali, N. A. Niaz, J. Nanomater. Biostruct. 8 (2013) 1271 – 1280.

[97]. S. A. Shahid, A. Nafady, I. Ullah, Y. H. Taufiq-Yap, I. Shakir, F. Anwar, U. Rashid, J. Nanomater. (2013) 1-6.

[98]. W. Lu, J. Chen, Y. Wu, L. Duan, Y. Yang, X. Ge, Nanoscale Res. Lett. 9 (2014) 1-7.

[99]. R. Wei, T. Zhou, J. Hu, J. Li, Mater. Res. Express. 1 (2014) 1-14.

[100]. P. Ellappan, L. R. Miranda, Inter. J. Photoenerg. (2014) 1-9.

[101]. C. Wang, H. Shi, P. Zhang, Y. Li, Appl. Clay Sci. 53 (2011) 646–649.

[102]. K.C. Namkung, A.E. Burgess, D.H. Bremner, H. Staines, Ultrason. Sonochem. 15 (2008) 171–176.

[103]. I. Ioan, S. Wilson, E. Lundanes, A. Neculai, J. Hazard. Mater. 142 (2007) 559–563.

[104]. M. Papadaki, R.J. Emery, M.A.A. Hassan, A.D. Bustos, I.S. Metcalfe, D. Mantzavinos, Sep. Purif. Technol. 34 (2004) 35–42.

[105]. J.H. Sun, S.P. Sun, J.Y. Sun, R.X. Sun, L.P. Qiao, H.Q. Guo, M.H. Fan, Ultrason. Sonochem. 14 (2007) 761–766.

[106]. A.G. Chakinala, D.H. Bremner, P.R. Gogate, K.C. Namkung, A.E. Burgess, Appl. Catal. B: Environ. 78 (2008) 11–18.

[107]. Q. Chen, F. Ji, T. Liu, P. Yan, W. Guan, X. Xu, Chem. Eng. J. 229 (2013) 57–65.

[108]. M. Bobu, A. Yediler, I. Siminiceanu, S. Schulte-Hostede, Appl. Catal. B: Environ. 83 (2008) 15–23.

[109]. B. Narendra Kumar, Y. Anjaneyulu, V. Himabindu, J. Chem. Pharm. Res. 3 (2011) 718-731.

[110]. S. Sivasankaran, A. Pandey, P. Ranjan, Inter. J. Scientific Eng. Res. 4 (2013) 1587-1593.

[111]. M. Sivakumar, A.B. Pandit, Ultrason. Sonochem. 8 (2001) 233–240.

[112]. P.R. Gogate, S. Mujumdar, J. Thampi, A.M. Wilhelm, A.B. Pandit, Sep. Purif. Technol. 34 (2004) 25–34.

[113]. M.A. Behnajady, N. Modirshahla, M. Shokri, B. Vahid, Global NEST Journal. 10 (2008) 8-15.

[114]. M.A. Behnajady, N. Modirshahla, M. Shokri, B. Vahid, Ultrason. Sonochem. 15 (2008) 1009–1014.

[115]. N. Talebian, M. R. Nilforoushan, F. J. Mogaddas, Ceramic. Inter. 39 (2013) 4913–4921.

[116]. S. Chakma, J. B. Bhasarkar, V. S. Moholkar, Inter. J. Res. Eng. Technol. 2 (2013) 177-183.

[117]. M. Salehi, H. Hashemipour, M. Mirzaee, Am. J. Environ. Eng. 2 (2012) 1-7.

[118]. P. Sathishkumar, R. V. Mangalaraja, O. Rozas, H. D. Mansilla, M. Gracia-Pinilla, S. Anandan, Sonophotocatalytic degradation of acid blue 113 in the presence of rare earth ions loaded TiO$_2$ nanophotocatalysts, 13er Congreso Internecional Encienicia Y Technologia De Metalurgia Materials, 2013.

[119]. S. R. Shirsath, D.V. Pinjari, P.R. Gogate, S.H. Sonawane, A.B. Pandit, Ultrason. Sonochem. 20 (2013) 277–286.

[120]. N. M. Mahmoodi, M. Arami, J. Photochem. Photobiol. A: Chem. 182 (2006) 60–66.

[121]. N. M. Mahmoodi, Desalination. 279 (2011) 332–337.

[122]. N. M. Mahmoodi, M. Bashiri, S. J. Moeen, Mater. Res. Bull. 47 (2012) 4403–4408.

[123]. J. Feng, R. S. K. Wong, X. Hu, P. Yue, Catal. Today. 98 (2004) 441–446.

[124]. R. Thiruvenkatachari, T. Kwon, I. Moon, J. Environ. Sci. Health A. 4 (2006) 1685–1697.

[125]. M. Ahmad, E. Ahmed, Z.L. Hong, W. Ahmed, A. Elhissi, N.R. Khalid, Ultrason. Sonochem. 21 (2014) 761–773.

[126]. R. Huang, Z. Fang, X. Yan, W. Cheng, Chem. Eng. J. 197 (2012) 242–249.

[127]. J. Feng, X. Hu, P.L. Yue, H.Y. Zhu, G.Q. Lu, Ind. Eng. Chem. Res. 42 (2003) 2058–2066.

[128]. J. Feng, X. Hu, P.L. Yue, Environ. Sci. Technol. 38 (2004 a) 269–275.

[129]. J. Feng, X. Hu, P.L. Yue, Environ. Sci. Technol. 38 (2004 b) 5773–5778.

[130]. M. Zarei, A. Khataee, M. Fathinia, F. Seyyednajafi, H. Ranjbar, Inter. J. Ind. Chem. 3 (2012) 1-11.

[131]. B. Neppolian, L. Ciceri, C. L. Bianchi, F. Grieser, M. Ashokkumar, Ultrason. Sonochem. 18 (2011) 135–139.

[132]. S.G. Anju, S. Yesodharan, E.P. Yesodharan, Chem. Eng. J. 189 (2012) 84– 93.

[133]. X. Wang, J. Jia, Y. Wang, J. Hazard. Mater. 185 (2011) 315–321.

[134]. M. V. Bagal, P. R. Gogate, Ultrason. Sonochem. 21 (2014) 1035–1043.

[135]. Tom Van Gerven, Guido Mul, Jacob Moulijn, Andrzej Stankiewicz, Chemical Engineering and Processing 46 (2007) 781–789

[136]. Shuo Zhang, Dong Wang, Liang Zhou, Xingwen Zhang, Pingping Fan, Xie Quan, Chemical Engineering Journal 217 (2013) 99‑107

[137]. Mohammad A. Behnajady andMahsa Hajiahmadi, International Journal of Photoenergy, Volume 2013, Article ID 289290, 11 pages.

[138]. Wei Wua, Shuang Gao, Weixia Tu, Jianfeng Chen, Pengyuan Zhang, Particuology 8 (2010) 453–457

[139]. Maria T. Pinho, Helder T. Gomes, Rui S. Ribeiro, Joaquim L. Faria, Adrián M.T. Silva, Applied Catalysis B: Environmental 165 (2015) 706–714

[140]. Sihai Hu & Hairui Yao & Kaifeng Wang & Cong Lu & Yaoguo Wu, Water Air Soil Pollut (2015) 226: 155

[141] Rui S. Ribeiro, Adrián M.T. Silva, Pedro B. Tavares, José L. Figueiredo,Joaquim L. Faria, Helder T. Gomes, Catalysis Today, Article in press.

[142]. C. Gottschalk, J. A. Libra, A. Saupe, Ozonation of Water and Waste Water, Wiley-VCH, 2000.

[143]. J. Hoigne, Mechanisms, Rates and selectivities of oxidations of organic compounds initiated by ozonation of water, In Handbook of Ozone Technology and Applications, Ann Arbor Science Publ., Ann Arbor, MI, 1982.

[144]. H. J. Fenton, J. Chem. Soc. 65 (1884) 889–899.

[145]. R.W. Matthews, Water Res. 20 (1986) 569–578.

List of Figures

Fig. 1. Schematic mechanism of TiO_2 photocatalysis
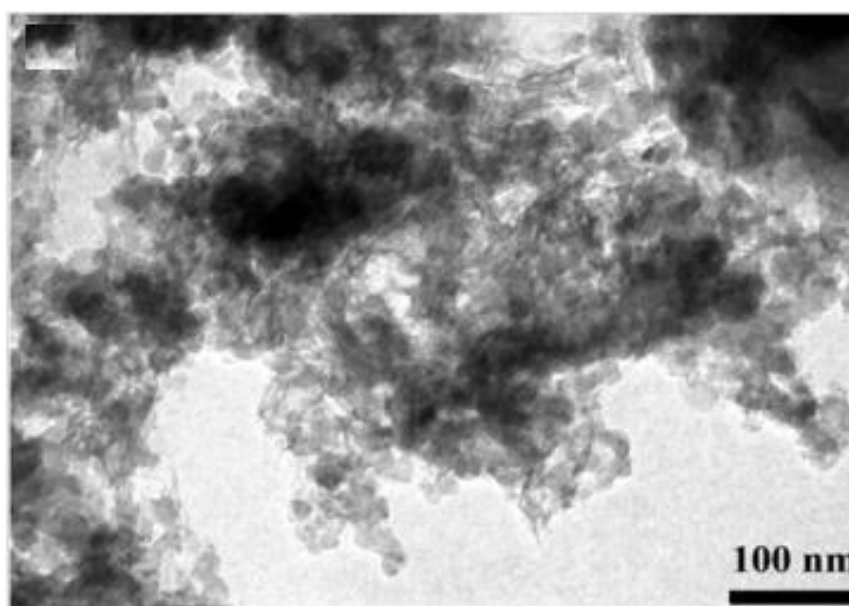
Fig.2. TEM image of Ce doped TiO_2 nanoparticles [Reprinted from (8). Copyright (2015) with the permission from Elsevier]
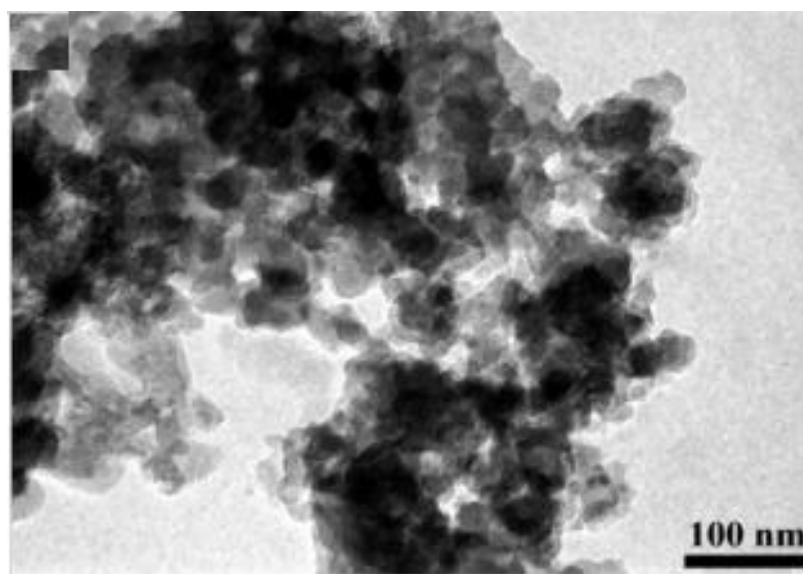
Fig.3. TEM image of TiO$_2$ [Reprinted from (8). Copyright (2015) with the permission from Elsevier]
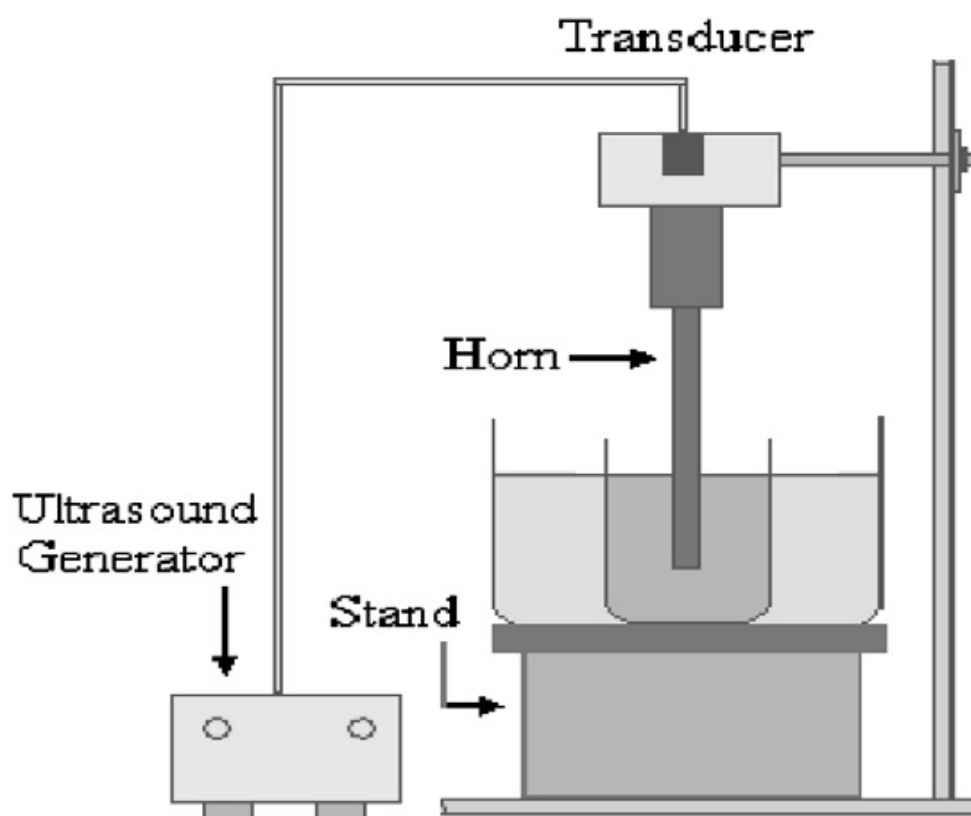
Fig.4. Experimental set up for sonochemical synthesis of nanoaprticles [Reprinted from (8). Copyright (2015) with the permission from Elsevier]

List of Tables

Table 1: Photocatalytic nanoparticles used for Single AOP's

Type of System	Type of Nano Catalyst	Degraded component	Highlights	Article Ref.
Photocatalysis	TiO_2	Acid red 44	Studied the influence of pH on adsorption and degradation of dye on to TiO_2 nano crystalline powder with an average particles diameter of 30 nm in the presence of visible light respectively.	[75]
Photocatalysis	TiO_2/CdO–ZnO	Blue azo dye	100 mg/L of dye solution having pH =3, at temperature 85 ^{0}C and with the aid of 400 mg/L hydrogen peroxide in the presence of TiO_2 films shows the lower degradation of dye than on TiO_2/CdO–ZnO	[76]
Photocatalysis	S-doped TiO_2	Micrococcus lylae (gram-positive bacterium)	A visible light used for killing bacteria via doping sulfur onto TiO_2 photocatalyst	[77]
Photocatalysis	ZnO/Al film	Phenol	ZnO nano-size particles with average diameter of 52 nm were used. 20 mg/L of phenol solution were used and visible light was irradiated for 3 h, studies concluded that more than 40 % of the initial phenol was totally mineralized over two pieces of ZnO/Al thin film. Authors are concluded ZnO/Al is a promising visible light responded photocatalyst	[78]
Photocatalysis	Polyaniline (PAn) sensitized nanocrystalline TiO_2 composite (PAn/TiO_2)	methylene blue (MB)	Degradation of methylene blue (MB) in aqueous solution was investigated under natural light irradiation; MB could be degraded more efficiently on the PAn/TiO_2 than on the pure TiO_2.	[79]
Photocatalysis	Zr^{4+} doped TiO_2, commercial TiO_2 (Degussa P25)	4-chlorophenol	Experimental parameters such as initial concentration of 4-chlorophenol, catalyst loading, pH and light intensity were optimized to achieve maximum degradation efficiency. Zr^{4+} doped TiO_2 shows the maximum degradation than both nano TiO_2 and commercial TiO_2 (Degussa P25).	[80]
Photocatalysis	ZnO	methyl orange	The smallest 10 nm ZnO nanoparticle prepared by chemical deposition method indicated the lower efficiency contrast to 200 nm ZnO	[81]

			powders prepared by thermal evaporation method. The results indicated that preparation method was the decisive factor rather than size and morphology.	
sonocatalytic and sonophotocatalytic	$Na_5PV_2Mo_{10}O_{40}$ supported on nanoporous anatase TiO_2	coperxon Navy Blue-RL, Nylosan Black 2-BC, Methyl Orange, Congo Red, Solophenyl Red-3BL, Ponceau S, Bromothymol Blue, Methylene Blue and Rhodamin B	Sonocatalytic and sonophotocatalytic decomposition of different dyes. Composite showed higher photocatalytic and sonocatalytic activity than pure polyoxometalate or pure TiO_2	[82]
Photocatalysis	zinc sulfide as undoped and doped with manganese, nickel and copper	methylene blue and safranin	The maximum degradation efficiency was obtained in the presence of $Zn_{0.98}Mn_{0.02}S$, $Zn_{0.94}Ni_{0.06}S$ and $Zn_{0.90}Cu_{0.10}S$. The higher degradation efficiency was obtained at alkaline pH of 11.0	[83]
Photoelectrocatalysis	salicylic acid (SA)-modified TiO_2 nanotube array electrode	p-nitrophenol (PNP)	The degradation efficiencies increased from 63 to 100 % under UV light, and 79−100 % under visible light ($\lambda > 400$ nm), compared with TiO_2 nanotube array electrode.	[84]
photocatalysis	TiO_2	C.I. Acid Orange 10 (AO10), C.I. Acid Orange 12 (AO12) and C.I. Acid Orange 8 (AO8)	Crystallites mean size 5−10 nm immobilized on glass plates by heat attachment method. Photocatalytic decolorization kinetics of the dyes were obtained in the order of AO10 >AO12 >AO8. overall TOC removal larger than 94 % for a reaction time of 6 h.	[85]
Photocatalysis	Non metal-doped TiO_2 nanoparticles (N-F-TiO_2)	microcystin-LR (MC-LR)	Co-doping with nitrogen and fluorine are responsible for higher photocatalytic activity than TiO_2 nanoparticles with only fluorine or nitrogen doping. Under acidic conditions (pH 3.0 ± 0.1), the highest MC-LR degradation rate was achieved with N-F-TiO_2.	[86]
Photocatalysis	Er^{3+}:$YAlO_3$/ZnO composite	Acid red B	Prepared by ultrasonic dispersion and liquid boiling method. Dye were degraded under solar light irradiation.	[87]
Photocatalysis	Co-doped TiO_2 nanotubes (TNTs)	basic violet 10 (BV10)	Hydrothermal treatment was employed to synthesis visible-light-driven photocatalysis. Synthesized tubes are hollow scrolls with a typical outer diameter of about 10−15 nm,	[88]

43

			inner diameter 5–10 nm and length of several micrometers.	
Photocatalysis	TiO_2, ZnO, and CdS	chromium Cr (VI)	The maximum removal of Cr (VI) was observed at pH=2 out of these photocatalysts TiO_2 showed highest capacity for Cr (VI) removal than TiO_2 thin film	[89]
Photocatalysis	GO-based hybrid Ag/AgX (X = Br, Cl) nanocomposites	methyl orange (MO)	The GO-involved nanocomposites (Ag/AgX/GO) display distinctly enhanced photocatalytic activities compared to bare Ag/AgX nanospecies. The hybridization of Ag/AgX with GO nanosheets shows the nice adsorptive capacity of MO molecules	[90]
Photocatalysis	ZnO	Ponceau S (PS) diazo dye	ZnO nanoparticles of size 40 nm have been prepared and used as a photocatalyst compared to pristine ZnO Photodecolorization	[91]
Photocatalysis	Pt modified nano-sized tungsten trioxides (Pt/WO_3)	microcystin-LR (MC-LR), Cyano bacteria	Photocatalytic activity was higher during the degradation of MC-LR with Pt/WO_3 than with pure WO_3 or TiO_2	[92]
Photocatalysis	$BiVO_4$	ciprofloxacin (CIP)	Facile microwave-assisted synthesis of $BiVO_4$ nano crystal showed excellent visible-light response. Further Pt loading were carried out to create the charge collectors, transporters, active sites.	[93]
Photocatalysis	N-doped TiO_2	Olive mill wastewater (OMWW)	Sol-gel nanoparticles coated on glass spheres of 1 mm in diameter. 150W visible light batch photoreactor were used. (COD) was chosen as a key parameter of the organic matter degradation	[94]
Photocatalysis	$CuO-Al_2O_3-ZrO_2$-TiO_2	Direct sky blue-5B	Nanocomposite was synthesized by co-precipitation method and photocatalytic activity under sun light shows about 96 % degradation of dye over 100 min of degradation study.	[95]
Photocatalysis	TiON/Cu/Co (copper and cobalt co-modified nitrogen doped titania)	Erichrome black-T (EBT)	Due to lower cobalt ion concentration in the doped samples, the TiON/Cu/Co composite responded with extraordinary photocatalytic properties. Photocatalytic efficiency of TiON/Cu/Co was found to be 95 % in 100 min duration.	[96]
Photocatalysis	$ZrFe_2O_5$	Toluidine Blue O (TBO) dye	Nanoparticles were synthesized using coprecipitation technique. degradation	[97]

			efficiency was observed as 92% after 140 min under visible light	
Photocatalysis	graphene decorated CdS particles (G/M-CdS)	Rhodamine B	CdS Nanoparticles having 640 nm were synthesized using one-pot solvo-thermal route. Syntheiszed composite reveals the high photodegradation rate under visible light irradiation	[98]
Photocatalysis	L-Glutatione (GSH) modified ultrathin SnS_2 nanosheets	Methyl orange (MO) and Chromium Cr (VI)	Nano sheets synthesized via a one-pot, facile and rapid solvo-thermal approach. Superior photocatalytic performance was observed by complete removal of methyl orange and Cr (VI) in 20 min and 60 min respectively.	[99]
Photocatalysis	Cerium doped TiO_2	Nitrobenzene (NB)	Decomposition of Nitrobenzene (NB) in the presence of visible light as the artificial light source. Cerium doped catalyst was found to have better degradation of nitrobenzene due to its shift in the band gap from UV to visible region as compared to undoped TiO_2 catalyst. Catalyst dosage of 0.1 g/l, pH of 9, and light intensity of 500W have been employed.	[100]
Photocatalysis	Kaolinite/TiO_2	Methyl orange	TiO_2/kaolinite calcined at 200 °C shows a high photocatalytic activity due to the smaller crystallite size	[101]

Table 2: Hybrid AOP's involving nanomaterials

Type of System	Type of Nano Catalyst	Degraded component	Highlights	Article Ref.
UV+H_2O_2	Immobilized titanium(IV) oxide	Acid Red 14	Photocatalytic degradation process has been employed to study the degradation of dye on pilot scale (7 L), UV-C lamp (200–280 nm and 15W, Philips) were used.	[120]
photocatalytic ozonation (UV+O_3)	copper ferrite ($CuFe_2O_4$) nanoparticle	Reactive Red 198 and Reactive Red 120	Nanoparticles prepared by co-precipitation method. Photocatalytic ozonation of dyes on Copper Ferrite nanoparticle was a very effective method for dye degradation.	[121]
photocatalytic ozonation	Nickel–zinc ferrite magnetic nanoparticle (NZFMN)	Reactive Red 198 and Direct Green 6	NZFMN dosage, dye concentration, salt and pH were studied. RR198 and DG6 were completely decolorized (100%)	[122]
Uv+H_2O_2	Fe^{3+}-doped TiO_2 and Fe-bentonite (Fe–B) nanocomposite	Orange II dye	Fe–B catalyst exhibits good catalytic activity in the discoloration and mineralization of Orange II in the presence of UV-C light (254 nm) and H_2O_2 at an initial solution pH of 6.60. Negligible leaching of Fe ions from the nanocatalyst was observed.	[123]
photofenton oxidation (UV-H_2O_2-Fe), photocatalytic ozonation (UV-O_3-Fe), photofenton ozonation (UV-O_3-H_2O_2-Fe)	Br, Mn and Co	terephthalic acid (TPA), isophthalic acid (IPA), benzoic acid (BA)	Among all the three processes, Photofenton ozonation was found to be most efficient by achieving almost complete destruction of all the three targeted organics in less than 30 minutes of reaction	[124]
Sono-photocatalysis	pristine ZnO, ZnO/CNTs composites	Rhodamine B	Sono-photocatalysis was always faster than the photocatalysis processe due to more formation of reactive radicals as well as the increase of the active surface area of ZnO/CNTs photocatalyst.	[125]
Sono-Fenton process	Fe_3O_4 magnetic nano particles (MNPs)	Bisphenol-A	Reported about 95% degradation of BPA and half total organic carbon (TOC) in solution was eliminated. Fe_3O_4 MNPs showed good stability and activity even after five recycles under pH range from 3 to 9	[126]
Photo assisted-Fenton process	Iron-oxide and silicate nanoparticles, Fe^{3+} doped TiO_2 and Bentonite-Fe	Orange II	Heterogeneous photocatalysts	[127,128,129]
photoelectron Fenton (PEF) + photocatalysis	Mn^{2+} and supported TiO_2	phenol	Synergetic effect has been studied.	[130]
Sono-photocatalytic	Bi_2O_3/$TiZrO_4$	4-chlorophenol (4-CP)	7 nm particles synthesized by an ultrasonic assisted hydrothermal method. Compared sonolytic, photocatalytic and sonophotocatalytic processes.	[131]
Sono-photocatalysis	ZnO and TiO_2	Phenol	13.7% and 7.0% of	[132]

			degradation was obtained, when exposed to US for 2 h in presence of ZnO and TiO2 respectively. sonophotocatalysis resulted in 85% degradation in the case of ZnO and 65% in the case of TiO2 in 2 h.	
Photocatalysis+ water jet cavitation	TiO$_2$	C.I. reactive red 2	They are observed that RR2 degradation efficiency decreased from 60.5 to 53.5% at 90 min as the diameter of throat tube increased from 2 mm (Tube 1) to 3 mm (Tube 2).	[133]
Hydrodynamic cavitation +Photocatalysis	TiO$_2$	Diclofenac sodium (Pharmaceutical Drug)	Degradation of diclofenac sodium is about 95% with 76% reduction in TOC using hydrodynamic cavitation in conjunction with UV/TiO$_2$/H$_2$O$_2$	[134]